

**ELECTRICAL PROPERTY-INVESTIGATION OF POROUS CLAY
HETEROSTRUCTURES DERIVED FROM NATURALLY-OCCURRING
CLAY MINERALS FOR SMART PACKAGING**

Kornkamol Srithammaraj

A Dissertation Submitted in Partial Fulfilment of the Requirements
for the Degree of Doctor of Philosophy
The Petroleum and Petrochemical College, Chulalongkorn University
in Academic Partnership with
The University of Michigan, The University of Oklahoma,
and Case Western Reserve University

2017

บทคัดย่อและแฟ้มข้อมูลฉบับเต็มของวิทยานิพนธ์ตั้งแต่ปีการศึกษา 2554 ที่ให้บริการในคลังปัญญาจุฬาฯ (CUIR)
เป็นแฟ้มข้อมูลของนิสิตเจ้าของวิทยานิพนธ์ที่ส่งผ่านทางบัณฑิตวิทยาลัย

The abstract and full text of theses from the academic year 2011 in Chulalongkorn University Intellectual Repository (CUIR)
are the thesis authors' files submitted through the Graduate School.

Thesis Title: Electrical Property-Investigation of Porous Clay
Heterostructures derived from Naturally-Occurring Clay
Minerals for Smart Packaging
By: Ms. Kornkamol Srithammaraj
Program: Polymer Science
Thesis Advisors: Assoc. Prof. Hathaikarn Manuspiya
Prof. Rathanawan Magaraphan

Accepted by The Petroleum and Petrochemical College, Chulalongkorn University, in partial fulfilment of the requirements for the Degree of Doctor of Philosophy.

..... College Dean
(Prof. Suwabun Chirachanchai)

Thesis Committee:

.....
(Prof. Suwabun Chirachanchai) (Assoc. Prof. Hathaikarn Manuspiya)

.....
(Prof. Rathanawan Magaraphan) (Asst. Prof. Manit Nithitanakul)

.....
(Asst. Prof. Chiravoot Pechyen)

ABSTRACT

4982006063: Polymer Science Program
Kornkamol Srithammaraj: Electrical Property-Investigation of
Porous Clay Heterostructures derived from Naturally-Occurring
Clay Minerals for Smart Packaging
Thesis Advisors: Assoc. Prof. Hathaikarn Manuspiya and Prof.
Rathanawan Magaraphan 155 pp.
Keywords: Porous clay heterostructures/ Organic-Inorganic hybrid/ Ethylene
adsorption/Smart packaging/ Shelf-life

Porous Clay Heterostructure (PCH) is an interesting material to use as entrapping system such as ethylene scavenger, respected to its high surface area with uniform and specific pore size. PCHs have been prepared by the surfactant-directed assembly of mesostructured silica within the two-dimensional galleries of clays. Then, the PCH was synthesized within the galleries of Na-bentonite clay by the polymerization of tetraethoxysilane (TEOS) in the presence of surfactant micelles. In addition, mesoporous clay with organic-inorganic hybrid (HPCH) is modified via co-condensation reaction of TEOS with candidate conductive functional groups (thiol group) and metal loading (silver), designated as MPPCH and Ag-PCH, to enhance surface conductivity of PCH material for using as sensor packaging. Subsequently, all modified PCHs were utilized as ethylene scavenger and blended with polypropylene for producing ethylene scavenging films in food packaging application with various ratios of clay. The morphological, structural, thermal, and mechanical properties were studied and reported in this work. In addition, the modified PCHs and polypropylene/modified PCHs nanocomposite films were also evaluated the potential uses in active packaging and sensor packaging.

บทคัดย่อ

กรกมล ศรีธรรมราช : การศึกษาสมบัติทางไฟฟ้าของดินเหนียวรูพรุนที่สังเคราะห์จากแร่ดินเหนียวธรรมชาติสำหรับบรรจุภัณฑ์ฉลาด (Electrical Property-Investigation of Porous Clay Heterostructures derived from Naturally—Occurring Clay Minerals for Smart Packaging) อาจารย์ที่ปรึกษา : รศ. ดร. หทัยกานต์ มนัสปิยะ และ ศ. ดร. รัตน์วรรณ มกรพันธุ์ ๑๕๕ หน้า

แร่ดินเหนียวรูพรุนเป็นวัสดุที่น่าสนใจอย่างหนึ่งสำหรับระบบดักจับ เช่น ตัวดักจับก๊าซเอธิลีน เนื่องด้วยการมีพื้นที่ผิวที่สูงและมีรูพรุนที่พิเศษ แร่ดินเหนียวรูพรุนสามารถเตรียมได้จากการเข้าไปขยายชั้นแร่ดินเหนียวด้วยสารลดแรงตึงผิว จากนั้นเติมสารจำพวกซิลิกาเข้าไปเพื่อทำการพอลิเมอไรเซชันหรือการเกิดพอลิเมอร์รอบๆไมเซลล์ของสารลดแรงตึงผิว นอกจากนี้ได้มีการเพิ่มหมู่ฟังก์ชันอินทรีย์เข้าไป เช่น หมู่ด้านการนำไฟฟ้า โดยปฏิกิริยาควบแน่นร่วมกันของสารอินทรีย์และอนินทรีย์ เพื่อเพิ่มประสิทธิภาพด้านไฟฟ้าของดินเหนียวรูพรุนในการที่จะนำมาใช้งานบรรจุภัณฑ์แบบเซนเซอร์ ดินเหนียวรูพรุนที่มีการดัดแปรหมู่ฟังก์ชันทั้งหมดจะถูกนำมาใช้งานเป็นตัวดักจับก๊าซเอธิลีนและจะถูกนำมาผสมกับพอลิโพรพิลีนพร้อมด้วยอัตราส่วนของดินเหนียวรูพรุนที่แตกต่างกัน เพื่อผลิตเป็นฟิล์มดักจับก๊าซเอธิลีนสำหรับบรรจุภัณฑ์อาหาร แร่ดินเหนียวรูพรุนที่มีการดัดแปรหมู่ฟังก์ชันจะถูกนำมารวสอบคุณสมบัติต่างๆ เช่น ลักษณะทางสัณฐานวิทยา โครงสร้างทางเคมี คุณสมบัติทางความร้อน และคุณสมบัติเชิงกล นอกจากนี้ฟิล์มนาโนคอมพอสิตจะถูกนำมาประเมินประสิทธิภาพและศักยภาพในรูปแบบของบรรจุภัณฑ์แอ็กทีฟและเซนเซอร์

ACKNOWLEDGEMENTS

This thesis work is funded by the Petroleum and Petrochemical College; and the Center of Excellence on Petrochemicals and Materials Technology, Thailand. Furthermore the author would like to express her thanks to the Higher Education Research Promotion and National Research University Project of Thailand, Office of the Higher Education Commission (FW 0649A) and the 90th Anniversary of the Chulalongkorn University Fund (Ratchadaphiseksomphot Endowment Fund) for partially fund.

This work would not have been possible without the assistance of the following individuals. First of all, the author would like to gratefully give special appreciation to her advisors, Assoc. Prof. Hathaikarn Manuspiya and Prof. Rathanawan Magaraphan for their intensive suggestions, valuable guidance, vital help, hopeful inspiration, and kindly support throughout this research and also her crisis. In addition, the author deeply thanks to Asst. Prof. Manit Nithitanakul and Asst. Prof. Chiravoot Pechyen for serving on her thesis committee.

The author would like to express special thanks to Professor Amar S. Bhalla and Professor Ruyan Guo who gave valuable advices, discussion and opportunity for doing the research in the Multifunctional Electronic Materials and Devices Research Laboratory (MeMDRL), Department of Electrical and Computer Engineering, College of Engineering, The University of Texas at San Antonio, Texas, United State.

Finally, the author would like to take this opportunity to thank all professors, PPC friends, and friends in the Multifunctional Electronic Materials and Devices Research Laboratory (MeMDRL), Department of Electrical and Computer Engineering, College of Engineering, The University of Texas at San Antonio, Texas, United State, for their friendly assistance, cheerfulness, creative suggestions, and encouragement. Also, the author is greatly indebted to her parents and her family for their support, love and understanding.

TABLE OF CONTENTS

	PAGE
Title Page	i
Abstract (in English)	iii
Abstract (in Thai)	iv
Acknowledgements	v
Table of Contents	vi
List of Tables	ix
List of Figures	xi
 CHAPTER	
I INTRODUCTION	1
II LITERATURE REVIEW	4
III EXPERIMENTAL	26
IV MODIFIED POROUS CLAY HETEROSTRUCTURES BY ORGANIC-INORGANIC HYBRIDS FOR NANOCOMPOSITE ETHYLENE SCAVENGING/SENSOR PACKAGING FILM	33
4.1 Abstract	33
4.2 Introduction	34
4.3 Experimental	36
4.4 Results and Discussions	40
4.5 Conclusions	47
4.6 Acknowledgements	47
4.7 References	48

CHAPTER		PAGE
V	INFLUENCE OF THIOL GROUPS ON THE ETHYLENE ADSORPTION AND CONDUCTIVITY PROPERTIES OF THE MODIFIED POROUS CLAY HETEROSTRUCTURES (PCHS) USING AS ETHYLENE SCAVENGER IN SMART PACKAGING	51
	5.1 Abstract	51
	5.2 Introduction	51
	5.3 Experimental	53
	5.4 Results and Discussions	57
	5.5 Conclusions	76
	5.6 Acknowledgements	77
	5.7 References	77
VI	SILVER-LOADED ON THE SURFACE OF THE POROUS CLAY HETEROSTRUCTURE (PCH) FOR USING AS ETHYLENE SCAVENGER IN FOOD PACKAGING	82
	6.1 Abstract	82
	6.2 Introduction	82
	6.3 Experimental	84
	6.4 Results and Discussions	88
	6.5 Conclusions	109
	6.6 Acknowledgements	110
	6.7 References	110

CHAPTER	PAGE
VII INVESTIGATION OF POLYPROPYLENE/MODIFIED POROUS CLAY HETEROSTRUCTURE NANOCOMPOSITE FILMS: DIELECTRIC PROPERTY AND THERMAL EXPANSION	113
7.1 Abstract	113
7.2 Introduction	113
7.3 Experimental	114
7.4 Results and Discussions	117
7.5 Conclusions	125
7.6 Acknowledgements	125
7.7 References	125
VIII CONCLUSIONS AND RECOMMENDATIONS	129
REFERENCES	132
APPENDICES	142
Appendix A Prolonging Shelf-life of Fresh Fruits	142
Appendix B Percentages of Weight Loss	146
Appendix C Disease Incidence	147
Appendix D Measurement of Respiration Rate	148
Appendix E Antibacterial Test	150
Appendix F Food Safety Test	152
Appendix G Breakdown Strength Measurement	153
CURRICULUM VITAE	154

LIST OF TABLES

TABLE		PAGE
CHAPTER IV		
4.1	Elemental analysis from X-ray fluorescence spectrometry result	44
4.2	Specific surface areas from the N ₂ adsorption-desorption	44
CHAPTER V		
5.1	Elemental analysis from XRF result	63
5.2	Specific surface areas from the N ₂ adsorption-desorption	64
5.3	Resistivity and conductivity of bentonite, MPPCH (1:1), MPPCH (2:1) and MPPCH (4:1)	66
5.4	Thermal properties of PP and PP/modified PCHs nanocomposites	67
5.5	Crystallization behavior of PP and PP/modified PCHs nanocomposites	71
5.6	Young's modulus, tensile strength, and % elongation of PP and PP/modified PCHs nanocomposites with various compositions	73
5.7	Conductivity of polypropylene (PP) and PP/modified PCHs nanocomposite films	75
CHAPTER VI		
6.1	Basal spacing of BTN, organoclay, and porous clay	88
6.2	Elemental analysis from XRF result	95
6.3	The specific surface areas from the N ₂ adsorption-desorption	97
6.4	The conductivity of bentonite and Ag-PCHs	99
6.5	Crystallization behavior of PP and PP/modified Ag-PCHs nanocomposites	102
6.6	Thermal properties of PP and PP/modified PCHs nanocomposites	103
6.7	Young's modulus, tensile strength, and % elongation of PP and 10 wt% Ag-PCH/PP nanocomposites with various compositions	106
6.8	Conductivity of polypropylene (PP) and PP/modified PCHs nanocomposite films	109

LIST OF TABLES

TABLE		PAGE
CHAPTER VII		
7.1	Dielectric constant of PP and PP/modified PCHs nanocomposite films	122
7.2	The value from thermal expansion analysis	124

LIST OF FIGURES

FIGURE	PAGE
CHAPTER II	
2.1	Structure of montmorillonite. 9
2.2	TEM images of saponite heterostructure. 12
2.3	Schematic illustration of mechanism for formation of hybrid porous clay heterostructure (HPCH) through surfactant-directed assembly of organosilica in the galleries of clay. 14
2.4	Grafting of mercaptopropylsilane groups to the inner and outer walls of mesostructural silica intercalated in smectite clay. 15
2.5	Schematically illustration of three different types of thermodynamically achievable polymer/layered silicate nanocomposites. 19
2.6	Basic configuration of a capacitor. 23
2.7	A parallel-plate capacitor. 23
2.8	Capacitor symbols (a) in circuit and (b) polarized fixed. 24
2.9	Two conducting plates separated by a dielectric material with area (A) and separation distance (d). 25
CHAPTER IV	
4.1	X-ray diffractometer patterns of (a) BTN and (b) organoclay. 40
4.2	The transmission electron microscopy images of porous clay heterostructure. 41
4.3	Scanning electron microscopy images of (a) bentonite, (b) porous clay heterostructure, (c) hybrid organic-inorganic porous clay heterostructures (HPCH) and (d) mercaptopropyl functionalized MPPCH. 42

LIST OF FIGURES

FIGURE	PAGE
CHAPTER IV	
4.4	Fourier transform infrared spectroscopy spectra of (a) bentonite, (b) organoclay, (c) porous clay heterostructures and (d) hybrid organic–inorganic porous clay heterostructures. 43
4.5	Ethylene adsorption capacity of bentonite, porous clay heterostructures and hybrid organic– inorganic porous clay heterostructures. 45
4.6	The conductivity of polypropylene/clay nanocomposite films as a function of time attached to the ethylene gas. 46
CHAPTER V	
5.1	XRD patterns of (a) Bentonite, (b) Organoclay, and (c) PCH. 58
5.2	XRD patterns of MPPCH (1:1), MPPCH (2:1) and MPPCH (4:1). 58
5.3	SEM images of (a) BTN, (b) MPPCH (1:1), (c) MPPCH (2:1) and (d) MPPCH (4:1). 59
5.4	FTIR spectra of (a) bentonite, (b) organoclay, (c) MPPCH (1:1), (d) MPPCH (2:1), and (e) MPPCH (4:1). 62
5.5	Ethylene reduction capacity of BTN, MPPCH (1:1), MPPCH (2:1) and MPPCH (4:1). 65
5.6	TG-DTA curves of pure PP and modified PCHs nanocomposites. 67
5.7	DSC heating scan thermograms of pure PP and PP/modified PCHs nanocomposites. 69
5.8	DSC cooling scan thermograms of pure PP and PP/modified PCHs nanocomposites. 70
5.9	Mechanical properties of PP and PP/modified PCHs nanocomposite films: (a) Young's modulus (b) Tensile strength, and (c) % Elongation. 72
5.10	Ethylene reduction capacity of PP, 1 wt% MPPCH (2:1)/PP, 3 wt% MPPCH (2:1)/PP, and 5 wt% MPPCH (2:1)/PP nanocomposite films. 74

LIST OF FIGURES

FIGURE	PAGE
CHAPTER V	
5.11 The conductivity of PP and PP/modified PCHs nanocomposite films as a function of ethylene adsorption time.	76
CHAPTER VI	
6.1 XRD patterns of (a) Bentonite, (b) organoclay (CTAC), and (c) PCH.	89
6.2 XRD patterns of Bentonite (BTN), porous clay heterostructure (PCH) and all modified PCHs (Ag-PCHs).	90
6.3 SEM images of (a) BTN, (b) PCH, (c) 1wt% Ag-PCH, (d) 5wt% Ag-PCH, (e) 10wt% Ag-PCH, (f) 20wt% Ag-PCH, and (f) 30wt% Ag-PCH.	91
6.4 Transmission electron microscopy images of (a) porous clay heterostructure (PCH), (b) silver loaded porous clay heterostructure (Ag-PCH), and (c) silver particles.	93
6.5 XPS spectra for wide analysis.	96
6.6 Ethylene adsorption of BTN, PCH, and Ag-PCHs at the equilibrium state.	98
6.7 DSC heating scan thermograms of pure PP and PP/modified Ag-PCHs nanocomposites.	101
6.8 DSC cooling scan thermograms of pure PP and PP/modified Ag-PCHs Nanocomposites.	101
6.9 TG-DTA curves of pure PP and modified Ag-PCH nanocomposites	103
6.10 Mechanical properties of PP and 10wt% Ag-PCH/PP composite films with various contents of clay loading: (a) Young's modulus (b) Tensile strength, and (c) %Elongation.	105
6.11 Ethylene reduction capacity of PP, 1wt% (10wt%Ag-PCH)/PP, 3wt% (10wt%Ag-PCH)/PP, and 5wt% (10wt%Ag-PCH)/PP nanocomposite films.	107

FIGURE		PAGE
CHAPTER VI		
6.12	The conductivity of PP and Ag-PCHs/PP nanocomposite films as a function of time adsorbing to the ethylene gas.	108
6.13	Structure of PCH and Ag-PCH (Scheme 1).	96
CHAPTER VII		
7.1	Dielectric constant and loss tangent of PP and Ag-PCH at function of temperature.	118
7.2	The dielectric constant and loss tangent in function of frequency at 20 °C (293K).	121
7.3	The plot between $\ln \tau - 1000/T$.	122
7.4	The loop of thermal expansion experiment.	123
7.5	Tg point of the cooling cycle.	124

CHAPTER I

INTRODUCTION

Nowadays, smart packaging is very popular for innovative technology in packaging. The smart packaging is a package that not only retains the product but also adds functionality to the product itself, or to aspects of product consumption, convenience and security. The package operates as a smart system incorporating both smart and conventional materials and must be capable of adding value across the packaging supply chain. Smart packaging is usually divided into 2 types: active packaging and intelligent packaging.

Active packaging is triggered by filling, exposure to UV, release of pressure and then continues until the process is exhausted. Many examples of active packaging are widget, oxygen scavenger, plain tinplate cans for white fruits and modified- atmosphere flexible packaging for meat. The functions of active packaging are to extend the shelf-life or to maintain or improve the condition of packaged foods. They contain deliberately incorporated components intended to release or absorb substances into or from the packaged food or from the environment surrounding the food. Active materials are allowed to cause changes in the composition or the organoleptic characteristics of the food on condition (Regulation on food contact materials, 1935/2004).

Intelligent packaging is a package which function switches on and off in response to change external and internal conditions. Intelligent materials are defined as materials that monitor the condition of packaged food or the environment surrounding the food and attached as labels, incorporated into, or printed onto a food packaging material offer enhanced possibilities to monitor product quality and give more detailed information throughout the supply chain (Han, Ho, and Rodrigues, 2005). Intelligent tags such as electronic labeling, designed with ink technology in a printed circuit and built-in battery radio-frequency identity tags, all placed outside the primary packaging, are being developed in order to increase the efficiency of the flow of information and to offer innovative communicative functions. Diagnostic indicators were first designed to provide information on the food storage conditions, such as temperature, time, oxygen or carbon dioxide content, and thus, indirectly,

information on food quality, as an interesting complement to end-use dates (D. Dainelli *et al.*, 2008).

For food packaging, the main problem of food packaging is quick spoilage because of ethylene gas. Ethylene (C_2H_4) acts as a plant hormone which accelerates respiration, leading to maturity and senescence, and ripening of many kinds of fruits. Furthermore, ethylene accumulation can cause yellowing of green vegetables and may be responsible for a number of specific post harvest disorders in fresh fruits and vegetables. Ethylene can also be removed by using a number of chemical processes. Many suppliers offer C_2H_4 -scavengers based on potassium permanganate ($KMnO_4$), which oxidizes ethylene to acetate and ethanol. In this process, color changes from purple to brown indicating the remaining C_2H_4 -scavenging capacity. Products based on $KMnO_4$ cannot be integrated into food-contact materials, but are only supplied in the form of sachets because $KMnO_4$ is toxic and has a purple color. Rengo Co. (Japan) developed 'Green Pack', a sachet of $KMnO_4$ embedded in silica. The silica adsorbs the ethylene and the permanganate oxidizes it to acetate and ethanol. The technology of C_2H_4 -scrubbing has also been transferred to household refrigerators. Systems containing a zeolite coated with $KMnO_4$ are now available and are meant to be used in consumer refrigerators. Other C_2H_4 -adsorbing technologies are based on inclusion of finely dispersed minerals such as zeolites, clays and Japanese soya into packaging films. Most of these packaging films, however, are opaque and not capable of adsorbing C_2H_4 sufficiently. Even though the incorporated minerals may adsorb ethylene, they also alter the permeability of the films: C_2H_4 and CO_2 diffuse much more rapidly and O_2 enters more readily than through pure PE. These effects can improve shelf-life and reduce headspace C_2H_4 -concentrations independently of any C_2H_4 -adsorption. In fact, any powdered material can be used to reach such effects. C_2H_4 -scavengers are not yet very successful, probably because of insufficient adsorbing capacity. A large proportion of the fresh fruits and vegetables harvested each year are lost due to fungal contamination and physiological damage. The C_2H_4 -adsorbing packaging concepts could possibly contribute to an increase in the export of fresh produce (L. Vermeiren, 1999).

According to the structure of porous clay structure (PCH) which has high surface area, it can adsorb gas such as oxygen and ethylene gas. The modification of

PCH would enhance the efficiency of PCH to eliminate ethylene gas from the atmosphere. When modified PCH and organically modified PCH blend with thermoplastic polymer, it can be applied as smart packaging films to prolong the shelf life of the fresh products.

From the contents above, one of the goals of this research is to modify the PCH and organically modified PCH derived from naturally-occurring clay minerals for utilizing as ethylene scavenger in food packaging. Subsequently, these synthesized mesoporous materials were blended with polypropylene and investigated the properties which correlated to their functions as ethylene scavenger of polypropylene-clay nanocomposites. Moreover, the nanocomposite materials will play their roles as ethylene indicating system in smart packaging as well.

This research proposal includes the literature reviews of related work, research objectives, methodology, results, discussions, and conclusion. The results were divided into 4 chapters; chapter 4 describes the various modified porous clays to evaluate the effective functions for active packaging and chapter 5 describes about the effect of the amount of thiol group that were incorporated into the modified porous clays to exhibit the conductive property. The chapter 6 is about silver loaded on the surface of modified PCH to enhance higher the conductivity and play the role in ethylene adsorption and the last chapter 7 focuses on the another application of PP in electronic part which investigated by dielectric property.

CHAPTER II

THEORETICAL BACKGROUND AND LITERATURES

2.1 Packaging Technology

Packaging is one of the main processes to preserve the quality of food products for transportation, storage, and end use. It slows quality decay and makes distribution and marketing more efficient. Packaging has four basic functions: protection, communication, convenience, and containment (Han, 2005). Packages protect products from the external environment; communicate with the customer through written texts, brand logo, and graphics; accommodate the lifestyle of the customer, for example saving time (ready-to-eat and heat-and-eat meals) or making the manipulation and handling of packaged food easier for the customer (examples of convenient features are easy opening, resealability, and microwavability), and act as containers for differently shaped and sized products, with the goal of optimizing logistic efficiency (Yam and Lee, 2012). Secure delivery and the preservation of packaged foods before consumption are the main goals throughout the food supply chain. However, loss of food quality attributes occurs during distribution and storage due to biological, chemical, and physical degradation (Han, 2013). Up-to-date, two new concepts have greatly contributed to achieving an advanced concept of packaging for safer and healthier food: the active packaging and intelligent packaging concepts.

2.1.1 Active Packaging

Active packaging is “the package that is intended to extend the shelf-life or to maintain or improve the condition of packaged food. They are designed to deliberately incorporate components that would release or absorb substances into or from the packaged food or the environment surrounding the food” (European Commission, 2004). To improve the functionality of food packages and give them additional functions, different active substances can be incorporated into the packaging material (Preeti *et al.*, 2011). Several active packaging systems have been widely reported, such as O₂ and ethylene scavengers, moisture regulators, CO₂ scavengers and emitters, antioxidant and antimicrobial controlled-release packages,

and devices to control the release or adsorption of flavors and odors (Ghaani *et al.*, 2016).

2.1.1.1 Oxygen Scavengers

High levels of oxygen in the package always accelerate quality deterioration of respiring fruits and lead to an increase in ethylene production. Excess level of oxygen causes the oxidative changes in vitamins, pigments, lipids, flavor compounds that favors the growth of aerobic microbes (Sanjeev and Ramesh, 2006). While controlling the oxygen concentration, it is beneficial in protecting the fresh fruits against the quality deterioration that is closely associated with oxygen, such as off-flavor formation, color change, nutritional value reduction, and safety losses. Also low level of oxygen helps in reducing the respiration and ethylene production that keeps the fruits fresh longer. Oxygen scavengers are active additives used in the packaging system to absorb residual oxygen by means of chemical reaction that remains after the package is sealed. Commonly used substances are iron powder and ascorbic acid.

2.1.1.2 Humidity Absorbers

Fruits produce water by transpiration. To maintain high quality of fresh fruits, it is important to control the atmospheric relative humidity during the storage. Excessive relative humidity inside the package promotes fungal and bacterial growth, while excessive water loss from packaged fruits leads to shrinkage and loss of quality and sensory properties (Baldwin *et al.*, 1999). Various moisture scavengers have been used to modify the package humidity including silica gel, natural clays (e.g., montmorillonite), calcium oxide, calcium chloride, and modified starch (Chakraverty, 2001). Silica gels can absorb up to 35% of their own weight in water that are very useful to maintain dry conditions within packages of dry foods, down to below 0.2 water activity while zeolites can absorb up to 24% (Brody *et al.*, 2001).

2.1.1.3 Ethylene Absorber

Ethylene (C₂H₄), the growth-stimulating hormone, is responsible for initiating fruit ripening especially in case of climacteric fruits. During the senescence stage, ethylene causes the increase in fruit respiration rate, textural and color changes in climacteric fruits more as compared to nonclimacteric fruits. Therefore, by controlling the concentration of the ethylene in the package extends the shelf

life of fruit product (Martínez-Romero *et al.*, 2007). There are many commercial materials to use as ethylene scavenger such as Potassium permanganate (KMnO₄), Palladium (Pd), light-activated titanium dioxide (TiO₂), and activated carbon (Martínez-Romero *et al.*, 2007; Scully and Horsham, 2007).

2.1.1.4 Carbon Dioxide Emitter

When there is high level of carbon dioxide in the headspace of packaged fruits, it retards the growth of aerobic microorganisms and thus reduces the respiration and senescence processes (Cao *et al.*, 2007). This technology uses the reaction of sodium bicarbonate and hydrating agents such as water with acidulates to produce carbon dioxide (Ozdemir and Floros, 2004). One application of this technology is developed by SARL Codimer (Paris, France) called Verifrais™ package.

2.1.1.5 Antimicrobial Active Packaging System

Surface microbial spoilage is the primary cause of shelf-life termination of fresh produce. The main reasons for microbial contamination are transportation, packaging, uncontrolled harvesting and processing operations (Erdogrul and Sener, 2005). Adding antimicrobial agents such as hydrogen peroxide, peroxyacetic acid, ozone, chlorinated water, and plant extracts into the washing water demonstrates effective antimicrobial activity but is not successful for the total elimination of the microbial spoilage on fruit surfaces (Garcia *et al.*, 1998a; Mehyar and Han, 2004). This sort of direct application of antimicrobial agents has a limited effectiveness because most of the antimicrobial agents interact quickly with food compounds and thereby reduce their effectiveness (Mehyar and Han, 2006). The antimicrobial agent in active films may either make chemical bond to the surface of the film (called immobilized films) or migrate to the food surface (Pap *et al.*, 2002).

2.1.2 Intelligent Packaging

Intelligent packaging also called as smart packaging is the packaging which can exist as a monitoring system to monitor some properties of the food. It is able to inform the manufacturer, retailer and consumer of the state of these properties (Renata, 2014). Intelligent packaging devices are capable of providing assurances of tamper evidence, product safety and quality. These are also being utilized in applications like authenticity of product, anti-theft and product traceability (Chakraverty,

2001). Once the package is tampered, the seal or the label may undergo a permanent color change. Then the intelligent packaging will serve as informer to consumer about such an event that occurred such as package tampering. Intelligent packaging devices include biosensors, time-temperature indicators, physical shock indicators, microbial growth indicators, and anti-theft, tamper proof, anti-counterfeiting technologies.

2.1.2.1 Time–Temperature Indicators (TTIs)

Temperature is definitely the most effectual factor for respiration, microbial, and chemical reactions that impact plant metabolic activity (Erturk and Picha, 2008). A skillful control of temperature can retard the deterioration process of fresh fruits. Generally, the respiration rate of plants increases twice for each increase of 10 °C. Time–temperature indicators or integrators (TTIs) are defined as simple and user friendly devices that are used to record and monitor overall influence of temperature on the quality of food product from the manufacturer point up to the consumer point (Giannakourou *et al.*, 2005). In addition, TTIs have also been used to assess the sterilization and pasteurization process (Tucker *et al.*, 2009; Khwaldia *et al.*, 2004; Tucker *et al.*, 2007). During transportation and distribution of frozen or chilled foods, TTIs are important for food quality and safety and are commonly used there. These are also used as freshness indicators for evaluating the shelf life of perishable products. Most TTIs are in the form of self-adhesive labels that can easily adhere on the product or package. For instance, Bionest, the largest Spanish organic strawberry producer, deployed active RFID tag that supplies information on the remaining shelf-life of strawberries.

2.1.2.2 Oxygen and Carbon Dioxide Indicators

Packaging of fresh fruit is a complicated process because it is capable of respiring even after harvesting and therefore may change its own atmosphere when present inside a package (De Jong *et al.*, 2005). Indicators are efficient of signaling whether there is a gas leakage in the package, or they may be assessed to check the low or high concentration or absence of oxygen and/or carbon dioxide.

In active packaging, there are many selective additives, depending on their applications. In this research, the researchers are interested in synthesizing ethylene scavenger for using in the packaging in order to absorb the ethylene gas and also pro-

long shelf-life of produce by retarding the ripening. In addition, Bentonite is used as the raw material in the process because it is from natural, cheap and abundant in Thailand.

2.2 Clay Minerals

Clay minerals, or phyllosilicate, consist of sheets of silica tetrahedral and alumina octahedral which are held together by only weak interatomic forces between the layers. Owing to their chemical composition and crystal structure, they are divided into four main groups which are illite, smectite, vermiculite and kaolite. Among these, the one that is found to be useful in the field of polymer composites is a group of expandable clay known as smectite clay.

Smectite clay is phyllosilicates or layer silicates having a layer lattice structure in which two-dimensional oxoanions are separated by hydrated cations (Kloprogge *et al.*, 1998). Montmorillonite (MMT), which is the main constituent of bentonites, is a mainly species of smectite clay. The structure of MMT is made of several stacked layers, with a layer thickness around 0.96 nm and a lateral dimension of 100-200 nm (Lertwimolnum and Vergnes, 2005). Its crystal lattice consists of a central octahedral sheet of alumina fused between two external silica tetrahedral sheets (in such a way that the oxygen from the octahedral sheet also belong to the silica tetrahedral), as shown in Fig. 2.1. These layers organize themselves in a parallel fashion to form stacks with a regular gap between them, called interlayer or gallery (Manias *et al.*, 2001).

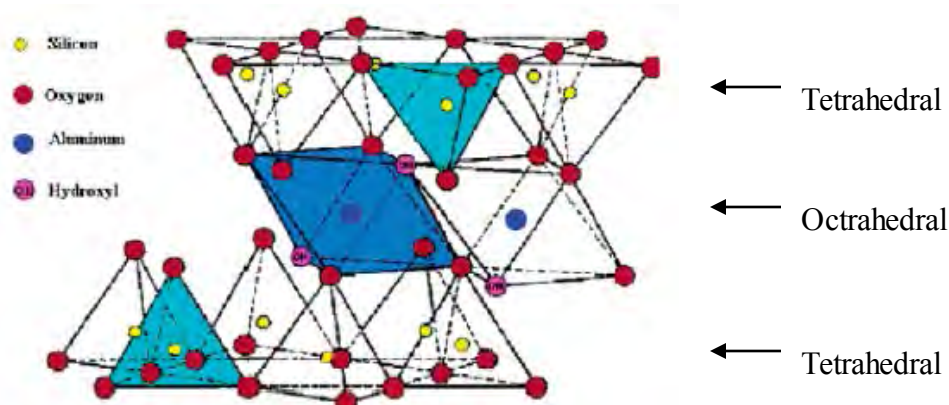


Figure 2.1 Structure of montmorillonite (Morlat *et al.*, 2004).

Isomorphous substitution within the layers (for example, Al^{3+} replaced by Mg^{2+} or Fe^{2+} , or Mg^{2+} replaced by Li^{1+}) generates negative charges that are counter-balanced by alkali and alkaline earth cations situated inside the galleries. This type of layered silicate is characterized by a moderate surface charge known as the cation exchange capacity (CEC), and generally expressed as mequiv/100 gm. This charge is not locally constant, but varies from layer to layer, and must be considered as an average value over the whole crystal (Manias *et al.*, 2001; Sinha Ray Okamoto., 2003).

In the present work, bentonite is a clay mineral used for the preparation of polymer-clay nanocomposites. Bentonite is a clay mineral derived from the alteration of volcanic ash, comprising predominantly of montmorillonite. Bentonite has unique water absorbing and swelling characteristics. These characteristics make bentonite a very desirable industrial mineral. The adsorption and ion exchange properties of clay minerals effect on many parameters. In addition to electrolyte concentration, pH of solution (H^+ ion) controls the swelling behavior of expandable clay minerals.

Altin *et al.* (1999) determined surface area, pore volume distribution, and porosity of montmorillonite after being exposed to aqueous solutions with various pH values. For the pH-adjusted montmorillonite, the results demonstrated that the micropore and mesopore surface areas were greatly increased by increasing pH due to increasing pH creates a more porous structure, since the interlayer repulsive force become dominant. Then pore volume distributions showed that lowering pH of montmorillonite reduced the mesoporous and microporous.

2.3 Porous Clay Heterostructure (PCH)

A variety of ordered mesoporous materials have been synthesized by surfactant-templated methods. Porous clay heterostructure (PCH) is a recent class of solid porous materials formed by the intercalation of surfactant within the intragalleries of clays. Various types of expandable clay could be employed such as hectorite, vermiculite, synthetic saponite and montmorillonite for the synthesized of these highly porous clays.

Helena *et al.* (2009) synthesized porous clay heterostructures (PCHs) via a surfactant-directed assembly of Si precursor (tetraethylorthosilicate – TEOS) and laponite clay. The self-assembly of PCH induced a break up of plate-like laponite clay. Formation of PCH structures led to an increase of specific surface area, total pore volume and average pore diameter. The porous silicate network in PCH obtained with the use of organoclay:TEOS ratio = 1:75 was much more resistant to treatment at elevated temperature than the one developed in the solid prepared with double amount of TEOS.

A synthetic saponite was synthesized into the porous clay heterostructure (PCH) and used as a catalytic support for the deposition metal (Cu, Fe) oxides. Transition metal oxides were introduced into the ammonia treated PCH support by the ion-exchange method. The treatment of the PCH with ammonia resulted in a slight used decrease in a surface area and porosity. Effectiveness of the ion-exchange method, used for the introduction of the transition metals, depended on the nature of the cations compensating the negative charge of the PCH surface. In the ammonium form of PCH (PCH-NH₃), a higher amount of copper was introduced than in the PCH support not modified with ammonia. Such an effect was not observed for the Fe-containing samples. The surface acidity of the samples was investigated by temperature desorption of the ammonia (NH₃-TPD). From the results, parent PCH was characterized by a rather low surface acidity due to the lowest ammonia sorption while the introduction of the transition metal generated more site for the NH₃ sorption because of higher NH₃ sorption (Chmielarz *et al.*, 2006).

Benjelloun *et al.* (2001) studied the cationic exchange capacities (CECs) of two porous clay heterostructures (PCHs), derived from natural montmorillonite

(PMH) and synthetic saponite (PSH). Three methods for the formation of NH_4^+ -exchanged PCH forms are describe and evaluated: (1) adsorption of ammonia under a gas flow on calcined and extracted PCHs in acidified methanol; (2) direct exchange in NH_4Cl solutions; (3) solvent extraction with $\text{NH}_4\text{Ac}/\text{EtOH}/\text{H}_2\text{O}$. The obtained ammonium containing materials are subsequently exchanged for K^+ cations in aqueous solution in order to determine the CEC of the PCH solids. Several extraction media were tested for their efficiency in extracting the hexadecyltrimethylammonium surfactant from the PCH precursor. The best results were obtained with methanol:water mixture with 9:1 vol%. The resulting extracted materials had a higher specific surface area and porosity and even a slightly narrower pore size distribution than the calcined ones with maxima of $997 \text{ m}^2/\text{g}$. and $0.76 \text{ cm}^3/\text{g}$ for montmorillonite PCH (PMH) and $1118 \text{ m}^2/\text{g}$ and $0.97 \text{ cm}^3/\text{g}$ for saponite PCH (PSH).

Polverejan *et al.* (2000) prepared porous clay heterostructures within the galleries of synthetic saponite clays with targeted layer charge densities in the range $x = 1.2-1.7 \text{ e}^-$ units per $\text{Q}^+_x [\text{Mg}_6](\text{Si}_{8-x}\text{Al}_x)\text{O}_{20}(\text{OH})_4$ unit cell. The CEC value increase in propotional to the aluminum content of the clays. All three saponites were used to assemble porous clay heterostructures that were denoted SAP1.2-, SAP1.5-, and SAP1.7-PCH, respectively. The removal of the intragallery mixture of neutral alkylamine and quaternary ammonium ion surfactant (Q^+) by calcination afforded PCH intercalates with basal spacing of $33-35 \text{ \AA}$. The BET specific surface areas progressively decreased with increasing aluminum loading from 921 to $797 \text{ m}^2 \text{ g}^{-1}$ and the framework pore volumes decreased from 0.44 to $0.37 \text{ cm}^3 \text{ g}^{-1}$. Moreover, these materials exhibited the framework pore sizes were in the supermicropore to small mesopore region $15-23 \text{ \AA}$ as can be seen in TEM image (Fig. 2.2). In 2000, they synthesized acid-functionalized porous clay heterostructure from synthetic saponite through postsynthesis grafting reactions using AlCl_3 and NaAlO_2 as alumination agents under acid and basic condition, respectively. The amount of tetrahedral aluminum incorporated into the saponite gallery structure is correlated with the concentration of aluminum in the grafting solution. However, some loss of gallery mesostructure occurred at higher aluminum loadings (e.g., $\text{Si}/\text{Al} = 5$) with sodium aluminate. Depending on the choice of aluminum reagent (AlCl_3 or NaAlO_2), the Al-

SAP/PCH derivatives exhibited basal spacing of 32-34.8 Å, BET surface areas of 623-906 m²/g, pore volumes of 0.32-0.45 cm³/g, and pore sizes in the large micropore to small mesopore range (14-25 Å).

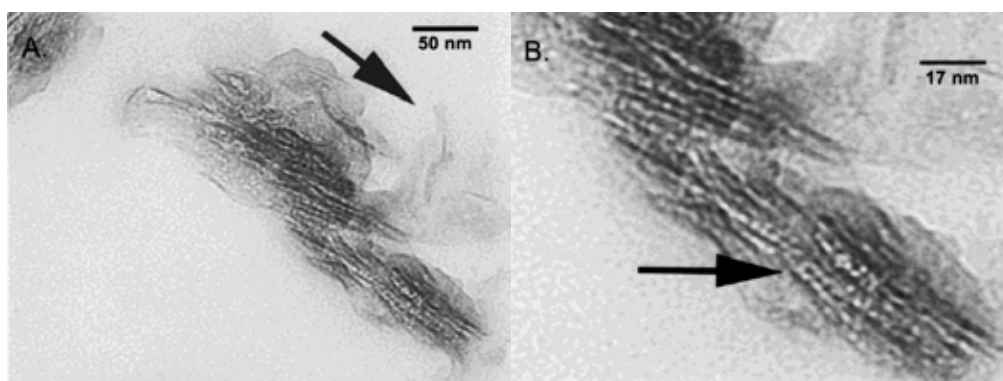


Figure 2.2 TEM images of saponite heterostructures (Polverejan *et al.*, 2000).

2.4 Hybrid Organic-Inorganic PCH

The interesting way to modify the physical and chemical properties of mesoporous silicates is the incorporation of organic components, either on the silicate surface or within the walls. Organic modification of the silicates permits precise control over the surface properties and pore size of the mesoporous materials for specific applications.

Surface modified mesoporous silica via covalent bonding of organic molecules can be achieved by using two general strategies which are post-synthesis modification (also called "grafting method") and co-condensation reaction (also called "one-pot synthesis") (Stein *et al.*, 2000; Sayari and Hamoudi, 2001).

1) *Post-synthesis modification*. In this approach, it refers to direct grafting of a mesoporous support by attachment of functional molecules to the surface of mesoporous, usually after surfactant removal either by calcination or solvent extraction. Furthermore, mesoporous silicates possess surface silanol (Si-OH) groups that can be present in high concentration and act as anchoring points for organic functionalization. Surface modification with organic groups is most commonly carried out by silylation with a suitable organosilane reagent.

2) *Co-condensation reaction*. In this method, it refers to co-condensation of tetraalkoxysilane and one or more organosilane precursors via sol-gel technique to produce organic functionalized mesoporous silicates. In this approach, the organic moieties are covalently linked via nonhydrolyzable Si-C bonds to a siloxane species, which hydrolyzes to form a silica network.

D. Nunes *et al.* (2008) prepared porous clay heterostructure (PCH) by chemical modification, by using a cationic surfactant, a neutral amine, and an equimolar mixture of bis(triethoxysilyl) benzene (BTEB) and tetraethyl orthosilicate (TEOS). The effect of different polymerization times of the silica sources and of the hydrocarbon chain length of the neutral amine was studied. The reaction time of 4 h led to a material with lower carbon content, higher specific surface area ($723 \text{ m}^2 \text{ g}^{-1}$). The structural modifications introduced in the final materials by the presence of organic aromatic moieties in the pillars were successful in terms of leading to a highly adsorbent species favoring VOCs over water, and thus tailored for the adsorption of hydrophobic VOCs.

Ishii *et al.* (2005) synthesized highly porous silica nanocomposites from a clay mineral by a new approach using a pillaring method combined with a selective leaching method. Preparation was conducted by applying an HCl/ethanol treatment after intercalation and condensation of tetraethoxysilane (TEOS) and/or methytriethoxysilane (MTS) into cetyltrimethylammonium (CTA) ion-exchanged vermiculite. The products are porous nanocomposites consisting of TEOS and/or MTS-derived polysiloxane and hydrated silica, resulting from the selective leaching process of the inorganic constituents and the extraction of CTA ions from CTA-exchanged vermiculite after the intercalation of TEOS and/or MTS. N_2 -adsorption isotherms revealed that the products had high porosity with $1205\text{--}715 \text{ m}^2 \text{ g}^{-1}$ of BET surface area, owing to the multiple pore formations in and between the silicate layers.

Wei *et al.* (2004) incorporated phenyl groups into the porous clay heterostructures within the galleries of montmorillonite via co-condensation reaction of tetraethoxysilane and phenylethoxysilane in the presence of surfactant templates (dodecylamine and cetyltrimethylammonium ion), as shown in Fig. 2.3. The surfactant templates were removed from the pores by solvent-extraction ($\text{C}_2\text{H}_5\text{OH}/\text{HCL}$). Depending on the loading of phenyl groups, the hybrid porous clay heterostructures had

BET surface areas of 390-771 m^2g^{-1} , pore volumes of 0.3-0.59 cm^3g^{-1} , and the framework pore sizes in the supermicropore to small mesopore range (1.2-2.6 nm).

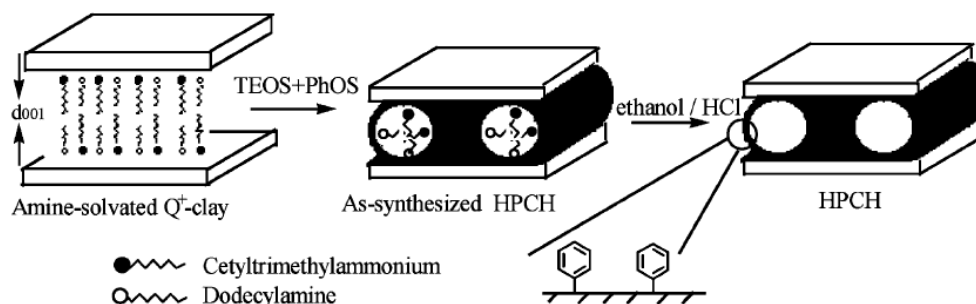


Figure 2.3 Schematic illustration of mechanism for formation of hybrid porous clay heterostructure (HPCH) through surfactant-directed assembly of organosilica in the galleries of clay (Wei *et al.*, 2004).

Nakatsuji *et al.* (2004) synthesized a microporous clay minerals with organic-inorganic pillared by using $\text{C}_2\text{H}_5\text{OH}/\text{HCL}$ extraction method after intercalation of tetraethoxysilane (TEOS) or TEOS/methyltriethoxysilane (MTS) into the cetyltrimethylammonium ion (CTA)-exchanged vermiculite. The BET surface areas increase to 500 m^2g^{-1} with an increase the HCl concentration to 0.4 moldm^{-3} . A water adsorption study showed that the product treated with a TEOS/MTS mixture had a hydrophobic surface as a result of the successful incorporation of methyl groups at the surface of the pillars.

2.5 Applications of Mesoporous Clay Heterostructures

The first major challenge for the adsorption field is to select the most promising types of sorbent from and extremely large readily available materials. The usage of natural mineral adsorbents is increasing because of their abundance and low price. Due to the ability to form mesoporous materials with closely reproducible pore size of the PCH and the ability to control surface properties of the hybrid organic-inorganic PCH, adsorption properties of these materials obtained from the intercala-

tion of clays attached to the interest. The most extensive work dealt with the adsorption of heavy metals.

Mercier and Pinnavaia (1998) demonstrated the first potential environmental application of a porous clay heterostructure. A heavy metal ion adsorbent that bind Hg^{2+} ions was prepared by grafting 3-mercaptopropyltrimethoxysilane to the intragallery framework walls of a porous fluorohectorite clay heterostructure (PCH) as illustrated in Fig. 2.4. The results revealed that the immobilized thiol groups (up to 67%) were accessible for Hg^{2+} trapping.

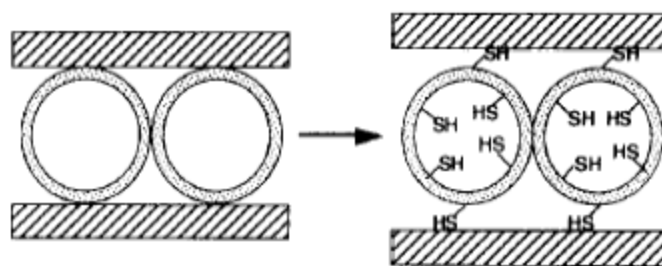


Figure 2.4 Grafting of mercaptopropylsilane groups to the inner and outer walls of mesostructural silica intercalated in smectite clay (Mercier and Pinnavaia, 1998).

Angela *et al.*, (2009) modified clay by acid treatment followed by immobilization of ligands containing thiol ($-\text{SH}$) groups by covalent grafting with surface and interlayer silanol groups. The modification was carried out under anhydrous conditions with (3-mercaptopropyl) trimethoxysilane. The functionalization process changed the hydrophilic nature of the clay mineral into hydrophobic. The result showed that the functionalized bentonite displayed good binding capacity for Ag^+ ions (1 mmol/g) compared to the ungrafted materials (0.1 mmol/g). Chemical modification by silane coupling agents may be a useful tool for the preparation of new adsorbents with high binding capacity and selectivity towards metal ions with applications for metal separation and pre-concentration purposes.

The adsorption properties of PCH have been considered in a number of studies, particularly when considering adsorption process as the recovery of volatile organic compounds or the enrichment of the more valuable fractions of natural or land fill gas. Pires *et al.* (2004) prepared porous materials from a natural smectite by

the gallery templated approach, using a quaternary ammonium cation (CTAB) and neutral amines with different chain length (octylamine and decylamine). The materials prepared in this work, after calcination at 650 °C, had A_{BET} values in the range of 600–700 m² g⁻¹ and micropore volumes near 0.3 cm³ g⁻¹. Furthermore, the samples presented pores with widths in the transition between micropores to mesopores. The possibility of using such materials as adsorbents of volatile organic compounds, due to their textural and hydrophobic characteristics, was studied by the adsorption of ethanol, methyl ethyl ketone, and water for comparison. The data from the adsorption showed that particularly one sample, decylamine, has interesting properties regarding the adsorption of VOCs.

Pinto *et al.* (2005, 2006) prepared composite adsorbent material supporting pillared clay in polyurethane foam for application in air filtering systems combining the ability of retaining noxious volatile organic compounds (VOC). The pillared clay was obtained from a natural montmorillonite by pillaring with aluminium oxide pillars. Adsorption isotherms of nitrogen and toluene were determined to evaluate the adsorption capacity of the adsorbent material before and after being support in the polyurethane. The result indicated that the pillared clay presented a decrease of about 97% in nitrogen adsorption capacity and also pronounced decrease in the toluene adsorption capacity. Moreover, they also studied the thermal regeneration of the composite material and the recycling of the adsorbents. The results showed a decrease in the adsorption capacity about 60% after regeneration process. However, the recycling of the adsorbent materials was possible since the adsorption capacity of the recycled material was in fact similar to the initial material before being support in the polyurethane.

Pires (2008) synthesized porous clays heterostructures from Wyoming clay and two types of silica sources, the tetraethoxysilane and the phenyltriethoxysilane. The use of the two silica sources allowed modifying the porosity and the surface chemistry of the adsorbents. The specific surface area, which reached up to 634 m²g⁻¹ for the sample where only tetraethoxysilane was used, decreased with the increase in the proportion of phenyltriethoxysilane. The amounts of adsorbed methane and ethane follow the trend of the porous volumes of each sample, but for carbon dioxide an inversion was found between the sample where only TEOS was used and the

sample prepared with the lowest proportion of PhOS. This observation could be explained by the specific interaction of the CO₂ molecule and it is a consequence of the change of the surface chemistry of the materials by the TEOS/PhOS ratio used in the synthesis. The selectivity for the separation of the binary mixtures: CO₂/CH₄, CO₂/C₂H₆ and C₂H₆/CH₄, was estimated using a methodology based on the determination of the equation of state for the Gibbs free energy of desorption of the solid adsorbent. The highest separation factors were obtained for the CO₂/CH₄ system when the samples synthesized with only TEOS or with the lowest amount of PhOS are used as adsorbents.

2.6 Polymer-Clay Nanocomposites

Polymer-clay nanocomposites exhibit outstanding properties that are synergistically derived from the organic and inorganic components. They exhibit superior mechanical properties, reduced gas permeability, improved solvent resistance and enhance ionic conductivity (Galgali *et al.*, 2001).

Several strategies have been considered to prepare polymer-clay nanocomposites. The preparative methods are divided into three main groups according to the starting materials and processing techniques (Sinha and Okamoto, 2003).

- *Intercalation of polymer or pre-polymer from solution*: This is based on a solvent system in which the polymer or pre-polymer is soluble and the silicate layers are swellable. The layered silicate is first swollen in a solvent, such as water, chloroform, or toluene. When the polymer and layered silicate solutions are mixed, the polymer chains intercalate and displace the solvent within the interlayer of the silicate. Upon solvent removal, the intercalated structure remains, resulting in polymer/layered silicate nanocomposite.

- *In situ intercalative polymerization method*: In this method, the layered silicate is swollen within the liquid monomer or a monomer solution so the polymer formation can occur between the intercalated sheets. Polymerization can be initiated either by heat or radiation, by the diffusion of a suitable initiator, or by an organic initiator or catalyst fixed through cation exchange inside the interlayer before the swelling step.

- *Melt intercalation method*: This method involves annealing, statically or under shear a mixture of the polymer and organically modified layered silicate above the softening point of the polymer. This method has great advantages over either in situ intercalative polymerization or polymer solution intercalation. First, this method is environmentally benign due to the absence of organic solvents. Second, it is compatible with current industrial process, such as extrusion and injection molding. The melt intercalation method allows the use of polymers which were previously not suitable for in situ polymerization or solution intercalation.

Depending on the strength of interfacial interactions between the polymer matrix and layered silicate (modified or not), three different types of PLS nanocomposites are thermodynamically achievable, as shown in Fig. 2.5 (Sinha and Okamoto, 2003).

- *Intercalated nanocomposites*: in intercalated nanocomposites, the insertion of a polymer matrix into the layered silicate structure occurs in a crystallographically regular fashion, regardless of the clay to polymer ratio. Intercalated nanocomposites are normally interlayer by a few molecular layers of polymer.

- *Flocculated nanocomposites*: conceptually this is same as intercalated nanocomposites. However, silicate layers are sometimes flocculated due to hydroxylated edge–edge interaction of the silicate layers.

- *Exfoliated nanocomposites*: in an exfoliated nanocomposite, the individual clay layers are separated in a continuous polymer matrix by an average distances that depends on clay loading. Usually, the clay content of an exfoliated nanocomposite is much lower than that of an intercalated nanocomposite.

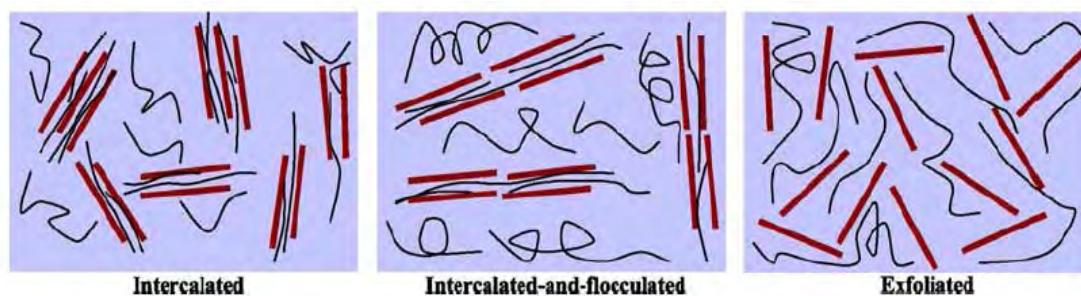


Figure 2.5 Schematically illustration of three different types of thermodynamically achievable polymer/layered silicate nanocomposites (Sinha and Okamoto, 2003).

Polypropylene (PP) is one of the most widely used plastics in large volume which is a fast growing thermoplastic that dominated the industrial applications due to it is relatively inexpensive, easily modified to meet a wide range of thermal and mechanical requirements and suitable for virtually all kinds of processing equipment. However, there are many disadvantages such as low toughness and low service temperature (Ding et al., 2005). Many research efforts focus on the preparation of polypropylene-clay nanocomposites. But PP does not include any polar groups in its backbone, it was thought that the homogeneous dispersion of the silicate layers in PP would not be realized. Hence, it is frequently necessary to use a compatibilizer such as maleic anhydride modified polypropylene (PP-g-MA). There are two important factors to achieve the exfoliation of the clay layer silicates: (1) the compatibilizer should be miscible with the polypropylene matrix, and (2) it should include a certain amount of polar functional groups in a molecule. Generally, the polypropylenes modified with maleic anhydride (MA) fulfill the two requirements and are frequently used as compatibilizer for polypropylene nanocomposites. However, they have mechanical properties lower than the native polypropylene, due to chain scission during grafting (Lertwimolnum and Vergnes, 2005).

Surlyn®/silicate hybrid materials were produced via diffusion-controlled polymer *in situ* sol-gel reactions for tetraethylorthosilicate (TEOS). The silicate uptake was highly dependent on the water affinity of the particular form of Surlyn®, that is, the acid or ionic form. Na⁺-neutralized Surlyn® demonstrated significantly higher swelling in water and a significantly higher uptake of silicate than the corresponding Zn²⁺ and un-neutralized Surlyn® versions. Evidently, the greater water ca-

capacity of the Na⁺ ionomer causes more rapid and complete hydrolysis and condensation reactions. The silicate phase consists of discrete, essentially round particles with diameters of tens of nanometers, a scale that is significantly smaller than the wavelength of visible light. This accounts for the fact that the composite films are optically transparent. Given the size of the *in situ* grown particles, these hybrid materials can be classified as nanocomposites (P. R. START., 2003).

The synthetic routes and materials properties of polypropylene/ montmorillonite nanocomposites are reviewed (Manias *et al.*, 2001). The nanocomposite formation is achieved in two ways: either by using functionalized polypropylenes and common organo-montmorillonites, or by using neat/unmodified polypropylene and a semi-fluorinated organic modification for the silicates. All the hybrids can be formed by solventless melt-intercalation or extrusion, and the resulting polymer/inorganic structures are characterized by a coexistence of intercalated and exfoliated montmorillonite layers. Small additions typically less than 6 wt% of these nanoscale inorganic fillers promote concurrently several of the polypropylene materials properties, including improved tensile characteristics, higher heat deflection temperature, retained optical clarity, high barrier properties, better scratch resistance, and increased flame retardance.

Alexandre and Dubois (2000) stated a study concern with the melt intercalation of PP chains modified with either maleic anhydride (PP-MA) or hydroxyl groups (PP-OH) in octadecylammonium-exchanged montmorillonite (CEC: 119 meq/100 g). When PP-MA (Mw: 30,000, acid value: 52 mg KOH/g) or PP-OH (Mw: 20,000, OH value: 54 mg KOH/g) was melt blended under shearing with a same given amount of modified montmorillonite at 200°C for 15 min, intercalated nanocomposites were recovered as demonstrated by the increase in the layer spacing from 21.7 Å for the initially organomodified montmorillonite to 38.2 and 44.0 Å for PP-MA and PP-OH based nanocomposites, respectively. Moreover, the results showed that intercalation increased when the PP-MA fraction was increased, going up to 72.2 Å for a PP-MA to clay ratio of 3:1.

2.7 Development in the Ethylene Scavenging System

The quality of food products may deteriorate biologically, chemically and/or physically during distribution and sale. Therefore, the packaging requirements for foodstuffs are more diverse and complex than those for other products. Active packaging is one of the innovative food packaging concepts that have been introduced as a response to the continuous changes in current consumer demands and market trends, can be defined as a type of packaging that changes the condition of the packaging to extend shelf-life or improve safety or sensory properties while maintaining the quality of food (Hong, 2002). It can be classified into active scavenging systems (absorbers) and active-releasing systems (emitter) (Kruijf *et al.*, 2002).

One of the most important active packaging concept as ethylene scavenging is a great interest. Ethylene (C_2H_4) has been recognized as a plant hormone controlling ripening and senescence in fruit and vegetable. If ethylene produced by fresh fruits accumulates in the packaging, it will speed up the respiration rates, reducing product storage life. Because of this, many packaging strategies for fresh fruits sensitive to ethylene seek to avoid ethylene accumulation inside the package, thereby limiting fruit senescence (Paz *et al.*, 2005). A lot of ethylene adsorbing substances are applied. Most of these are supplied as sachets or integrated into films.

There are diversified ethylene scavenging systems. Many supplier offer ethylene scavengers based on potassium permanganate, which oxidizing ethylene to acetate and ethanol. This substance is not integrated directly into food contact materials because of its toxicity. In addition, metal catalyst (e.g. palladium) on activates carbon can effectively remove ethylene. Other scavenging materials are based on inclusion of finely dispersed minerals such as zeolites and clays into packaging film. Unfortunately, these packaging films are not capable of adsorbing ethylene sufficiently, although the incorporated minerals may adsorb ethylene (Vermeiren *et al.*, 1999).

Kim *et al.*, (2005) studied binary adsorption of very low concentration ethylene and water vapor on mordenites (MORs), both in sodium type (NaMOR) and proton type (HMOR). In the binary adsorption, all MOR showed linear adsorption for ethylene in very low concentration range and the amount of ethylene decreased

as compared with the adsorption of single component. In case of the single component adsorption, the adsorption isotherm of ethylene on HMOR implied two kind of adsorption sites. The one, such as Brønsted acid site, has strong acidic property and strong interaction with ethylene. Conversely, the Si-O-Si and silanol group interact weakly with ethylene.

Ilkenhans *et al.*, (2008) observed a new palladium-promoted material with significant ethylene adsorption capacity. Materials were tested for ethylene scavenging ability in the presence of fruit. A banana was monitored by GC analysis for 24 h to measure changes in the gas composition in a 1-l vessel. After this time the ethylene level rose to $\sim 5 \mu\text{l l}^{-1}$. When the experiment was repeated with the Pd-based absorber, no ethylene was detected over 24 h (the minimum detection limit was $\sim 0.5 \mu\text{l l}^{-1}$ ethylene).

Kasinee *et al.*, (2008) synthesized PCH with methoxysilane (MTS) to obtain hybrid organic-inorganic PCH (HPCH) which then was blended with polypropylene to be evaluated as an ethylene scavenging film in active packaging application. The results showed that PCHs have surface areas of 501-668 m^2/g , an average pore diameter in the supermicropore to small mesopore range of 3.01-3.85 nm, and a pore volume of 0.43-0.64 cc/g , while HPCHs have a result of 469-582 m^2/g , 3.19-3.88 nm, and 0.33-0.49 cc/g , respectively. According to ethylene adsorption capacity and ethylene permeability test, HPCHs shows the enhancement of the hydrophobicity and plays an important role in ethylene adsorption. Both PCHs and HPCHs significantly effect on the ethylene barrier property of the nanocomposite films.

2.8 Capacitor

A capacitor is a device which stores electric charge. Capacitors vary in shape and size, but the basic configuration is two conductors carrying equal but opposite charges (Fig. 2.6). Capacitors have many important applications in electronics. Some examples include storing electric potential energy, delaying voltage changes when coupled with resistors, filtering out unwanted frequency signals, forming resonant circuits and making frequency-dependent and independent voltage dividers when combined with resistors. Some of these applications will be discussed in latter

chapters.

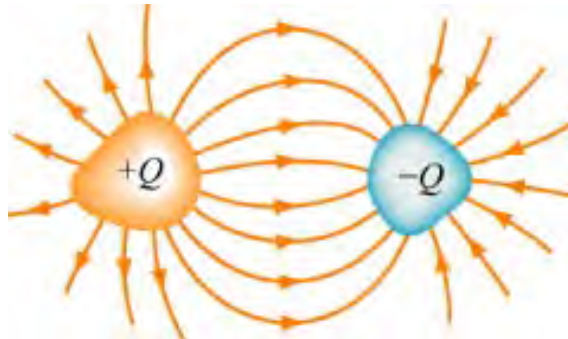


Figure 2.6 Basic configuration of a capacitor.

In the *uncharged* state, the charge on either one of the conductors in the capacitor is zero. During the charging process, a charge Q is moved from one conductor to the other one, giving one conductor a charge $+Q$, and the other one a charge $-Q$. A potential difference ΔV is created, with the positively charged conductor at a higher potential than the negatively charged conductor. Note that whether charged or uncharged, the net charge on the capacitor as a whole is zero.

The simplest example of a capacitor consists of two conducting plates of area A , which are parallel to each other, and separated by a distance d , as shown in Fig. 2.7.

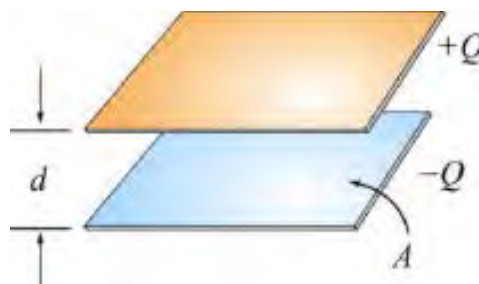


Figure 2.7 A parallel-plate capacitor.

Experiments show that the amount of charge Q stored in a capacitor is linearly proportional to ΔV , the electric potential difference between the plates.

$$Q = C|\Delta V| \quad (2.1)$$

Where C is a positive proportionality constant called *capacitance*. Physically, capacitance is a measure of the capacity of storing electric charge for a given potential difference ΔV . The SI unit of capacitance is the *farad* (F).

$$1 \text{ F} = 1 \text{ farad} = 1 \text{ coulombvoltage} = 1 \text{ C/V}$$

A typical capacitance is in the picofarad ($1 \text{ pF} = 10^{-12}\text{F}$) to millifarad range, ($1 \text{ mF} = 10^{-3}\text{F} = 1000 \text{ }\mu\text{F}$; $1 \text{ }\mu\text{F} = 10^{-6}\text{F}$). Figure 2.8 (a) shows the symbol which is used to represent capacitors in circuits. For a polarized fixed capacitor which has a definite polarity, Fig. 2.8 (b) is sometimes used.

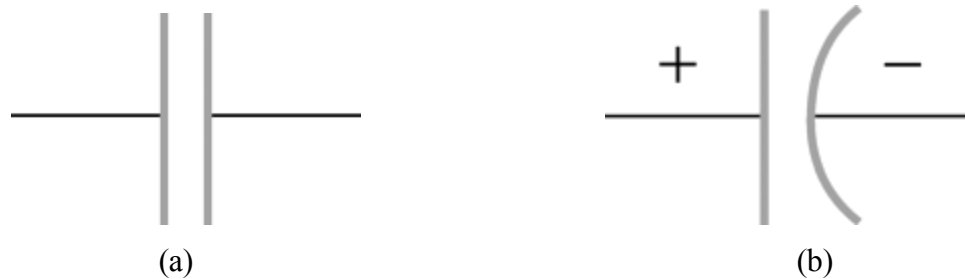


Figure 2.8 Capacitor symbols (a) in circuit and (b) polarized fixed.

In case of parallel-plate model, the simplest model capacitor, consists of two thin parallel conductive plates separated by a dielectric with permittivity ϵ (Fig. 2.9). This model may also be used to make qualitative predictions for other device geometries. The plates are considered to extend uniformly over an area A and a charge density $\pm\rho = \pm Q/A$ exists on their surface. Assuming that the length and width of the plates are much greater than their separation d , the electric field near the center of the device is uniform with the magnitude $E = \rho/\epsilon$. The voltage is defined as the line integral of the electric field between the plates.

$$V = \int_0^d E dz = \int_0^d \frac{\rho}{\epsilon} dz = \frac{\rho d}{\epsilon} = \frac{Qd}{\epsilon A} \quad (2.2)$$

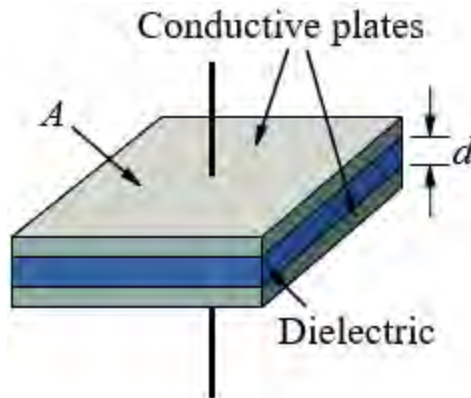


Figure 2.9 Two conducting plates separated by a dielectric material with area (A) and separation distance (d).

Solving this for $C = Q/V$ reveals that capacitance increases with area of the plates, and decreases as separation between plates increases.

$$C = \epsilon \frac{A}{d} \quad (2.3)$$

The capacitance is therefore greatest in devices made from materials with a high permittivity, large plate area, and small distance between plates.

In the present research work, ethylene adsorbing capacity of packaging films was enhanced by nanoclay filler which is synthesized to mesoporous structures and then also incorporated with organic moiety to improve organophilicity of this ethylene scavenger. Moreover, some part of this research work was relevance with conductivity test of the packaging films in order to evaluate the potential use of PCH and modified PCHs in ethylene indicating system.

CHAPTER III EXPERIMENTAL

3.1 Materials

Sodium bentonite (Na-BTN), with a cation exchange capacity (CEC) of 44.5 meq/100g of clay, was supplied by Thai Nippon Chemical Industry Co., LTD. (Thailand). Cetyl trimethyl ammonium bromide (CTAB), cetyltrimethyl ammonium chloride (CTAC) performing as the cationic surfactants, and chemical substances such as tetraethyl orthosilicate (TEOS), for use as a silica source, methyltriethoxysilane (MTS), (3-mercaptopropyl) trimethoxysilane (MPTMS), for modifying HPCH and MPPCH, Dodecylamine, Ascorbic acid, and Silver nitrate (AgNO_3), were purchased from Fluka, Acros, and Merck, respectively. Polypropylene (PP) (Moplen HP525N, MFI 11) and Surlyn® (PC 350, MFI 5) were provided by HMC Polymers Co., Ltd. (Thailand) and DuPont™.

3.2 Methodology

3.2.1 Synthesis of Porous Clay Heterostructures

Purified bentonite (BTN) was changed into a quaternary ammonium exchange form by ion exchange with CTAB and was stirred at 50 °C. After that, the sample was filtered, washed with a mixture of methanol and water and then air-dried overnight. The obtained organoclay was stirred in dodecylamine at 50 °C for 30min before adding the TEOS at a molar ratio of organoclay:dodecylamine:TEOS of 1:20:150. The resulting suspension was stirred at 37 °C for 4h. The suspension was filtered and air-dried overnight to form the as-synthesized PCH. Then the surfactant was removed from the as-synthesized PCH by solvent extraction using a mixture of methanol and HCl solution. Typically, 1g of the as-synthesized PCH was added to 5ml of HCl and 45ml of methanol and was refluxed for 2 h.

3.2.2 Synthesis of hybrid organic–inorganic porous clay heterostructures with functional groups

According to the previous PCH forming step, a mixture of TEOS and MTS in a mole fraction of 0.5:0.5 was added and stirred for a further 12 h at 35 °C. For the conductive functional group, the mixture of TEOS and MPTMS, in a mole fraction of 1:1, was added under N₂ atmosphere and stirred for a further 24h at room temperature. The obtained modified PCHs were collected by filtration and air-dried overnight at room temperature. Then the surfactant was removed from the as-synthesized modified PCH by solvent extraction. The modified PCHs by MTS and MPTMS are named HPCH and MPPCH, respectively.

3.2.3 Synthesis of Hybrid Organic-Inorganic PCHs with Conductive Functional Groups (MPPCHs)

According to the previous PCH forming step, the mixture of TEOS and MPTMS was added under N₂ atmosphere and stirred for a further 24 h at room temperature with various molar ratios of MPTMS: TEOS of 1:1, 2:1, and 4:1. The obtained modified PCHs were collected by filtration and air-dried overnight at room temperature. Then the surfactant was removed by solvent extraction using a mixture of methanol and HCl solution. Typically, 1 g of the modified PCHs was added into the 5 ml of HCl and 45 ml of methanol, and was refluxed for 2 h. The modified PCHs were abbreviated as MPPCH (1:1), MPPCH (2:1), and MPPCH (4:1), respectively.

3.2.4 Synthesis of Hybrid Organic-Inorganic PCHs by Silver Loading

Next, PCH was suspended in the mixture of AgNO₃ and ethanol with various contents of silver in 1 wt%, 5 wt%, 10 wt%, 20 wt%, and 30 wt% to PCHs at 30 °C. After 1 hour, the 0.1 M ascorbic acid was dropped into the suspension to reduce Ag⁺ to Ag⁰, designated as Ag-PCH. The Ag-PCH was collected by filtration and air-dried overnight

3.2.5 Preparation of Polypropylene/clay Nanocomposite Film

The 1, 3, and 5 wt% modified PCHs, 2 wt% surlyn[®], and PP were prepared by using twin-screw extruder (LabTech type LHFS1-271822 co-rotating;

non-intermeshing twin screw extruder) with an L/D ratio of 40 and a screw diameter of 20 mm. The operation temperature was performed at 160, 165, 170, 175, 180, 185, 190, 200, 210 and 215 °C from hopper to die respectively and the screw speed was 30 rpm.

3.2.6 Fabrication of Nanocomposite Films

The nanocomposite films were prepared by using blown film extrusion machine. The nanocomposite pellets were dried in an oven prior to blowing. The following extrusion conditions were employed: the rotation speed of the screw was around 50 rpm and the blowing ratio was 1.52. The barrel and mold temperature were 210 °C. The thickness of the films was controlled to about 40 μm .

3.3 Characterization

3.3.1 X-Ray Fluorescence Spectrometry

The elemental analysis of the pristine clay and the modified PCHs was carried out by using X-ray fluorescence (Axios PW4400, SciSpec Co., Ltd). The excitation source was an X-ray tube with thin silver as the primary filter, operating at a tube voltage of 35 kV.

3.3.2 X-Ray Diffractometry (XRD)

An X-ray diffractometer (XRD) was used to obtain the d -value of the bentonite and the organoclay to investigate the crystal structure of materials. The X-Ray diffraction patterns were measured on a Rigaku Model Rigaku Model Smart Lab Guidance (Rigaku, Japan) with Ni-filtered $\text{CuK}\alpha$ radiation at 40 kV and 30 mA. For WAXS mode, the powder samples were observed on the 2θ range of 2 to 10 degrees with a scan speed of 2 degrees/min and a scan step 0.01 degree. SAXS mode was operated at 45kV, 200mA, and on the 2θ range of 0.1 to 8 degrees with a scan speed of 0.5 degrees/min and a scan step 0.02 degrees.

3.3.3 Surface Area Analysis (SAA)

The N₂ adsorption desorption–isotherms were obtained at -196 °C on a Sorptomatic analyzer. The samples were degassed at 150 °C for 15 h in a vacuum furnace before analysis. Specific surface areas were calculated using the BET equation. The pore size distributions were constructed based on The Barrett, Joyner, and Halenda (BJH) method using the adsorption branch of the nitrogen isotherm.

3.3.4 Fourier Transform Infrared Spectroscopy (FT-IR)

The FT-IR spectra of bentonite, organoclays, and modified MPPCHs were obtained by using a Nicolet Nexus 670 FT-IR spectrometer (Becthai Co.Ltd, Bangkok, Thailand) in the frequency range of 4000-400 cm⁻¹ with 32 scans/min at a resolution of 2 cm⁻¹. The KBr pellet technique was used in the preparation of the powder samples. The incorporation of the organic group into the silicate network was investigated by using FT-IR.

3.3.5 Scanning Electron Microscopy (SEM)

Scanning electron microscopy was performed with Hitachi S-4800 Model to observe the surface morphology of all modified PCHs at 5 kV. The samples were sputtered with a thin layer of platinum for 180 seconds prior to the observation.

3.3.6 Transmission electron microscopy

JEOL Ltd, Tokyo, Japan has been supplied for JEM-2100 electron microscope with an accelerating voltage of 160kV to observe the structure of the pores and the dispersion of PCH in the polymer matrix of the nanocomposites. The TEM samples were prepared by suspension on 300 mesh copper grids.

3.3.7 Optical microscopy

The OM images were captured by Leica optical microscopy model DM RXP using the magnification of 20 times for objective lens and 10 times for the camera. The observation was done on surface of PP/modified PCHs nanocomposite films.

3.3.8 X-ray photoelectron spectroscopy (XPS)

Both qualitative and quantitative analysis of all specimens were examined by XPS (Kratos axis ultra DLD model) with a monochromatic x-ray source (Al K_{α} anode). The base pressure during experiments was 3×10^{-9} Torr and analyzed area was $700 \times 300 \mu\text{m}^2$. Pass energy 160 eV was used for wide scan in order to get percentage of atomic concentration of Si2p, C1s, O1s, Ag3d compositions. Moreover, for quantitative analysis, narrow scan with pass energy 40 eV was used for Si2p, C1s, O1s and Ag3d spectra. Then all spectra were referenced to the Ag3d_(3/2,5/2) peak at 368 eV and 374 eV, respectively.

3.3.9 Differential scanning calorimetry (DSC)

Differential Scanning Calorimeter (METTLER, DSC822) was used to measure the crystallization and melting behavior of the PP/modified PCHs nanocomposites. The samples were heated and cooled from 30-200 °C, using a heating/cooling rate of 10 °C min⁻¹ in a nitrogen.

3.3.10 Thermogravimetric Analysis (TGA)

TGA analysis was performed with a TA Instruments TGA 2950 over a temperature range 30-700 °C at a heating rate of 10 °C/min under N₂ atmosphere of 200 ml/min. The decomposition temperature and weight loss were measured.

3.3.11 Tensile Properties

Tensile test of PP/modified porous clay nanocomposite films were carried out by a LLOYD Universal Testing Machine model 4206 by ASTM D 638. A gage length of 50 mm was employed with a crosshead speed of 50 mm/min and preload 0.01 N.

3.3.12 Gas Chromatography for Ethylene Adsorption

A gas chromatograph with a flame ionization detector was utilized to examine the ethylene adsorption capacity of the modified PCHs. Ethylene adsorption was measured by placing each product in a chamber (0.6 l), then sealing it with a

screw-cap lid. Ethylene was injected into a jar to give a specific concentration of 5000 ppm. Ethylene concentration in the chamber was measured periodically, about once per hour by injecting into the gas chromatography (GC). The ethylene adsorption was calculated by taking the difference between the amount of ethylene added and the amount remaining in the headspace.

3.3.13 Conductivity Measurement

The electrical conductivity of the mesoporous materials were observed using Impedance test by LCR meter (Agilent E4980A) as the function between Z (ohm) and θ (radian). The clay pellets were covered with platinum and placed between the 2 probes and the tests were run at 20 Volts with varying frequency from 20 Hz to 1 MHz. Finally, the results were calculated by Nyquist's plot to obtain the semi circle and find the resistivity from the intersect of x axis at the high frequency.

3.3.14 Keithley Electrometer for Conductivity Measurement

The electrical conductivity of the nanocomposite films were observed using Keithley Electrometer with 6517B Hi-R test. The film was placed between the 2 probes in the vacuum box. The tests were run by varying the voltages in 1, 5, 10, 20 and 100 Volts and then calculated the electrical conductivity from plotting between the current and the applied voltage. The volume resistivity was calculated by using the Equation (3.1).

$$\text{Volume resistivity} = \frac{22.9}{\text{thickness, cm}} \times \frac{V}{I} (\text{ohm} \cdot \text{cm}) \quad (3.1)$$

3.3.15 Dielectric Property

The dielectric properties of the samples were measured at various frequencies and temperatures. The dielectric properties of the samples with a function of temperature (173 K to 373K) were measured by a LCR meter (HP 4284A) under He atmosphere with the heating and cooling rate of 3 K/min and also collected as a function in diameter. The tests were investigated the capacitance (C) of the samples.

Then, the dielectric constant (k) was calculated from the capacitance by using Equation (3.2).

$$C = \varepsilon_0 k \frac{A}{d} \quad (3.2)$$

Where C is capacitance of the composite (F), ε_0 is dielectric constant of the free space (8.85×10^{-12} F/m), A is electrode area (m^2), and d is distance between electrodes, i.e. thickness of the samples (m).

3.3.16 Thermal Expansion Property

Thermal expansion of the samples was carried out by using a dilatometer. The measurement was performed at the various temperature from 373 K to 173 K under the N_2 atmosphere. The samples were cut into the bar shape (3.00 mm \times 7.00 mm \times 3.00 mm) before testing. The parameters were calculated by using Equation (3.3).

$$\frac{\Delta L}{L_0} = \alpha \Delta T \quad (3.3)$$

Where ΔL is change in length (m), α is linear expansion coefficient (K^{-1}), ΔT is change in temperature (K).

3.3.17 Breakdown Strength Measurement

The breakdown strength of the nanocomposite films was observed by using 175Y8S electric puncture tester. The nanocomposite films were placed between the metal plates (sphere shape). All measurements were performed under the air atmosphere.

CHAPTER IV

MODIFIED POROUS CLAY HETEROSTRUCTURES BY ORGANIC– INORGANIC HYBRIDS FOR NANOCOMPOSITE ETHYLENE SCAVENGING/SENSOR PACKAGING FILM

4.1 Abstract

Porous clay heterostructures (PCHs) were prepared by the surfactant-directed assembly of mesostructured silica within the two-dimensional galleries of clays. PCH is an interesting material for use as an entrapping system (for example, as an ethylene scavenger) because of its high surface area with uniform and specific pore sizes. In the present work, the PCH was synthesized within the galleries of bentonite by the polymerization of tetraethoxysilane (TEOS) in the presence of surfactant micelles. In addition, mesoporous clay was modified by an organic–inorganic hybrid material through the co-condensation reaction of TEOS with the functional groups (methyl and thiol) designated as hybrid organic–inorganic PCH (HPCH) and mercaptopropyl functionalized PCH (MPPCH), respectively. The synthesized PCH, HPCH and MPPCH were blended with polypropylene (PP) to produce PCH/PP, HPCH/PP and MPPCH/PP for ethylene scavenging blown films. All nanocomposite films were evaluated as ethylene sensors by measuring the conductivity changes by the attachment time with the ethylene gas. According to the surface characterization, the specific surface areas of modified PCHs increased from 31 to about 500 m²/g. From the ethylene adsorption results, the PCH, HPCH and MPPCH show higher efficiency in adsorbing ethylene gas than those of bentonite because of the non-polar property of the modified functional groups. Subsequently, the electrical conductivity of the nanocomposite films decreased when they react with the longer attachment time to the ethylene gas, and the largest conductivity drop resulted from the MPPCH/PP nanocomposite films.

KEY WORDS: porous clay heterostructure (PCH); organic–inorganic hybrid; ethylene scavenger; sensor packaging

4.2 INTRODUCTION

Prolonging the shelf life of products requires packages that can preserve the freshness as long as they can before serving to consumers. This is the reason why the packaging industry would carry out research and develop these packages: active packaging and smart packaging. Active packaging is a package that can change the condition of the package to extend the shelf life of food products such as ethylene scavenger and oxygen scavenger. Smart packaging is the package that can indicate the shelf life and the freshness of food products during transportation and storage. It consists of a sensor or a component that can monitor and provide the information of the package; for example, when vegetables and fruits begin to ripen, the color of the package is changed for indicating the deteriorated conditions in the package. These packages are useful for sellers and consumers to consider the quality of the products.^{1,2} Because most of the products get spoiled very easily before reaching the consumers, our research group has introduced new filler that has been added into the packaging to prolong shelf life and monitor the deteriorated condition of the products.

Recently, one of the technologies in developing active and smart packaging is nanocomposite films containing mesoporous material to improve the properties of the films. The usual way to use mesoporous materials is the adsorption field, i.e. as ethylene scavengers and heavy metal adsorbents.³ Clay is one of the most popular starting materials for preparing mesoporous material. Porous clay heterostructure (PCH) is a well-known solid porous material derived from the intercalation of a surfactant within the galleries of the clays. Moreover, PCH can be modified by functional groups to be hybrid organic-inorganic PCH (HPCH) for use in many applications.⁴⁻⁷

The best way to modify the physical and chemical properties of mesoporous silicates is to incorporate organic components on the silicate surface. There are two methods of incorporating the organic compounds on the silicate surface post-synthesis: modification (grafting method) and co-condensation reaction (one-pot synthesis). Organic modification of the silicates can provide and control over the surface properties and pore size of the mesoporous materials and will improve the affinity of the organic compound for use in specific applications.⁸⁻¹⁰

To synthesize PCH, clay is expanded when the cations in the galleries of the clay are exchanged with a cationic surfactant, such as cetyltrimethylammonium bromide (CTAB), to allow an easier path to the galleries of clay. Then the clay galleries are further expanded by a neutral amine (dodecylamine). Next, a silica source such as tetraethyl orthosilicate (TEOS) partially replaces the neutral amine, and the reactions between the surfactant and the silica source exhibit micellar assemblies in the galleries of the clay.¹¹⁻¹⁶ Modification of the polymerization source allows for the control of the acidity of the intragalleries of the clay, which can also be tuned by the reaction with the reactive silanol group on the surface.^{14,17}

Recently, 3-mercaptopropyl triethoxysilane (MPTMS) was used to modify PCH for use in many applications such as heavy metal removal and proton exchange membrane. For heavy metal removal, heavy metals can be removed from waste water by binding with the thiol groups of the MPTMS, and then they are eluted by a solvent.¹⁸ From this application, small hydrocarbon molecules are bonded and captured in the pores by the thiol groups on the surface of clay, and then they are removed out from the system. Marshall *et al.*, (2007) used MPTMS to modify a new proton exchange membrane. Silica source or clay was functionalized with MPTMS to bind the thiol groups (—SH) on the surface of clay and then oxidized with H_2O_2 leading to sulfonic group ($\text{—SO}_3\text{H}$). The porous clay heterostructure was added into the Nafion membrane to improve proton exchange membrane in fuel cell system working at elevated temperatures.¹⁹

For packaging application, modified PCHs were blended with polypropylene (PP) to produce nanocomposites, and Surlyn® (DuPont) was used as a compatibilizer. The addition of Surlyn® resulted in a progressive enhancement in both moduli and complex viscosity, which could be attributed to the effect induced by the improved of clay dispersion.²⁰ In 1998, Wang et al. added zeolite into low-density polyethylene (LDPE) to perform the active packaging. The zeolite-filled polymer film showed a good ethylene adsorption.²¹ Next, the active packaging was developed to provide many applications such as ethylene scavenger, oxygen scavenger and carbon dioxide scavenger by adding some scavengers like O_2 absorber, KMnO_4 and CaCO_3 .¹ Recently, there were many attempts to develop the active packaging to be available for many applications. For example, microporous earthenware sheet was used as a choice to

combine with plastic box for maintaining the food product instead of only plastic sheet. It was able to provide a broader control of modified atmosphere packaging because of its unique permeability and also attain an optimal condition of the produce. In addition, CaCO_3 was added into PP to improve many properties of PP such as thermal and mechanical properties. CaCO_3 /PP film also decreased gas permeability of oxygen and carbon dioxide and showed the efficiency of CaCO_3 effect on the antimicroorganism growth.^{22,23}

The objective of adding the functional group on the surface of clay is to improve the ability in ethylene adsorption and electrical conductivity sensing during adsorbing the ethylene gas. The PCH was modified by methyltriethoxysilane (MTS) to have the attached methyl ($-\text{CH}_3$) group for increasing ethylene adsorption with non-polar property on the surface of clay that can be used as active filler in ethylene scavenger packaging. Furthermore, thiol group ($-\text{SH}$) was functionalized on the surface of clay to be an ethylene sensor. By entrapping the ethylene gas on the surface of the PCH, free electron densities on the methyl and thiol groups are reduced, and the electrical conductivity of the functionalized PCHs is expected to decrease. This changing mechanism can be applied to fabricate an ethylene sensor packaging film.

4.3 EXPERIMENTAL PARTS

4.3.1 Raw Materials

Pristine sodium bentonite, with a cation exchange capacity (CEC) of 44.5meq/100g, was kindly supplied by Thai Nippon Co., Ltd. (Thailand). CTAB, performing as the cationic surfactant, and chemical substances such as MTS and MPTMS were purchased from Fluka and Acros by S.M. Chemical Supplies Co., Ltd. (Thailand), respectively. PP (Moplen HP525N, MFI 11) was provided by HMC Polymers Co., Ltd. (Thailand).

4.3.2 Synthesis of Porous Clay Heterostructures

Purified bentonite (BTN) was changed into a quaternary ammonium exchange form by ion exchange with CTAB and was stirred at 50°C. After that, the sample was filtered, washed with a mixture of methanol and water and then air-dried

overnight. The obtained organoclay was stirred in dodecylamine at 50°C for 30 min before adding the TEOS at a molar ratio of organoclay:dodecylamine:TEOS of 1:20:150. The resulting suspension was stirred at 37°C for 4 h. The suspension was filtered and air-dried overnight to form the as-synthesized PCH. Then the surfactant was removed from the as-synthesized PCH by solvent extraction using a mixture of methanol and HCl solution. Typically, 1 g of the as-synthesized PCH was added to 5 ml of HCl and 45 ml of methanol and was refluxed for 2 h.

4.3.3 Synthesis of Hybrid Organic–Inorganic Porous Clay Heterostructures with Functional Groups

According to the previous PCH forming step, a mixture of TEOS and MTS in a mole fraction of 0.5:0.5 was added and stirred for a further 12 h at 35°C. For the conductive functional group, the mixture of TEOS and MPTMS, in a mole fraction of 1:1, was added under N₂ atmosphere and stirred for a further 24 h at room temperature. The obtained modified PCHs were collected by filtration and air-dried overnight at room temperature. Then the surfactant was removed from the as-synthesized modified PCH by solvent extraction. The modified PCHs by MTS and MPTMS are named HPCH and MPPCH, respectively.

4.3.4 Preparation of Nanocomposites

A 1 wt.% PCH, HPCH and MPPCH, 2 wt.% Surlyn® ionomer and PP were melt blended in a Collin model T-20 co-rotating twin-screw extruder with L/D=30 and D=25 mm; the processing conditions were as follows: temperature (°C) 80, 160, 180, 195, 205 and 215 from hopper to die, respectively, and the screw rotation was 50 rpm. Each composition was premixed in a tumble mixer before being introduced into the twin-screw extruder to be well mixed and extruded through a single strand die and then solidified with cold water and pelletized. The obtained pellet was dried in an oven.

4.3.5 Fabrication of nanocomposite films

The nanocomposite films were prepared by using blown film extrusion machine. The nanocomposite pellets were dried in an oven prior to blowing. The

following extrusion conditions were employed: the rotation speed of the screw was around 50 rpm, and the blowing ratio was 1.52. The barrel and mold temperature were 210 °C. The thickness of the films was controlled to about 40 µm.

4.3.6 Characterization

4.3.6.1 *X-ray Fluorescence Spectrometry*

Oxford Instruments, Tubney Woods Abingdon, Oxfordshire, UK has been supplied for X-ray fluorescence model 'ED2000' to analyze the elemental composition of pristine clay. The excitation source was an X-ray tube with thin silver as the primary filter, operating at a tube voltage of 35kV.

4.3.6.2 *X-ray Diffractometry*

An X-ray diffractometer (XRD) was used to obtain the d-value of the BTN, and the organoclay to investigate the crystal structure of materials. Rigaku, Woodlands, TX, USA has been supplied for Dmax 2002 diffractometer with Ni-filtered Cu K α radiation at 40kV and 30mA to observe the X-ray diffraction patterns. The powder samples were observed on the 2 θ range of 2–10° with a scan speed of 2°/min and a scan step 0.01°.

4.3.6.3 *Surface Area Analysis*

The N₂ adsorption–desorption isotherms were obtained at –196°C on a Sorptomatic analyzer. The samples were degassed at 150 °C for 15 h in a vacuum furnace prior to analysis. Surface areas were calculated using the Brunauer–Emmett–Teller (BET) equation. The pore size distributions were constructed based on the Barrett–Joyner–Halenda (BJH) method using the adsorption branch of the nitrogen isotherm.

4.3.6.4 *Fourier Transform Infrared Spectroscopy*

Becthai Co.Ltd, Bangkok, Thailand has been supplied for Nicolet Nexus 670 FT-IR to obtain the spectra of organoclay, PCHs, and HPCHs in the frequency range of 4000-400/cm with 32 scans/min at a resolution of 2/cm. The KBr pellet technique was used in the preparation of the powder samples. The incorporation of the organic group into the silicate network was investigated by using FT-IR.

4.3.6.5 Scanning Electron Microscopy

JEOL Ltd, Tokyo, Japan has been supplied for JSM-5410 LV model to observe the surface morphology of the PCH. The specimens were coated with gold under vacuum before observation to make them electrically conductive.

4.3.6.6 Transmission Electron Microscopy

JEOL Ltd, Tokyo, Japan has been supplied for JEM-2100 electron microscope with an accelerating voltage of 160 kV to observe the structure of the pores and the dispersion of PCH in the polymer matrix of the nanocomposites. The TEM samples were prepared by embedding the powder in resin and sectioning with an ultramicrotome. The thin sections were supported on 300 mesh copper grids.

4.3.6.7 Gas Chromatography For Ethylene Adsorption

A gas chromatograph with a flame ionization detector was utilized to examine the ethylene adsorption capacity of the porous clays. Ethylene adsorption was measured by placing each product in a jar (0.6l), then sealing it with a screw-cap lid. Ethylene was injected into a jar to give a specific concentration of 500 ppm. Ethylene concentration in the jar was measured periodically, about once per hour. The ethylene adsorption was calculated by taking the difference between the amount of ethylene added and the amount remaining in the headspace.

4.3.6.8 Keithley Electrometer For Conductivity Measurement

Keithley Instruments, Inc., Cleveland, OH, USA has been supplied for Keithley electrometer with 6517 Hi-R test for investigate the electrical conductivity of the nanocomposite films. The film was placed in the chamber, and then ethylene gas was injected into a jar to give a specific concentration of 500 ppm the same as in the ethylene adsorption part. The conductivity of the films was measured periodically, about once per hour by taking the film from the chamber and then placed between the two probes in the vacuum box. The tests were run by varying the voltages in 1, 5, 10, 20 and 100V and then by calculating the electrical conductivity from plotting between the current and the applied voltage.

4.4 Results and Discussions

4.4.1 Porous Clay Heterostructure Synthesis And Characterization

Intragalleries of clay. Bentonite, with a CEC of 44.5mmol/100g clay, was stirred with CTAB to prepare the organoclay. The corresponding XRD pattern showed the presence of the (001) reflection peak. As seen from Figure 1, the basal spacing of BTN was 1.16nm (Figure 1a). After the BTN was treated with CTAB, new peaks were observed at a lower angle (Figure 1b) indicating the increasing distance between the clay layers. The d- spacing of the organoclay was 3.87nm.

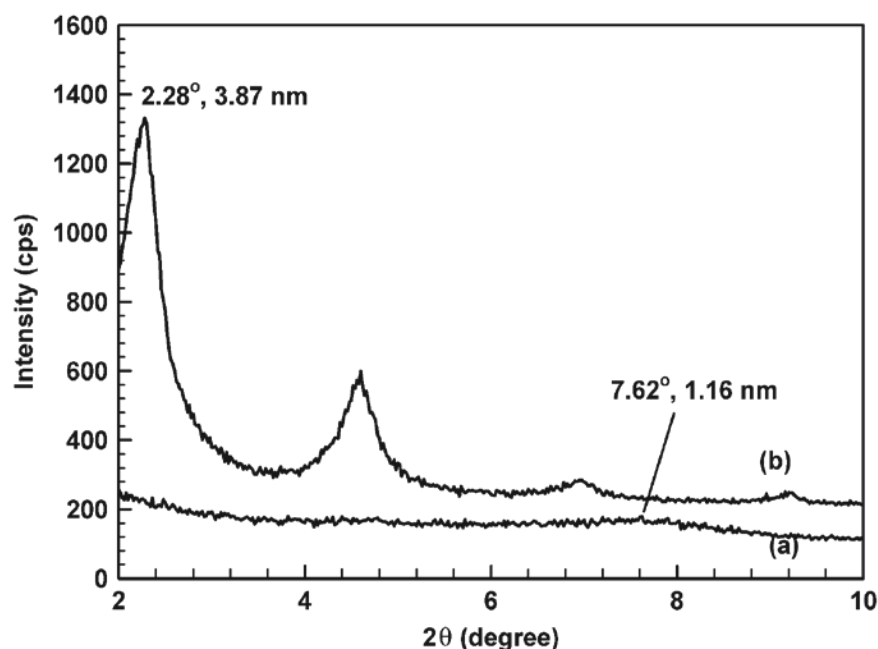


Figure 1 X-ray diffractometer patterns of (a) BTN and (b) organoclay.

4.4.2 Pore characterization of porous clay heterostructures, hybrid organic–inorganic porous clay heterostructures and mercaptopropyl functionalized PCHs

After intercalated by the surfactant, the organoclay was modified by co-condensation reaction of neutral amine and silica sources to polymerize around surfactant micelles. And then surfactant micelles were removed by solvent extraction, resulting in the formation of porous structures.

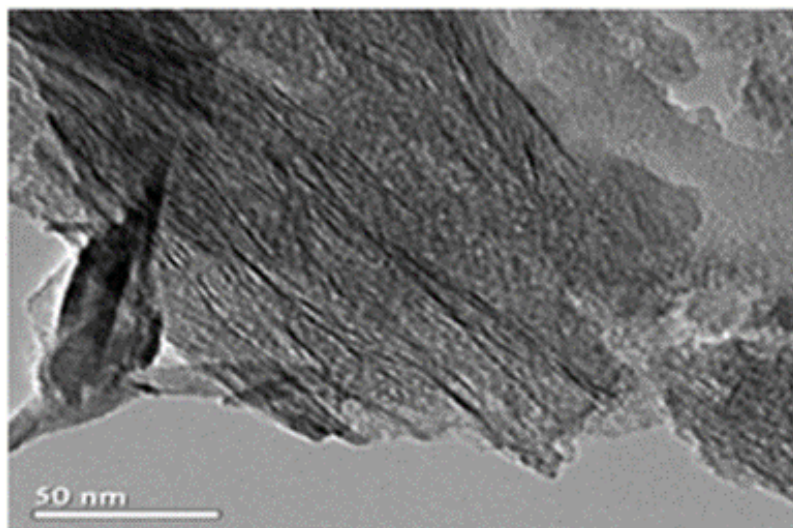


Figure 2 The transmission electron microscopy images of porous clay heterostructure.

The presence of the clay layers was confirmed by the TEM images of representative porous clay heterostructures (Figure 2). From the TEM images, the clay layers were discernible as solid dark lines and revealed aggregated domains of several layers. Although the clay layers were easily observed, the pore structure in the galleries of the clay was more difficult to notice because of their structures.

4.4.3 Morphology of bentonite, porous clay heterostructure, hybrid organic–inorganic porous clay heterostructure and mercaptopropyl functionalized PCHs.

Furthermore, the BTN exhibited a layered or plate-like structure in the SEM image (Figure 3a). After pore modification, addition of TEOS and the neutral amine co-surfactant causes a change in the particles appearance in SEM analysis. The SEM images of the PCH and HPCH (Figure 3b–c) revealed a rugged surface of the clay layers, compared with the flat and smooth pristine clay. This result implied that the molecular interactions forcing to self-assembly induce a break up of plate-like BTN. The morphology of MPPCH is also similar to those of modified PCHs as shown in Figure 3d.

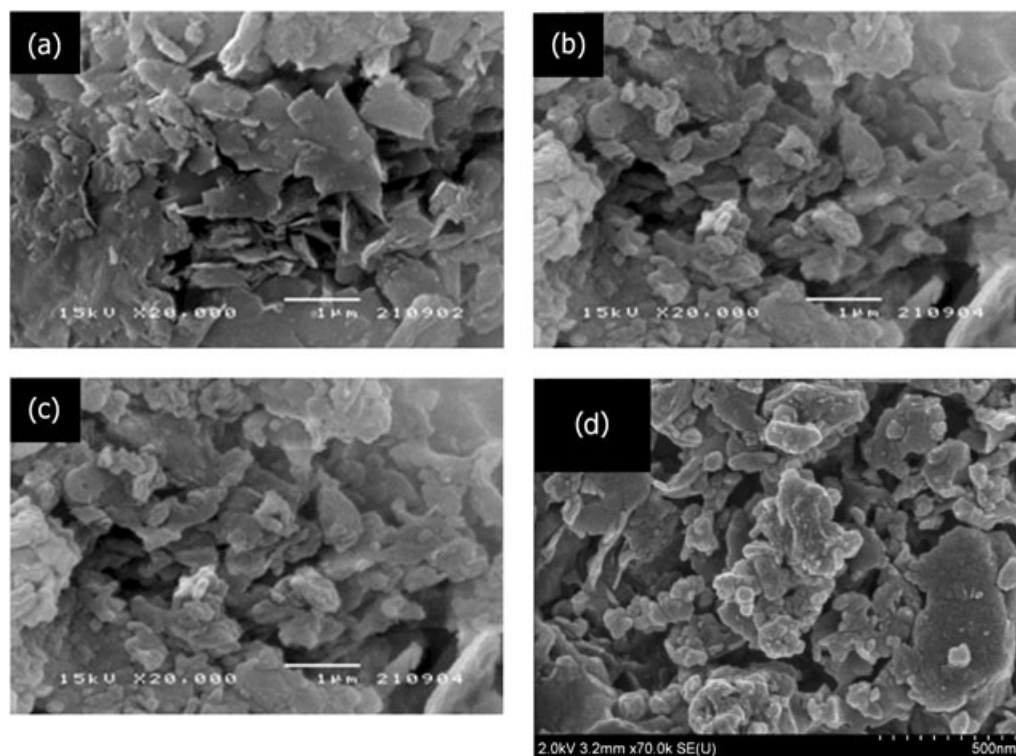


Figure 3 Scanning electron microscopy images of (a) bentonite, (b) porous clay heterostructure, (c) hybrid organic–inorganic porous clay heterostructures (HPCH) and (d) mercaptopropyl functionalized MPPCH.

4.4.4 Chemical Analysis

The FT-IR spectrum of BTN was given in Figure 4a. The broad peak at around 3500/cm was assigned to the stretching vibration of the silanol associated with the silica structure. The peaks at 1000, 1100 and 800/cm were assigned to the stretching vibration of the SiO_4 units, and the asymmetric and symmetric stretching vibrations of the Si—O—Si linkage, respectively. The presence of surfactant was evidenced by the FT-IR spectra of the organoclay (Figure 4b), indicating the asymmetric and symmetric vibrations of methyl and methylene groups of the cetyltrimethylammonium ion at 2920 and 2800/cm, respectively. The FT-IR spectra of the PCHs and the HPCHs (Figure 4c and d) were different from that of the starting BTN indicated by the absence of a peak at 1000/cm. So it inferred that the structures of the starting clay were changed after the modification. Moreover, the spectra of the HPCHs (Figure 4d) are evidenced that organic moiety is linked covalently to the silica

framework because of the presence of the peak at 1275/cm attributed to the Si-CH₃ bond.

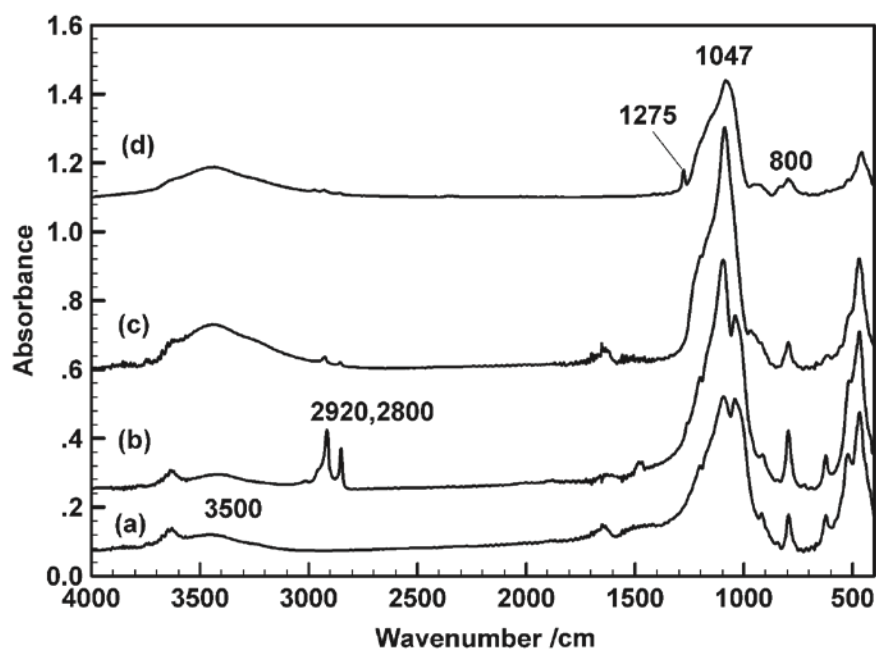


Figure 4 Fourier transform infrared spectroscopy spectra of (a) bentonite, (b) organoclay, (c) porous clay heterostructures and (d) hybrid organic-inorganic porous clay heterostructures.

In order to confirm the incorporation of the thiol group in the MPPCH, the X-ray fluorescence spectrometry (XRF) technique was required because the observed peak at 2550/cm in the FT-IR is too weak. From the XRF results (Table 1), the percentage of Sulphur in the MPPCH is 4.32, whereas that of Sulphur in the BTN is absent.

Table 1 Elemental analysis from X-ray fluorescence spectrometry result

Sample	Percent composition of elements											Total
	O	Na	Mg	Al	Si	K	Ca	Ti	Fe	Cu	S	
BTN	49.4	2.38	1.72	7.04	34.6	1.08	2.10	0.22	1.09	0.14	–	100
MPPCH	53.0	–	0.55	2.04	38.5	0.24	0.56	0.08	0.36	0.18	4.32	100

Notes: BTN, bentonite; mercaptopropyl functionalized PCH, MPPCH.

4.4.5 Surface area analysis

From the N₂ adsorption–desorption, the specific surface area of the BTN was 31 m²/g. After modification, the PCHs, HPCHs and MPPCHs possess surface areas of 507.7, 500.3 and 488.7 m²/g, average pore diameters in the small mesopore range of 5.07, 4.28 and 3.28 nm, and pore volumes of 0.64, 0.56 and 0.48 cm³/g, respectively (Table 2). These results strongly affirm that the surface areas of modified PCHs dramatically increase compared with that of pristine clay. Whereas, the incorporation of the functional groups is slightly reduces the pore diameters.

Table 2 Specific surface areas from the N₂ adsorption–desorption

Samples	Multipoint BET surface area (m ² /g)	Average pore diameter (nm)	BJH pore volume (cc/g)
BTN	31.0	–	–
PCH	507.7	5.07	0.64
HPCH	500.3	4.28	0.56
MPPCH	488.7	3.28	0.48

Note: BET, Brunauer–Emmett–Teller; BJH, Barrett–Joyner–Halenda; BTN, bentonite; PCH, porous clay heterostructures; HPCH, mercaptopropyl functionalized PCH; MPPCH.

4.4.6 Ethylene adsorption

The adsorption behavior of ethylene gas within the PCH, HPCH and MPPCH materials was examined using gas chromatography. Figure 5 shows the adsorption capacity of the PCHs, HPCHs and MPPCHs compared with that of BTN. The amount of ethylene adsorption proportionally increased with time. The amount of ethylene adsorption is in the following order: HPCH > MPPCH > PCH > BTN. This is explained based on the fact that a greater in non-polar property because of lower electronegativity; $C < S < O$: $2.55 < 2.58 < 3.44$ leads to a better ethylene adsorption. The greatest capacity of the HPCHs, prepared by the incorporation of a methyl group on the porous structures, is also because of the similarity of the functional group between the pore surface and the ethylene gas. From the results, it is clear that the insertion of the methyl groups on the HPCHs plays an important role in ethylene adsorption

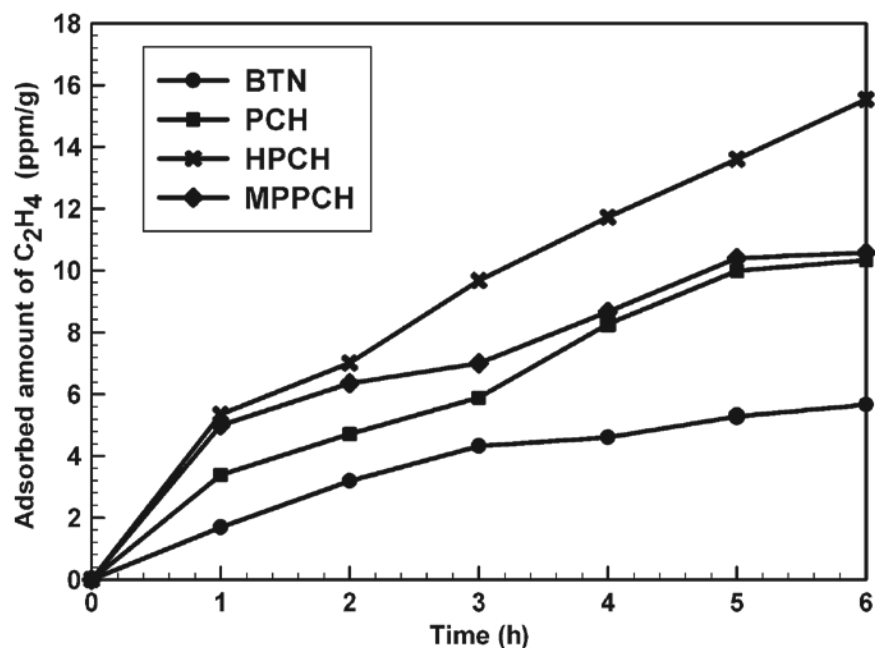


Figure 5 Ethylene adsorption capacity of bentonite, porous clay heterostructures and hybrid organic–inorganic porous clay heterostructures.

4.4.7 Nanocomposite film applications

Electrical conductivity of nanocomposite film upon the ethylene adsorption. The electrical conductivity measurement is taken as an approach to the performance of the modified PCHs/PP nanocomposite films as the ethylene sensor. Modified PCHs/PP nanocomposite films were fabricated and tested for their electrical conductivity after adsorbing ethylene gas at various attachment times. Figure 6 shows that the conductivity of the PCHs/PP nanocomposite films decreases with longer attachment time to the ethylene gas. The MPPCH/PP shows the largest decrease in electrical conductivity compared with the others. This is because when the ethylene gas diffuses into the pore, the ethylene gas reacts with the electrons on the —SH group. Ethylene gas is the electron donating group, whereas the —SH group is the electron withdrawing group; the gas is absorbed by a dipole–dipole interaction. This leads to the reduction in electrical conductivity. The concept of the conductivity drops will be applied in the future work to develop a new ethylene scavenger film. These modified PCHs/PP nanocomposite films are used as the ethylene gas sensor because the reduction of the electrical conductivity of the films is sensitive to the ethylene gas that is released from fresh vegetables and fruits.

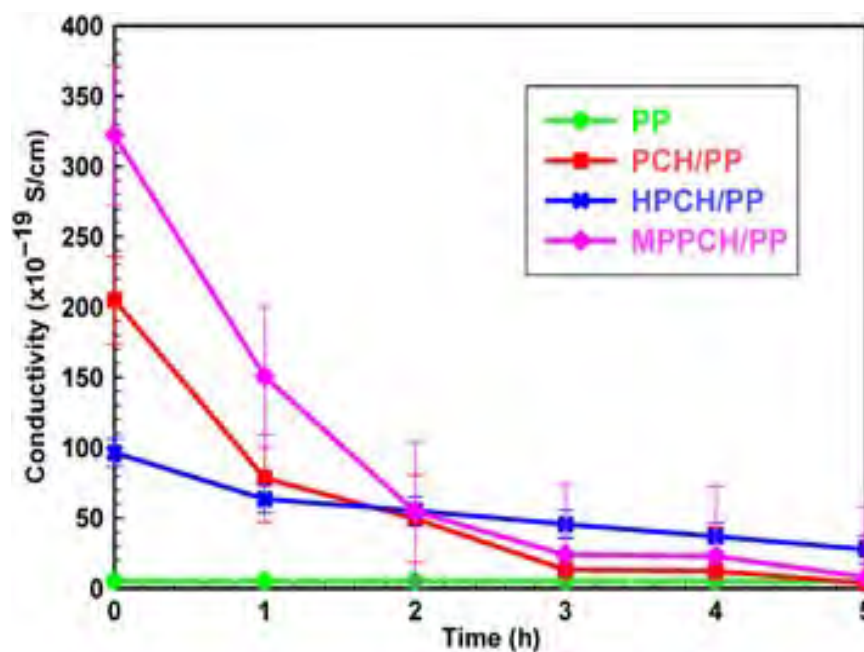


Figure 6 The conductivity of polypropylene/clay nanocomposite films as a function of time attached to the ethylene gas.

4.5 Conclusions

To fabricate a new ethylene scavenger material for packaging of tropical fruits, the modified mesoporous clay heterostructure was successfully synthesized through the surfactant-directed assembly of the mesostructured silica of clay. After treatment with TEOS/MTS and TEOS/MPTMS via the co-condensation reaction, the intercalated TEOS/MTS and TEOS/MPTMS were hydrolyzed and condensed, leading to the formation of micelles in the interlayer of the clay. The surfactants were removed by solvent extraction, and then porous materials were obtained. From the XRD results, after treatment with CTAB, the d-spacing of organoclay increases, indicating the successful insertion of the surfactant between the clay layers. According to the N₂ adsorption-desorption, the specific surface areas of the PCHs, HPCHs and MPPCHs are much higher than those of pure BTN as the plate-like structure was transformed to a pore structure. From the ethylene adsorption results, the HPCHs have a higher efficiency in adsorbing ethylene gas than the others because the methyl groups that incorporate in the PCH lead to a non-polar surface, which causes the best ethylene adsorption. Otherwise, the thiol groups that incorporates in the PCH, MPPCHs, exhibit the best ethylene sensing by its higher sensitivity because of the largest drop of the electrical conductivity when it binds to the ethylene gas by the dipole-dipole interaction. As supported by above results, these modified PCHs including HPCHs and MPPCHs are potentially used as packaging fillers to capture ethylene gas and could be further developed as ethylene sensor applied from conductivity sensitivity results. Future investigation will focus on the evaluation of these PCH/PP, HPCH/PP and MPPCH/PP nanocomposite films in smart packaging applications by monitoring the shelf life of Thai tropical fruits such as mangoes and bananas that own a high segment in Thai fruit's export.

4.6 Acknowledgements

This work was supported by the Higher Education Research Promotion and National Research University Project of Thailand, Office of the Higher Education Commission (FW 0649A). Partial funding was received from the Polymer Processing

and Polymer Nanomaterials Research Unit, The Petroleum and Petrochemical College, Chulalongkorn University. One of the authors would like to acknowledge the scholarship from the Center of Excellence for Petroleum, Petrochemicals and Advanced Materials, Thailand.

4.7 References

1. Vermeiren L, Devlieghere F, van Beest M, de Kruijf N, Debevere J. Developments in the active packaging of foods. *Trends in Food Science and Technology* 1999; 10: 77–86. doi:10.1016/S0924-2244(99)00032-1.
2. Goddard NDR, Kemp RMJ, Lane R. An overview of smart technology. *Packaging Technology and Science* 1997; 10: 129–143. doi:10.1002/(SICI)1099-1522(19970501/30).
3. Ishii R, Nakatsuji M, Ooi K. Preparation of highly porous silica nanocomposites from clay mineral: a new approach using pillaring method combined with selective leaching. *Microporous and Mesoporous Materials* 2005; 79: 111–119. doi:10.1016/j.micromeso.2004.10.033.
4. Galarnau A, Barodawalla A, Pinnavaia TJ. Porous clay heterostructures formed by gallery-templated synthesis. *Nature* 2002; 374: 529–531. doi:10.1038/374529a.
5. Zhu HY, Ding Z, Barry JC. Porous solids from layered clays by combined pillaring and templating approaches. *The Journal of Physical Chemistry B* 2002; 106(44): 11420–11429. doi:10.1021/jp014463i
6. Stein A, Melde BJ, Schroden RC. Hybrid inorganic–organic mesoporous silicates-nanoscope reactors coming of age. *Advance Materials* 2009; 12(9): 1403–1419. doi:10.1002/1521-4095(200010)
7. Burkett SL, Sims SD, Mann S. Synthesis of hybrid inorganic–organic mesoporous silica by co-condensation of siloxane and organosiloxane precursors. *Chemical Communication* 1996; 1367–1368. doi:10.1039/CC9960001367
8. Pires J, Araujo AC, Carvalho AP et al. Porous materials from clays by the gallery template approach: synthesis, characterization and adsorption properties.

- Microporous and Mesoporous Materials 2004; 73(3): 175–180. doi:10.1016/j.micromeso.2004.05.009
9. Wei L, Tang T, Huang B. Novel acidic porous clay heterostructure with highly ordered organic–inorganic hybrid structure: one-pot synthesis of mesoporous organosilica in the galleries of clay. *Microporous and Mesoporous Materials* 2004; 67(2–3): 175–179. doi:10.1016/j.micromeso.2003.11.002
 10. Pichowicz M, Mokaya R. Porous clay heterostructures with enhanced acidity obtained from acid-activated clays. *Chemical Communication* 2001; 2100–2101. doi:10.1039/b106660a
 11. Polverejan M, Pauly TR, Pinnavaia TJ. Acidic porous clay heterostructures (PCH): intragallery assembly of mesoporous silica in synthetic saponite clays. *Chemistry of Materials* 2000; 12(9): 2698–2704. doi:10.1021/cm0002618
 12. Polverejan M, Liu Y, Pinnavaia TJ. Aluminated derivatives of porous clay heterostructures (PCH) assembled from synthetic saponite clay: properties as supermicroporous to small mesoporous acid catalysts. *Chemistry of Materials* 2002; 14(5): 2283–2288. doi:10.1021/cm011559g
 13. Zhou C, Li X, Ge Z, Li Q, Tong D. Synthesis and acid catalysis of nanoporous silica/alumina- clay composites. *Catalysis Today* 2004; 93–95: 607–613. doi:10.1016/S0925-5214(98)00091-X
 14. Nunes CD, Pires J, Carvalho AP, Calhorda MJ, Ferreira P. Synthesis and characterisation of organo-silica hydrophobic clay heterostructures for volatile organic compounds removal. *Microporous and Mesoporous Materials* 2008; 111(1–3): 612–619. doi:10.1016/j.micromeso.2007.09.008
 15. Chmielarz L, Kuśtrowski P, Drozdek M et al. Selective catalytic oxidation of ammonia into nitrogen over PCH modified with copper and iron species. *Catalysis Today* 2006; 114: 319–325. doi:10.1016/j.cattod.2006.01.020
 16. Chmielarz L, Kuśtrowski P, Dziembaj R, Cool P, Vansant EF. Selective catalytic reduction of NO with ammonia over porous clay heterostructures modified with copper and iron species. *Catalysis Today* 2007; 119: 181–186. doi:10.1016/j.cattod.2006.08.017

17. Taguchi A, Schüth F. Ordered mesoporous materials in catalysis. *Microporous and Mesoporous Materials* 2008; 111(1–3): 612–619. doi:10.1016/j.micromeso.2007.09.008
18. Mercier L, Pinnavaia TJ. A functionalized porous clay heterostructure for heavy metal ion (Hg²⁺) trapping. *Microporous and Mesoporous Materials* 1998; 20(1–3): 101–106. doi:10.1016/S1387-1811(97)00019-X
19. Marschall R, Bannat I, Caro J, Wark M. Proton conductivity of sulfonic acid functionalised mesoporous materials. *Microporous and Mesoporous Materials* (2007); 99(1–2): 190–196. doi:10.1016/j.micromeso.2006.08.037
20. Liu H, Hyung Tag Lim HT, Ahn KH, Lee SJ. Effect of ionomer on clay dispersions in polypropylene-layered silicate nanocomposites. *Journal of Applied Polymer Science* 2007; 104: 4024–4034. doi:10.1002/app.26036
21. Wang Y, Easteal AJ, Chen XD. Ethylene and oxygen permeability through polyethylene packaging films. *Packaging Technology and Science* 1998; 11: 169–178. doi:10.1002/(SICI)1099-1522(199807/08)
22. Yun JH, An DS, Lee K - E, Jun BS, Lee DS. Modified atmosphere packaging of fresh produce using microporous earthenware material. *Packaging Technology and Science* 2006; 19: 269–278. doi:10.1002/pts.730
23. Avella M, Bruno G, Errico ME et al. Innovative packaging for minimally processed fruits. *Packaging Technology and Science* 2007; 20: 325–335. doi:10.1002/pts.761

CHAPTER V

INFLUENCE OF THIOL GROUPS ON THE ETHYLENE ADSORPTION AND CONDUCTIVITY PROPERTIES OF THE MODIFIED POROUS CLAY HETEROSTRUCTURES (PCHS) USING AS ETHYLENE SCAVENGER IN SMART PACKAGING

5.1 Abstract

Porous Clay Heterostructures (PCHs) were prepared by the surfactant-directed assembly of silica source (tetraethylorthosilicate-TEOS) and sodium-bentonite (Na-BTN) clay. These PCHs were subsequently modified to an organic-inorganic hybrid material by the co-condensation reaction of TEOS with (3-mercaptopropyl trimethoxy silane (MPTMS) in 1:1, 2:1, and 4:1 molar ratios of MPTMS to TEOS to obtain conductive porous clays, here referred to as modified MPPCHs. Various weight percentage of MPPCHs at 1 wt%, 3 wt%, and 5 wt% were blended with polypropylene (PP) and fabricated into the PP/modified MPPCHs nanocomposite films. Analysis revealed that the surface areas of modified MPPCHs increased significantly from Na-BTN; however, the higher MPTMS contents resulted in less porous surface areas. An ethylene adsorption study showed that modified MPPCHs exhibited higher adsorption efficiency of ethylene gas than that of Na-BTN due to the non-polar property of the modified functional groups. Subsequently, the electrical conductivity of the modified MPPCHs with various contents of thiol group was investigated to evaluate potential use in ethylene scavenger/sensor applications.

Keywords: Organic-Inorganic Hybrid, Modified MPPCHs, Conductive porous clay heterostructure, Ethylene scavenger, Sensor

5.2 Introduction

Ethylene gas is a plant hormone which facilitates ripening and ageing of many agricultural products cultivated throughout the world. Shelf-life of stored fruit and produce is often limited by natural production of this gas from ripening produce. To

prolong shelf-life of products, the ethylene gas should be removed from the storage system. There are many ways to protect produce from the ethylene gas. For example, 1-Methylcyclopropene (1-MCP), palladium, and zeolite acted as ethylene scavengers which block the ethylene binding sites, block the ethylene gas production from the plants, and also adsorb the ethylene gas [1-5]. Besides the ethylene scavengers, the polymer and polymer nanocomposite films may be employed as active packaging to prolong the shelf-life of produce [6-15].

In previous work, porous clay heterostructures (PCHs) were synthesized in order to absorb the ethylene gas from fruit ripening [16,17] because of their high surface areas, selective porous structure after surfactant removal [18-21]. Then, PCHs were functionalized by methyltriethoxysilane (MTS) and (3-mercaptopropyl) triethoxysilane (MPTMS) providing for hybrid organic-inorganic PCHs (HPCHs) and mercaptopropyl PCHs (MPPCHs), respectively [22-26]. MPPCH contained a thiol group (-SH) which normally removed heavy metal by binding the negative charge of the -SH to metal ion (Hg^+ , Cu^{2+} , and Ag^+) [27-32]. It also has the ability to adsorb organic compounds such as volatile organic compounds and dye molecules [33,34]. Previous works that modify montmorillonite, acid-activated montmorillonite, and organo-montmorillonite as the template or support to adsorb organic compounds or pesticide in the water were reviewed [35,36]. The acid-activation and organophilic treatment are easy-processing and well selective. However, comparing to PCH, they exhibit the lower surface area and less pore size. Since, PCH is synthesized by intercalation of surfactant in order to enlarge the distance of clay layer and then introduced silica sources to polymerize around surfactant micelle template, leading to high surface area and mesopore structure. Due to high surface area, the PCH is chosen to use as the template in this work and then modify to display more selectivity to adsorb various organic molecules.

All PCHs, HPCHs, and MPPCHs were tested for ethylene adsorption to use as ethylene scavenging materials for the purpose of prolonging the shelf-life of food products. The variation in electrical conductivity of MPPCHs when it reacts with ethylene was investigated as an operating principle to exploit for the sensing of ethylene gas. The MPPCHs electrical conductivity measurements were sensitive to

ethylene even though MPPCHs adsorbed less ethylene gas than that of HPCHs. However, MPPCH/Polypropylene (PP) nanocomposite film showed the best sensitivity to ethylene gas in electrical conductivity measurements, exhibiting the largest drop in conductivity when reacting to ethylene gas [16,17].

In this work, MPPCHs were synthesized with concentrations of MPTMS to TEOS in the molar ratios of 1:1, 2:1, and 4:1 which are denoted here respectively as MPPCH (1:1), MPPCH (2:1), and MPPCH (4:1). And, then the modified PCHs were blended with polypropylene (PP) in the ratio of 1wt%, 3wt%, and 5wt% of clay content, respectively. The objective of adding various ratios of the thiol group on the surface of clay and various clay contents in the PP matrix were to study the influence of these factors in ethylene adsorption effectiveness and electrical conductivity sensing of MPPCH/Polypropylene (PP) nanocomposite films for using as the ethylene gas scavenger/sensor films.

5.3 Experimental

5.3.1 Raw Materials

Sodium bentonite (Na-BTN), with a cation exchange capacity (CEC) of 44.5 meq/100g of clay, was supplied by Thai Nippon Chemical Industry Co. Ltd. (Thailand). Cetyl trimethylammonium bromide (CTAB), performing as the cationic surfactant, and chemical substances such as tetraethyl orthosilicate (TEOS), for use as a silica source and 3-mercaptopropyl trimethoxysilane (MPTMS), for modifying MPPCH, were purchased from Fluka and Acros, respectively. PP (Moplen HP525N, MFI 11) and Surlyn® (PC 350, MFI 5) were provided by HMC Polymers Co., Ltd. (Thailand) and DuPont™.

5.3.2 Synthesis of Hybrid Organic-Inorganic PCHs with Conductive Functional Groups (MPPCHs)

Na-BTN was changed into a quaternary ammonium exchange form by ion exchange with cetyltrimethylammonium bromide (CTAB) and was stirred at 50 °C for 24 h. After that, the sample was filtered, washed with a mixture of methanol

and water, and then air-dried for 24 h to obtain organoclay. The obtained organoclay was stirred in dodecylamine at 50 °C for 30 min and then adding the TEOS at a molar ratio of organoclay:dodecylamine:TEOS of 1:20:150 to synthesize the porous clay heterostructures (PCHs). According to the previous PCH forming step, the mixture of TEOS and MPTMS was added under N₂ atmosphere and stirred for a further 24 h at room temperature with various molar ratios of MPTMS: TEOS of 1:1, 2:1, and 4:1. The obtained modified PCHs were collected by filtration and air-dried overnight at room temperature. Then the surfactant was removed by solvent extraction using a mixture of methanol and HCl solution. Typically, 1 g of the modified PCHs was added into the 5 ml of HCl and 45 ml of methanol, and was refluxed for 2 h. The modified PCHs were abbreviated as MPPCH (1:1), MPPCH (2:1), and MPPCH (4:1), respectively.

5.3.3 Preparation of Polypropylene/clay Nanocomposite Film

The 1 wt%, 3 wt%, and 5 wt% of MPPCHs, 2 wt% of surlyn[®] (compatibilizer), and Polypropylene (PP) were prepared by using twin-screw extruder (Labtech) with with an L/D ratio of 40 and a screw diameter of 20 mm. The operation temperature was performed at 160 °C, 165 °C, 170 °C, 175 °C, 180 °C, 185 °C, 190 °C, 200 °C, 210 °C and 215 °C from hopper to die respectively and the screw speed was 30 rpm.

5.3.4 Fabrication of Nanocomposite Films

The nanocomposite films were prepared by using blown film extrusion machine. The nanocomposite pellets were dried in an oven prior to blowing. The following extrusion conditions were employed at the rotation speed of the screw around 50 rpm and the blowing ratio was 1.52. The barrel and mold temperature were 210 °C. The thickness of the films was controlled to about 40 μm.

5.3.5 Characterization

5.3.5.1 *X-Ray Fluorescence Spectrometry (XRF)*

The elemental analysis of the pristine clay and the modified PCHs (MPPCHs) was carried out by using X-ray fluorescence (Axios PW4400). The excitation source was an X-ray tube with thin silver as the primary filter, operating at a tube voltage of 35 kV.

5.3.5.2 X-Ray Diffractometry (XRD)

An X-Ray diffractometer (XRD) was used to obtain the d -value of the bentonite and the organoclay to investigate the crystal structure of materials. The X-Ray diffraction patterns were measured on a Rigaku Model Smart Lab Guidance (Rigaku, Japan) with Ni-filtered CuK_α radiation at 40 kV, 30 mA and on the 2θ range of 2 to 10 degrees with a scan speed of 2 degrees/min and a scan step 0.01 degree for WAXS mode. SAXS mode was operated at 45kV, 200mA, and on the $2q$ range of 0.1–8 degrees with a scan speed of 0.5 degrees/min and a scan step 0.02 degree.

5.3.5.3 Surface Area Analysis (SAA)

The N_2 adsorption–desorption isotherms were obtained at -196°C on a Sorptomatic analyzer. The samples were degassed at 150°C for 15 h in a vacuum furnace before analysis. Specific surface areas were calculated using the BET equation. The pore size distributions were constructed based on The Barrett, Joyner, and Halenda (BJH) method using the adsorption branch of the nitrogen isotherm.

5.3.5.4 Fourier Transform Infrared Spectroscopy (FT-IR)

The FT-IR spectra of bentonite, organoclays, and modified MPPCHs were obtained by using a Nicolet Nexus 670 FT-IR spectrometer in the frequency range of $4000\text{--}400\text{ cm}^{-1}$ with 32 scans/min at a resolution of 2 cm^{-1} . The incorporation of the organic group into the silicate network was investigated by using FT-IR.

5.3.5.5 Scanning Electron Microscopy (SEM)

Scanning electron microscopy was performed with Hitachi S-4800 Model to observe the surface morphology of the modified MPPCHs.

5.3.5.6 Gas Chromatography for Ethylene Adsorption

A gas chromatograph with a flame ionization detector was utilized to examine the ethylene adsorption capacity of the modified MPPCHs.

Ethylene adsorption was measured by placing each product in a chamber (0.6 l), then sealing it with a screw-cap lid. Ethylene was injected into a jar to give a specific concentration of 5000 ppm. Ethylene concentration in the chamber was measured periodically, about once per hour. The ethylene adsorption was calculated by taking the difference between the amount of ethylene added and the amount remaining in the headspace.

5.3.5.7 Conductivity Measurement

The electrical conductivity of the mesoporous materials were observed using Impedance test by LCR meter (Agilent E4980A). The clay pellets were covered with platinum and placed between the 2 probes and the tests were run at 20 Volts with varying frequencies from 20 Hz to 1 MHz. Finally, the results were calculated by Nyquist's plot to obtain the semi-circle and find the resistivity from the intersection of x axis at the high frequency.

5.3.5.8 Keithley Electrometer for Conductivity Measurement

The electrical conductivity of the nanocomposite films were observed using Keithley Electrometer with 6517 Hi-R test. The film was placed between the 2 probes in the vacuum box. The tests were run by varying the voltages in 1, 5, 10, 20 and 100 Volts and then calculated the electrical conductivity from plotting between the current and the applied voltage. The volume resistivity is calculated by using the Equation (1)

$$\text{Volume resistivity} = \frac{22.9}{\text{thickness, cm}} \times \frac{V}{I} \text{ (ohm} \cdot \text{cm)} \quad (1)$$

5.3.5.9 Thermal and Mechanical Property of Polypropylene/clay Nanocomposite

Thermogravimetric analysis (TGA) was used to investigate the thermal stability of the PP/modified porous clay nanocomposites as compared to pure PP. The samples were heated from 30 °C – 700 °C at a rate of 10 °C min⁻¹ in a nitrogen atmosphere of 200 ml/min. Differential Scanning Calorimeter (METTLER, DSC822^e) was used to measure the crystallization and melting behavior of the PP/modified porous clay nanocomposites. The samples were heated and cooled from 30 °C - 200 °C, using a heating/cooling rate of 10 °C min⁻¹ in a nitrogen atmosphere.

Tensile test of PP/modified porous clay nanocomposite samples were carried out by a LLOYD Universal Testing Machine model 4206 by ASTM D 638. A gage length of 50 mm was employed with a crosshead speed of 50 mm/min and preload 0.01 N.

5.4 Result and Discussion

5.4.1 Characterization of Bentonite and MPPCHs

As seen from Figure 1 (a) in small graph, the characteristic peak of bentonite was d_{001} plane at 7.62° which indicate the basal spacing of bentonite to 1.16 nm. After bentonite was treated with quaternary alkylammonium ion, the new peaks (d_{001}) was observed at lower angle (Figure 1 (b)) indicating the increasing of distance between interlayer spaces. The d -value of organoclay was 3.87 nm.

After porous modification with silica source, the modified MPPCHs were examined by SAXS mode (Rigaku Corporation, Japan). In Figure 2, none of diffraction peaks like those of bentonite and organoclay was presented. Disorder of silica framework which was formed in the interlayer spaces of bentonite shielded highly regular interstratifications of the clay layers. So the XRD patterns in Figure 2 showed only diffuse scatterings. It meant that the structure of PCH and all modified MPPCHs were not the long period structures but represented the pore structure.

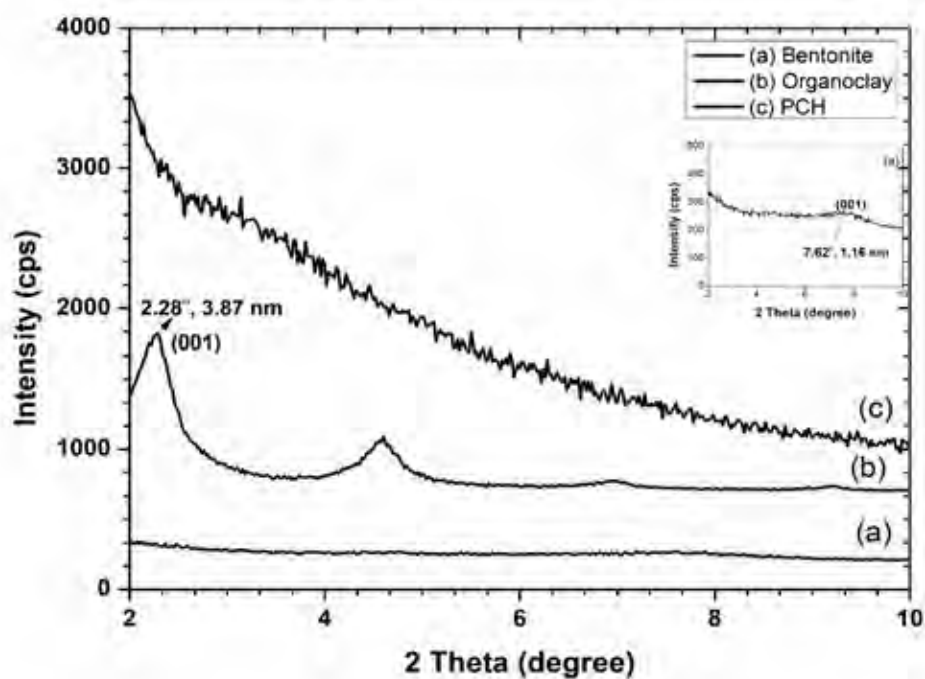


Figure 1 XRD patterns of (a) Bentonite, (b) Organoclay, and (c) PCH.

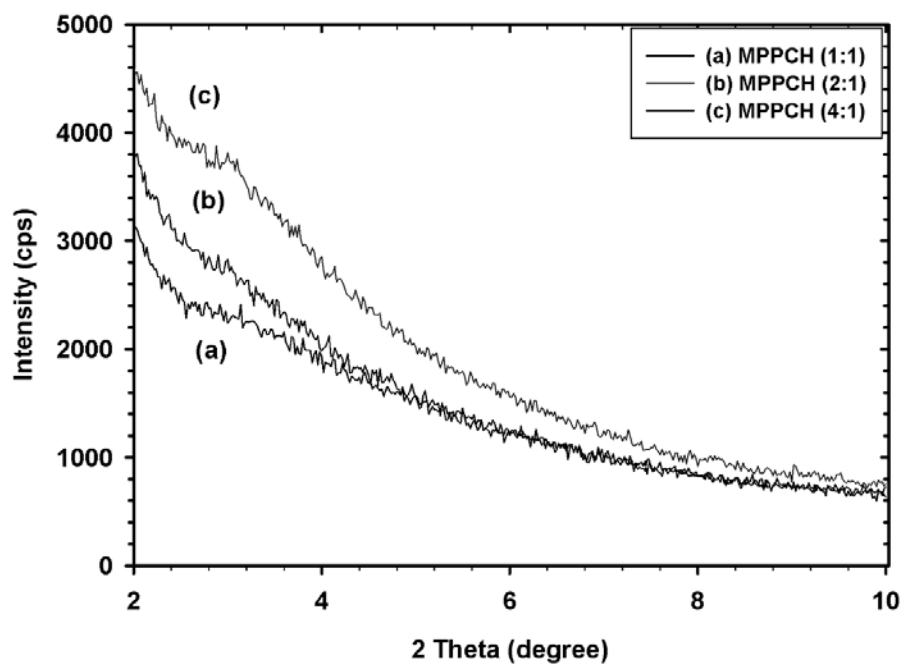
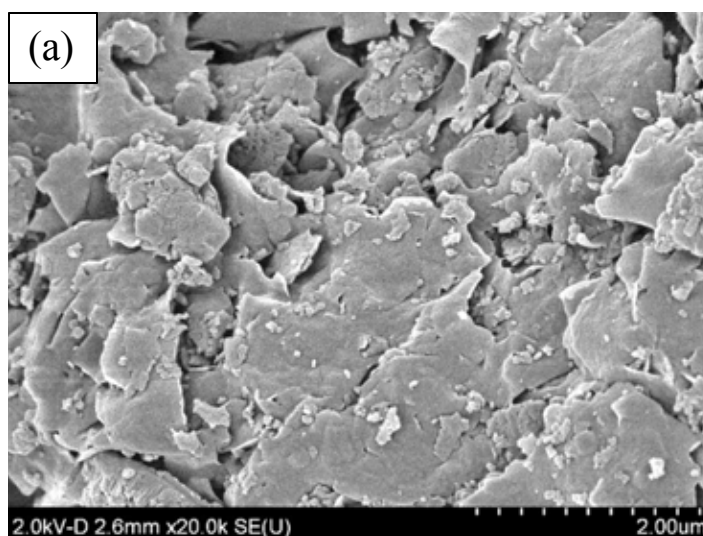


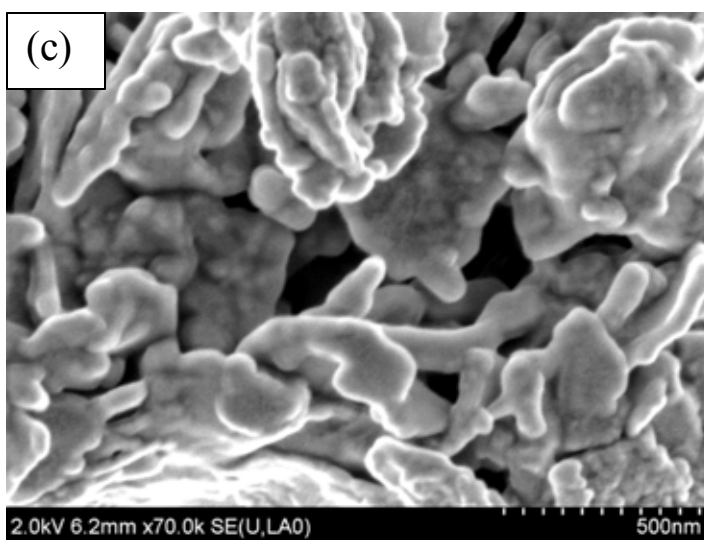
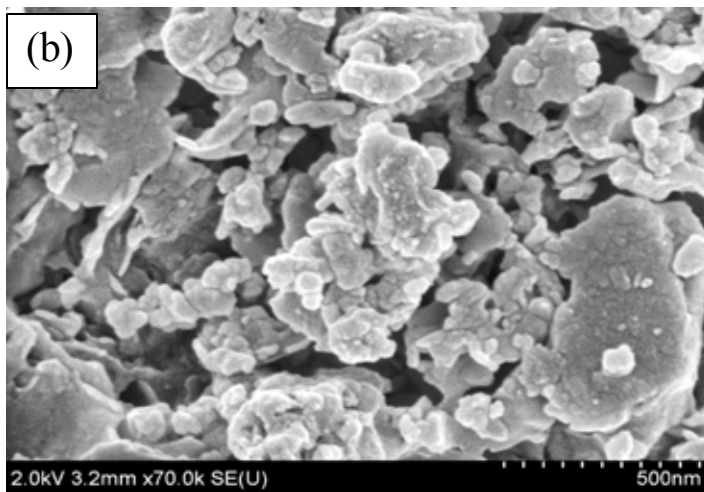
Figure 2 XRD patterns of (a) MPPCH (1:1), (b) MPPCH (2:1), and (c) MPPCH (4:1).

5.4.2 Morphology of MPPCHs

First, the interlayer spaces of bentonite were expanded by the intercalation of the surfactant cetyltrimethylammonium ion. Next, a neutral amine co-surfactant was intercalated between interlayer spaces to form micelle templates. Then silica sources (MPTMS/TEOS with various molar ratios 1:1, 2:1 and 4:1, respectively) were introduced to polymerize surrounding the surfactant micelles in the interlayer spaces of bentonite. By solvent extraction method, the surfactant templates were removed from MPPCHs, resulting in the formation of porous structures.

Normally, the bentonite exhibited a layered or plate-like structure in SEM image (Figure 3(a)). After porous modification, the SEM images of MPPCHs (Figure 3(b)-(d)) revealed a roughness and porosity on the surface of clay comparing to bentonite surface.





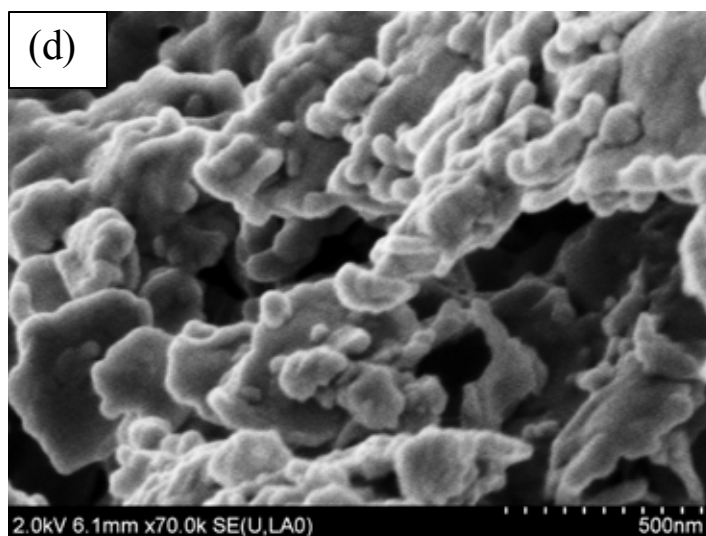


Figure 3 SEM images of (a) BTN, (b) MPPCH (1:1), (c) MPPCH (2:1) and (d) MPPCH (4:1).

5.4.3 Chemical Structure Analysis

The FTIR spectrum of bentonite was given in Figure 4 (a). The broad peak around 3500 cm^{-1} was assigned to the stretching vibration of the silanol associated with the silica structure. The peaks at 1640 , 1000 , 1100 and 800 cm^{-1} were assigned to the stretching vibration of the SiO_2 units, SiO_4 units, the asymmetric and symmetric stretching vibrations of the Si-O-Si linkage, respectively. The presence of surfactant was proved by FTIR spectra of organoclay (Figure 4 (b)) indicating the asymmetric and symmetric vibrations of methyl and methylene groups of cetyltrimethyl ammonium ion at 2920 and 2800 cm^{-1} , respectively. The FTIR spectra of MPPCHs (Figure 4 (c)-(e)) were indifferent from that of bentonite, however, the peak at 2550 cm^{-1} indicating $-\text{SH}$ group was very weak. Therefore it roughly inferred that the structure of starting bentonite was changed after the modification.

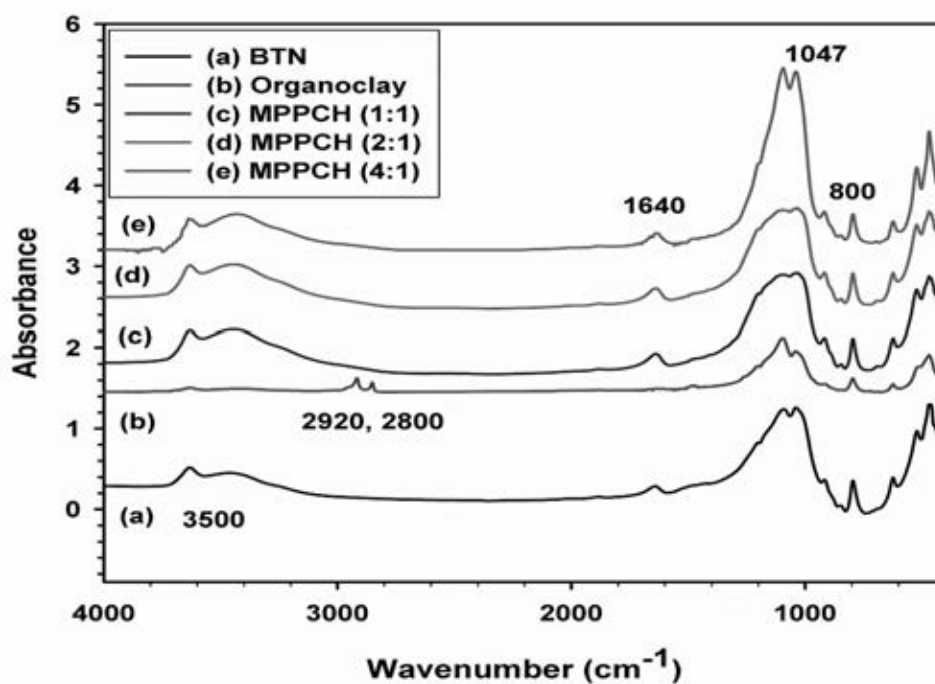


Figure 4 FTIR spectra of (a) bentonite, (b) organoclay, (c) MPPCH (1:1), (d) MPPCH (2:1), and (e) MPPCH (4:1).

In order to confirm the incorporation of thiol group in the modified MPPCHs (Figure 4 (c)-(e)), the XRF technique was required. From XRF results as shown in Table 1, the contents of sulfur in MPPCH (1:1), MPPCH (2:1) and MPPCH (4:1) were 4.32%, 8.84% and 11.58% while the content of sulfur in bentonite was none.

Table 1 Elemental analysis from XRF result

Sample	% composition of elements										
	O	Na	Mg	Al	Si	K	Ca	Ti	Fe	S	Total
BTN	49.4	2.61	1.72	7.04	34.6	1.08	2.24	0.22	1.09	-	100
MPPCH (1:1)	53.0	-	0.73	2.21	38.5	0.24	0.56	0.08	0.36	4.32	100
MPPCH (2:1)	49.8	-	1.15	2.48	36.2	0.32	0.44	0.10	0.70	8.84	100
MPPCH (4:1)	47.7	-	1.09	2.35	35.4	0.30	0.70	0.12	0.70	11.58	100

5.4.4 Specific Surface Area Analysis

From N₂ adsorption-desorption, the specific surface area of bentonite was 31 m²/g. After modification, the specific surface areas of MPPCH (1:1), MPPCH (2:1) and MPPCH (4:1) were dramatically increased to 488.7, 290.6, and 168.4 m²/g, respectively as shown in Table 2. Average pore diameter and pore volume of MPPCH (1:1), MPPCH (2:1), and MPPCH (4:1) were 3.28, 3.20, 2.00 nm and 0.48, 0.30, 0.25 cc/g. From the results, the surface areas, average pore diameter and pore volume decreased when the amount of thiol group in modified MPPCHs increased. One reasonable explanation was that the increasing contents of thiol groups resulted in intensified occupation of the interlayer spaces and increased in wall thickness of the pore that led to small pore volume [18]. With high contents of thiol group, the pores had been partially clogged by the organic groups which lead to low N₂ adsorption-desorption isotherm, referred to specific surface areas decreasing.

Table 2 Specific surface areas from the N₂ adsorption-desorption

Sample	Multipoint BET surface area (m ² /g)	Average pore diameter (nm)	BJH pore volume (cc/g)
BTN	31.0	-	-
MPPCH (1:1)	488.7	3.28	0.48
MPPCH (2:1)	290.6	3.20	0.30
MPPCH (4:1)	168.4	2.00	0.25

Note: BET, Brunauer–Emmett–Teller; BJH, Barrett–Joyner–Halenda; BTN, bentonite; porous clay heterostructure; PCH, mercaptopropyl functionalized PCH; MPPCH.

5.4.5 Ethylene Reduction of MPPCHs

The ethylene gas adsorption behaviour of the MPPCH (1:1), MPPCH (2:1) and MPPCH (4:1) materials was examined by gas chromatography technique (GC). The results showed that the ethylene reduction capacity of the MPPCH (1:1), MPPCH (2:1) and MPPCH (4:1) proportionally decreased with time dependent, compared to that of BTN (Figure 5). The amount of ethylene reduction was in the following order: MPPCH (4:1) > MPPCH (2:1) > MPPCH (1:1) > bentonite. This was explained based on the fact that a greater amount of thiol groups led to a better ethylene adsorption. Adding more functional groups led to more non-polar surface of the modified MPPCHs. So they reacted with ethylene gas more than bentonite. The MPPCH (4:1) adsorbed the largest amount of the ethylene gas adsorption due to the largest dropping value.

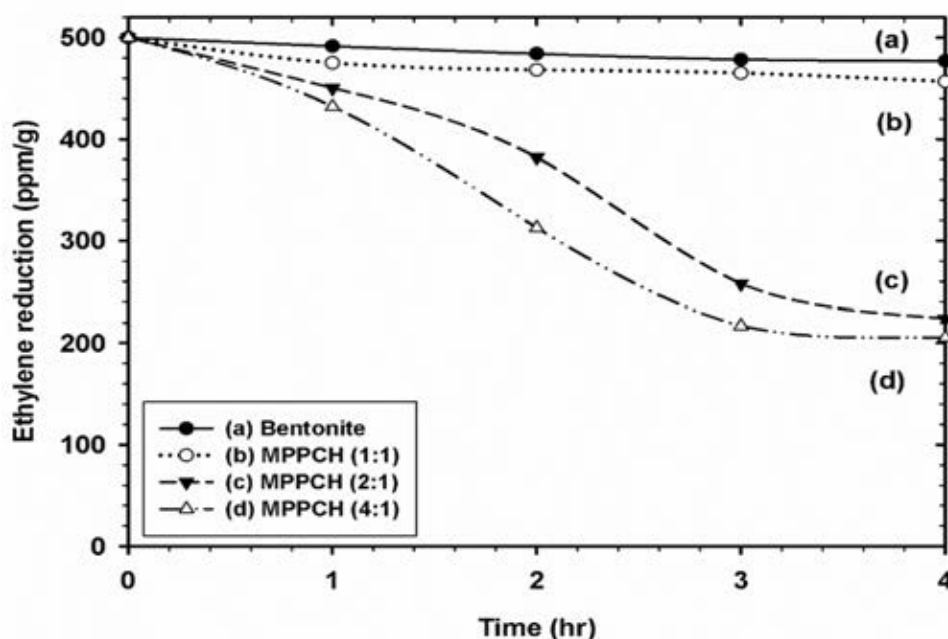


Figure 5 Ethylene reduction capacity of BTN, MPPCH (1:1), MPPCH (2:1) and MPPCH (4:1).

5.4.6 Conductivity of Modified Porous Clays

The electrical conductivity measurement was taken as an approach to the performance of the modified porous clay heterostructures as an ethylene sensor. Modified porous clay heterostructures were synthesized with several contents of MPTMS: TEOS in molar ratios of 1:1, 2:1, and 4:1 and then evaluated their electrical conductivity. From Table 3, the resistivity of bentonite was 552.3 k Ω /cm and the resistivity values of MPPCH (1:1), MPPCH (2:1), and MPPCH (4:1) were 298.9, 213.5, and 126.1 k Ω /cm. The resistivity converted to the conductivity by the following order; 1.81×10^{-6} , 3.34×10^{-6} , 4.68×10^{-6} , and 7.92×10^{-6} S/cm assigned for Bentonite, MPPCH(1:1), MPPCH(2:1), and MPPCH(4:1), respectively. This was explained that the greatest amount of thiol groups led to the largest conductivity values. It concluded that the conductivity of modified porous clay heterostructure increased with an increasing the amount of thiol group in the modified MPPCHs. The MPPCH (4:1) also showed the greatest conductivity value compared to the others. This was because

MPPCH (4:1) had the highest amount of thiol group, the conductive organic functional group, incorporating within the modified porous clays. From measurement results, it was implied that the thiol group played an important role in conductivity part.

Table 3 Resistivity and conductivity of bentonite, MPPCH (1:1), MPPCH (2:1) and MPPCH (4:1)

Sample	Resistivity (kΩ/cm)	Conductivity(S/cm)
Bentonite	552.3	1.81x10 ⁻⁶
MPPCH (1:1)	298.9	3.34x10 ⁻⁶
MPPCH (2:1)	213.5	4.68x10 ⁻⁶
MPPCH (4:1)	126.1	7.92x10 ⁻⁶

5.4.7 Thermal and Mechanical Properties

After surface modification, MPPCH (2:1) was firstly to be chosen and blended with polypropylene (PP) through twin screw extruder to obtain nanocomposite pellets and studied the effect of amount of clay on the properties of nanocomposite materials. Thermogravimetric analysis (TGA) was performed to study the thermal stability of PP/MPPCH nanocomposites compared to PP. The degradation temperature of samples was determined by Perkin Elmer Pyris Diamond TG/DTA instrument. The pellets were loaded on platinum pan and heated from 30 °C to 700 °C at a heating rate of 10 °C/min and flow under N₂ 200 ml/min.

TG-DTA curves of PP and the PP/modified PCHs nanocomposites were delineated in Figure 6 and all results of thermal properties were listed in Table 4 and Table 5. The thermal degradation of PP and all PP/MPPCHs nanocomposites were generated in a single stage, and indicating that thermal stability of the nanocomposites was marginally increased when compared to that of virgin PP.

Generally, the shift considerably toward higher temperature was attributed to the formation of a high-performance carbonaceous-silicate char, building up on the surface. Despite all these, the results implied that the addition of these

modified porous clays just slightly improved the thermal stability of PP which might be responsible for some destruction of clay layers on MPPCHs materials or due to the intercalation or the separation of the silicate layers as well as better dispersion of the silicate layers.

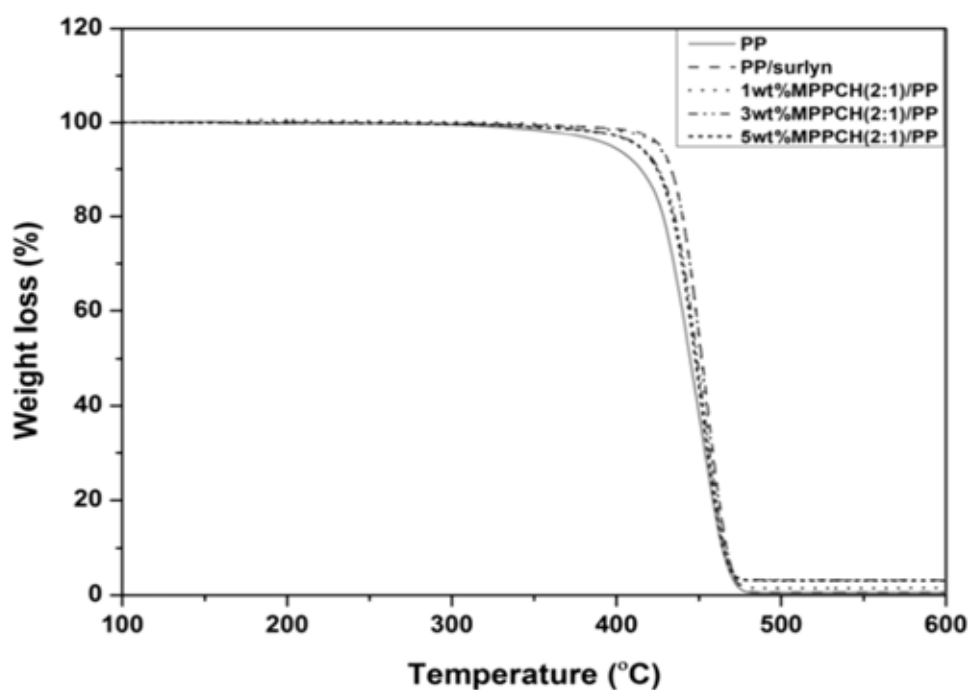


Figure 6 TG-DTA curves of pure PP and modified PCHs nanocomposites.

Table 4 Thermal properties of PP and PP/modified PCHs nanocomposites

Samples	T _d peak (°C)	Char residue at 600 °C (%)
PP	452.5	0.07
2 wt% Surlyn®/PP	455.7	0.07
1 wt% MPPCH(2:1)/Surlyn®/PP	455.7	0.87
3 wt% MPPCH(2:1)/Surlyn®/PP	456.6	2.67
5 wt% MPPCH(2:1)/surlyn®/PP	456.9	4.98

The crystallization and melting behavior of PP/MPPCHs nanocomposites compared to PP were measured by Differential Scanning Calorimeter (DSC) using Mettler DSC 822 STAR^e System. The pellets were heated from 30 °C to 200 °C at a heating rate of 10 °C/min in order to eliminate the influence of thermal history and then cooled down from 200 °C to 30 °C to observe melt crystallization behavior. After that, reheated to 200 °C to observe melting behavior.

The crystallinity of samples was calculated by this equation,

$$\% \text{ Crystallinity} = \frac{\Delta H_{\text{sample}}}{\Delta H^{\circ}} \times 100 \quad (2)$$

Where, ΔH_{sample} = enthalpy of fusion of the sample (J/g)

ΔH_{PP} = enthalpy of fusion of completely crystalline (207 J/g)

Melting temperatures of PP and PP/MPPCHs nanocomposites are observed by DSC heating scan thermograms in Figure 7. The melting temperature of PP is 164.0 °C while the melting temperature of the PP/MPPCHs is around 163 °C – 164 °C. These results suggested that the additions of a compatibilizer (surlyn® ionomer) and various types of porous clay have minimal effect on the melting temperatures. The increase in thermal stability and melting temperature are due to the intercalation or the separation of the silicate layers as well as better dispersion of the silicate layers.

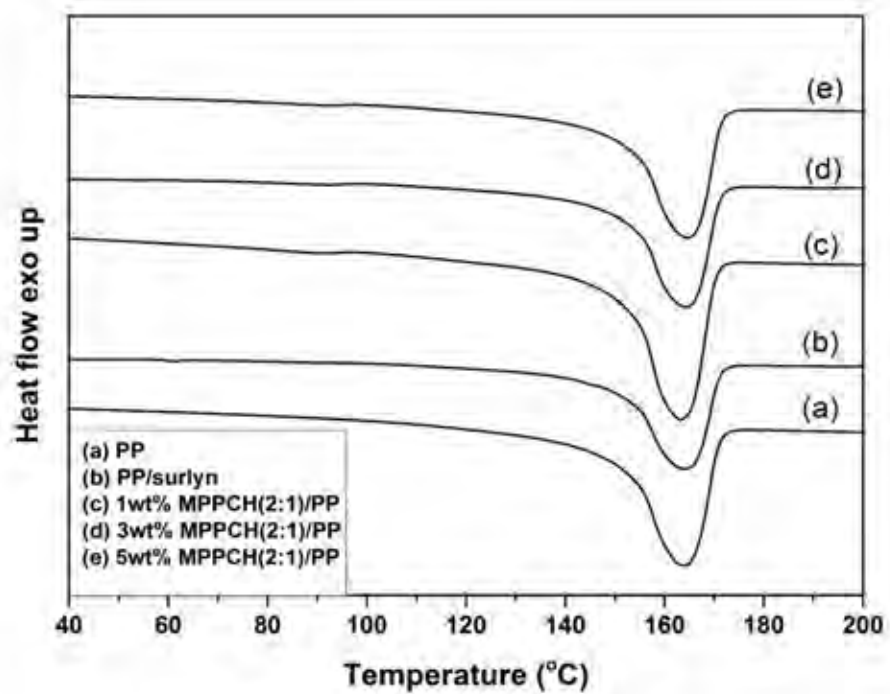


Figure 7 DSC heating scan thermograms of pure PP and PP/modified PCHs nanocomposites.

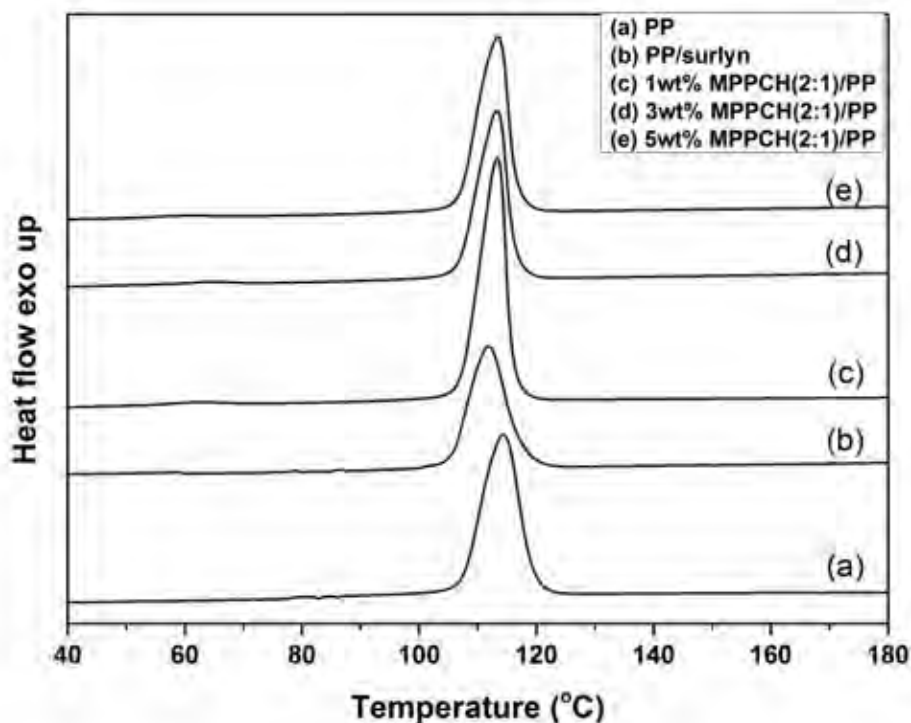


Figure 8 DSC cooling scan thermograms of pure PP and PP/modified PCHs nanocomposites.

Crystallization behaviors of PP and the nanocomposites were presented by DSC cooling scan thermograms in Figure 8 and Table 5. The results showed that the crystallization of PP was significantly affected by both the presence of a compatibilizer (surlyn®-ionomer) and modified porous clays. As shown in Figure. 8, the PP presented the crystallization temperature at 114.5 °C whereas the PP/MPPCHs exhibited similar crystallization behavior to the 2 wt% surlyn®/PP, which their crystallization peaks shifted to lower temperature and presented around 111 °C–113 °C. In addition, all PP/MPPCHs nanocomposites displayed the lower percentage of crystallinity than that of pure PP, indicating that the PP-clay interface played an important role in the crystallization behavior. These results referred to the good dispersion of modified PCHs in the PP matrix.

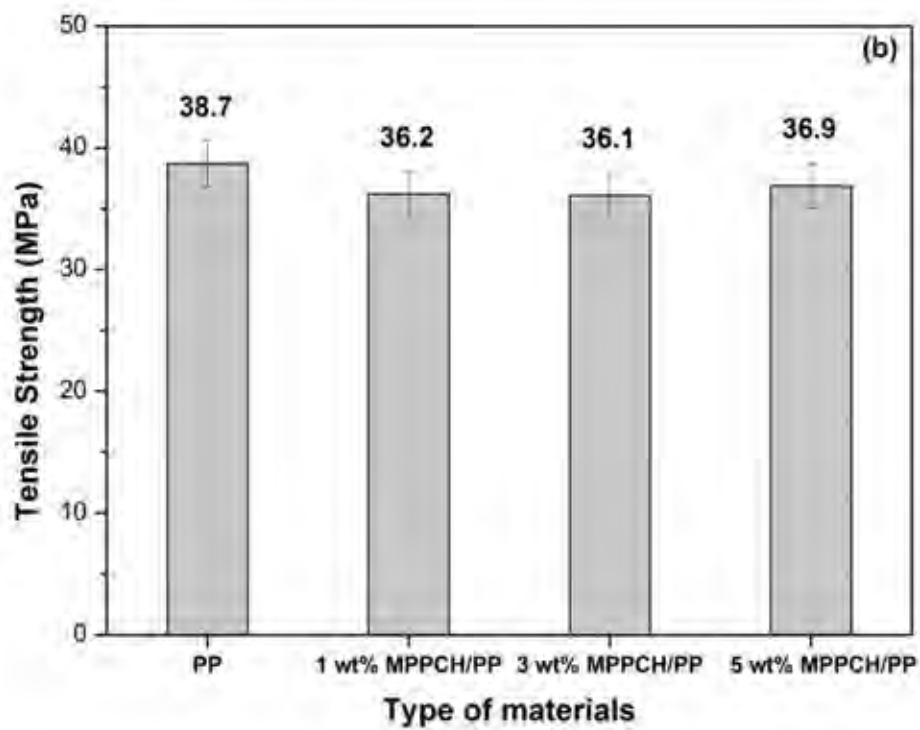
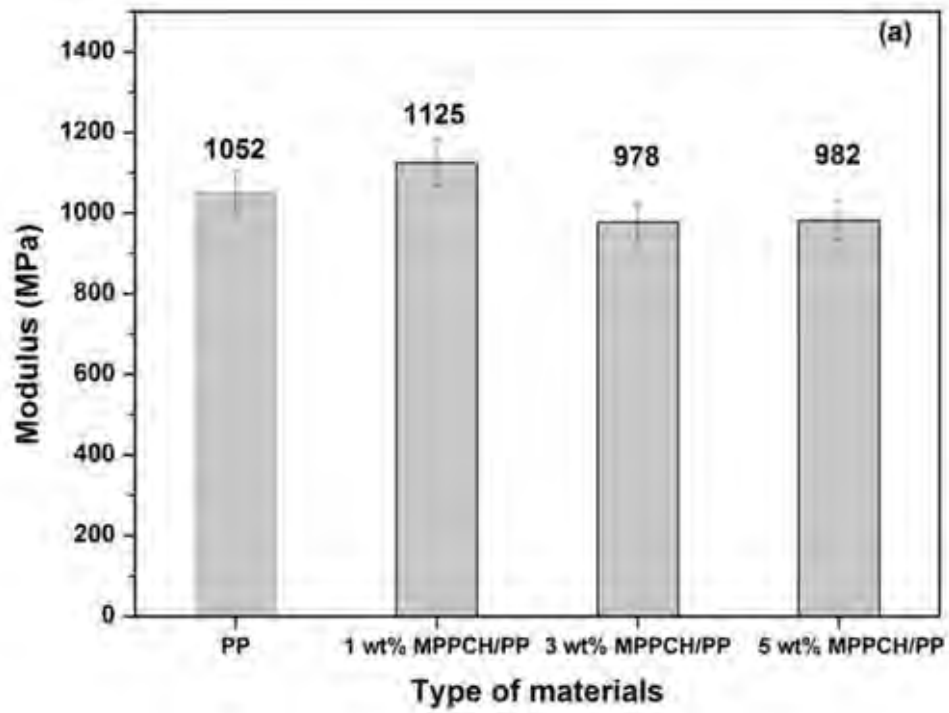
Table 5 Crystallization behavior of PP and PP/modified PCHs nanocomposites

Sample	T _c peak (°C)	T _m peak (°C)	ΔH _m (J/g)	Crystallinity (%)
PP	114.5	164.0	100.55	48.57
2 wt% Surlyn®/PP	111.5	164.1	95.05	45.00
1 wt% MPPCH(2:1)/Surlyn®/PP	113.3	163.2	91.17	42.72
3 wt% MPPCH(2:1)/Surlyn®/PP	113.2	164.2	88.33	40.53
5 wt% MPPCH(2:1)/Surlyn®/PP	113.5	164.7	92.31	41.47

5.4.8 Mechanical Property

The effect of clay contents on the mechanical property of all PP/MPPCHs nanocomposites was emphasized on the tensile modulus, tensile strength and % elongation. The results were shown in Figure 9 (a), (b) and (c), respectively. The average values of these mechanical properties were reported in Table 6. Tensile modulus and strength of 1 wt% MPPCH (2:1)/PP was greater than those of pure PP while the tensile modulus and strength of 3 wt% MPPCH (2:1)/PP and 5 wt% MPPCH (2:1)/PP were decreased. These can be described as the lower content of compatibilizer in PP/clay affects to the poor dispersion of modified porous clay in the composition. The decrease in tensile modulus and tensile strength of PP/clay nanocomposites can involve with the remaining of some impurities (quartz) in bentonite clay as inhomogeneous aggregates. The aggregations of clays or the impurities act as stress concentrators, allowing crack initiation and propagation, consequently decreasing the mechanical performance of the nanocomposites.

The percentage of elongation was represented in Figure 9 (c). The % elongation of both nanocomposites was reduced with increasing the clay contents. The reduction of elongation is due to the greater interaction between filler and polymer matrix, which probably leads to a lower polymeric chain mobility, making the material more rigid and the addition of rigid clay mineral can increase the stiffness of the material resulting in lower elongation.



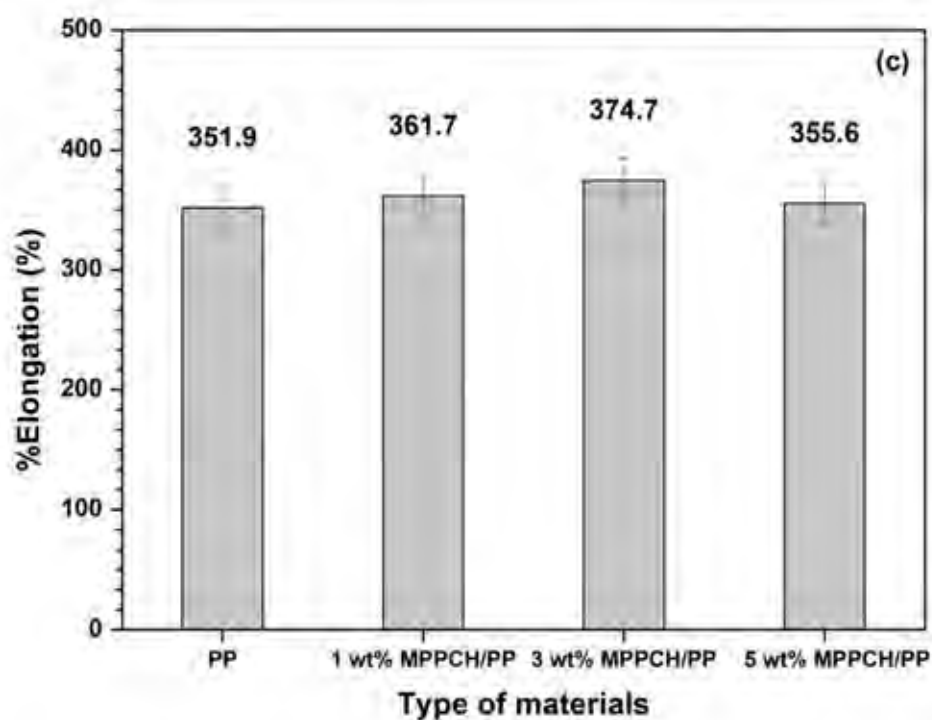


Figure 9 Mechanical properties of PP and PP/modified PCHs nanocomposite films: (a) Young's modulus (b) Tensile strength, and (c) %Elongation.

Table 6 Young's modulus, tensile strength, and % elongation of PP and PP/modified PCHs nanocomposites with various compositions

Sample	Young's Modulus (MPa)	Tensile strength (MPa)	Elongation (%)
PP	1052 ± 52.6	38.7 ± 1.9	351.9 ± 8.2
1 wt% MPPCH(2:1)/Surlyn®/PP	1125 ± 56.2	36.2 ± 1.8	361.7 ± 20.0
3 wt% MPPCH(2:1)/Surlyn®/PP	978 ± 48.9	36.1 ± 1.8	374.7 ± 23.3
5 wt% MPPCH(2:1)/Surlyn®/PP	982 ± 49.1	36.9 ± 1.8	355.6 ± 12.8

5.4.9 Ethylene Adsorption of nanocomposite films

Adsorption behaviour of ethylene gas within the PP/MPPCHs nanocomposite films was examined using gas chromatography. Figure 10 showed the amount of ethylene adsorption of PP and all the nanocomposite films. The amount of ethylene adsorption proportionally increased with the increasing of clay contents. Thus, the values of ethylene adsorption results were in the following order: 3 wt% MPPCH (2:1)/PP > 5 wt% MPPCH (2:1)/PP > 1 wt% MPPCH (2:1)/PP > PP. This was explained that the higher amount of clay led to the better ethylene adsorption. It concluded that the thiol group on the surface of clay adsorbed the ethylene gas and the amount of clay also affected to ethylene adsorption ability. In conclusion, 3 wt% MPPCH (2:1)/PP nanocomposite film performed the best ethylene adsorption threshold.

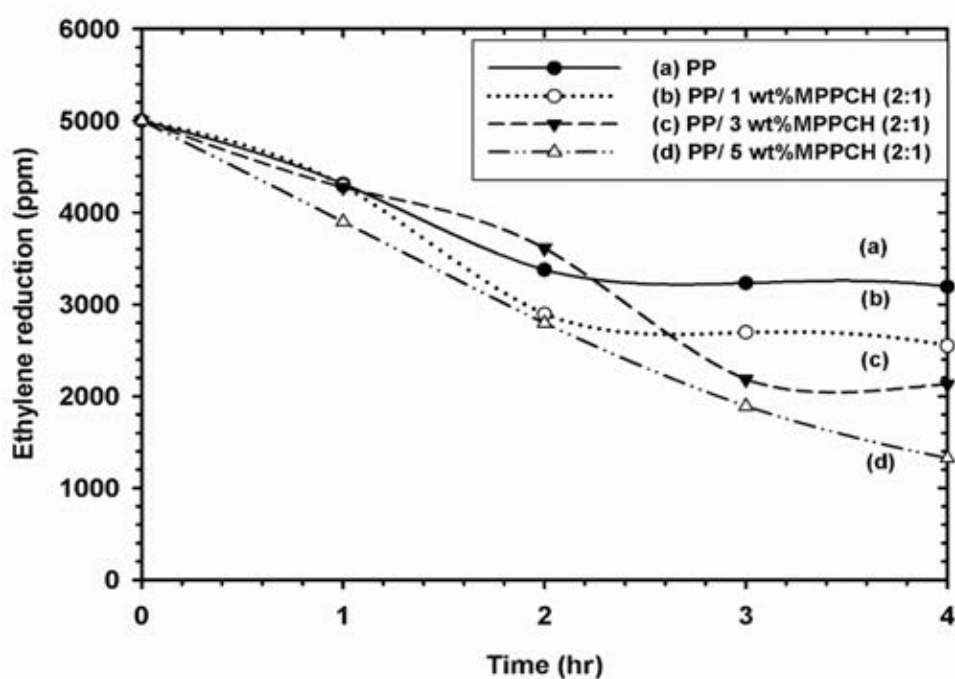


Figure 10 Ethylene reduction capacity of PP, 1 wt% MPPCH (2:1)/PP, 3 wt% MPPCH (2:1)/PP, and 5 wt% MPPCH (2:1)/PP nanocomposite films.

5.4.10 Conductivity of Nanocomposite Films

PP/modified PCHs nanocomposite films were the films which consisted of the modified PCHs; functionalizing with thiol group (–SH) that effected to the conductivity of the films. Whereas, PP is an insulator film, its conductivity did not change when adsorbed the ethylene gas. After studying the ethylene adsorption behaviour, the PP and PP/MPPCHs nanocomposite films were further evaluated the conductivity when they adsorbed the ethylene gas. The conductivity of PP/modified porous clay nanocomposite films decreased with time increasing. Hence, it replied that thiol group in the modified PCHs caused the reduction of the conductivity when the films interacted with the ethylene gas. In addition, the higher content of clay leads to the higher of the conductivity of the PP/modified porous clay nanocomposite films at the beginning. Finally, it can conclude that the PP/modified PCHs nanocomposite films performed significantly conductivity changing comparing to PP.

Table 7 Conductivity of polypropylene (PP) and PP/modified PCHs nanocomposite films

Samples	Conductivity* (Before) (S/cm)	Conductivity** (After) (S/cm)
Polypropylene (PP)	5.18×10^{-19}	5.18×10^{-19}
1 wt% MPPCH(2:1)/Surlyn®/PP	3.22×10^{-17}	7.92×10^{-19}
3 wt% MPPCH(2:1)/Surlyn®/PP	6.55×10^{-17}	5.61×10^{-18}
5 wt% MPPCH(2:1)/Surlyn®/PP	1.75×10^{-17}	2.18×10^{-18}

Note * Conductivity of materials before ethylene gas adsorption.

** Conductivity of materials after ethylene gas adsorption.

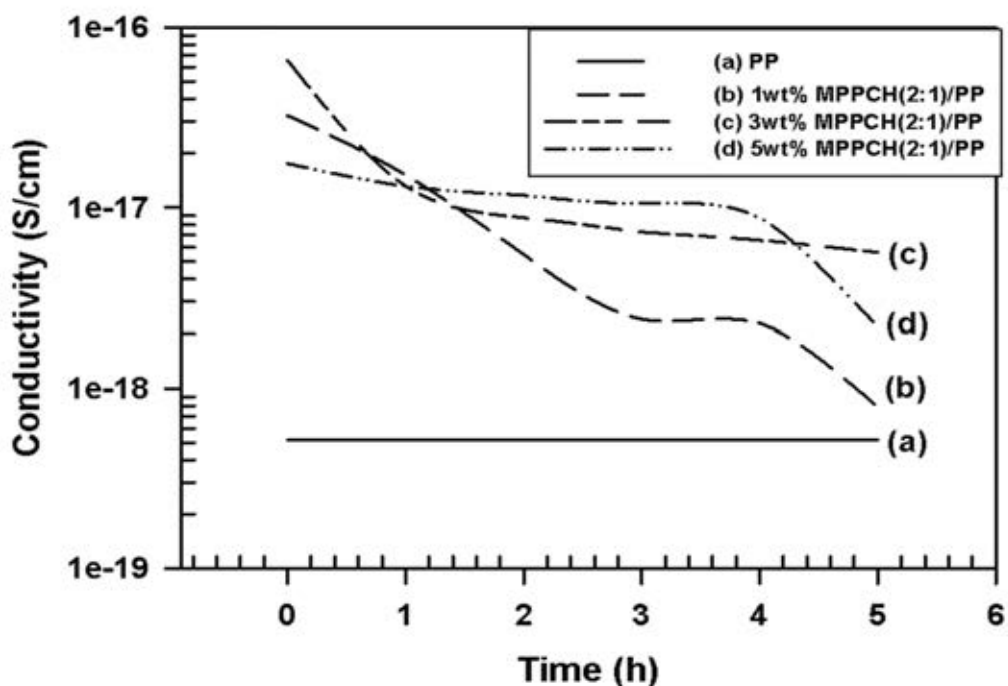


Fig11. The conductivity of PP and PP/modified PCHs nanocomposite films as a function of ethylene adsorption time.

5.5 Conclusion

In this work, the modified porous clay heterostructure was successfully synthesized through the surfactant-directed assembly of the interlayer spaces of bentonite and then functionalized with MPTMS/TEOS in molar ratios of 1:1, 2:1 and 4:1 via the co-condensation reaction leading to form micelles in the interlayer spaces of the bentonite. After surface modification, modified MPPCHs revealed the roughness surface and showed high specific surface areas and porosity comparing to the bentonite. From the ethylene adsorption results, the modified MPPCHs had higher efficiency in ethylene adsorption than that of bentonite because the organic group (thiol) that incorporated in the PCH led to a non-polar surface, which caused better ethylene adsorption. In addition, conductivity of all modified MPPCHs displayed higher conductivity than bentonite. The MPPCH (4:1) exhibited a great synergy

between ethylene adsorption and conductivity results. For the nanocomposite materials, the modified PCHs (MPPCHs) improve the thermal property of the nanocomposite due to the higher degradation temperature. However, high load of MPPCHs in PP possibly causes the drawback in nanocomposite film in term of stiffness. Loading of 3% by weight of MPPCH in PP nanocomposite is recommended. The PP/modified PCHs (MPPCHs) nanocomposite materials definitely present the better ethylene adsorption, greater conductivity value, and sharp retention of conductivity. Overall, modified PCHs (MPPCHs) and their nanocomposite films exhibit good performance as ethylene scavenger/sensor materials to be applied in the smart packaging.

5.6 Acknowledgment

This work are financially supported by 90th Anniversary of the Chulalongkorn University Fund (Ratchadaphiseksomphot Endowment Fund). Partially funds are supported by the the Petroleum and Petrochemical College and Centre of Excellent on Petrochemical and Materials Technology, Thailand.

5.7 References

1. Hassan FAS, Mahfouz SA (2012) Effect of 1-methylcyclopropene (1-MCP) on the postharvest senescence of coriander leaves during storage and its relation to antioxidant enzyme activity. *Scientia Horticulturae* 141:69-75. doi:<http://dx.doi.org/10.1016/j.scienta.2012.04.021>
2. Li L, Kaplunov T, Zutahy Y, Daus A, Porat R, Lichter A (2015) The effects of 1-methylcyclopropane and ethylene on postharvest rachis browning in table grapes. *Postharvest Biology and Technology* 107:16-22. doi:<http://dx.doi.org/10.1016/j.postharvbio.2015.04.001>
3. Meyer MD, Terry LA (2010) Fatty acid and sugar composition of avocado, cv. Hass, in response to treatment with an ethylene scavenger or 1-methylcyclopropene to extend storage life. *Food Chemistry* 121 (4):1203-1210. doi:<http://dx.doi.org/10.1016/j.foodchem.2010.02.005>

4. Rao TVR, Gol NB, Shah KK (2011) Effect of postharvest treatments and storage temperatures on the quality and shelf life of sweet pepper (*Capsicum annum* L.). *Scientia Horticulturae* 132:18-26. doi:<http://dx.doi.org/10.1016/j.scienta.2011.09.032>
5. Terry LA, Ilkenhans T, Poulston S, Rowsell L, Smith AWJ (2007) Development of new palladium-promoted ethylene scavenger. *Postharvest Biology and Technology* 45 (2):214-220. doi:<http://dx.doi.org/10.1016/j.postharvbio.2006.11.020>
6. Aharoni Y, Copel A, Gil M, Fallik E (1996) Polyolefin stretch films maintain the quality of sweet corn during storage and shelf-life. *Postharvest Biology and Technology* 7 (1-2):171-176. doi:[http://dx.doi.org/10.1016/0925-5214\(95\)00017-8](http://dx.doi.org/10.1016/0925-5214(95)00017-8)
7. Azeredo HMCd (2009) Nanocomposites for food packaging applications. *Food Research International* 42 (9):1240-1253. doi:<http://dx.doi.org/10.1016/j.foodres.2009.03.019>
8. Bodbodak S, Moshfeghifar M (2016) 4 - Advances in modified atmosphere packaging of fruits and vegetables A2 - Siddiqui, Mohammed Wasim. In: *Eco-Friendly Technology for Postharvest Produce Quality*. Academic Press, pp 127-183. doi:<http://dx.doi.org/10.1016/B978-0-12-804313-4.00004-9>
9. de Chiara MLV, Pal S, Licciulli A, Amodio ML, Colelli G (2015) Photocatalytic degradation of ethylene on mesoporous TiO₂/SiO₂ nanocomposites: Effects on the ripening of mature green tomatoes. *Biosystems Engineering* 132:61-70. doi:<http://dx.doi.org/10.1016/j.biosystemseng.2015.02.008>
10. Fagundes C, Moraes K, Pérez-Gago MB, Palou L, Maraschin M, Monteiro AR (2015) Effect of active modified atmosphere and cold storage on the postharvest quality of cherry tomatoes. *Postharvest Biology and Technology* 109:73-81. doi:<http://dx.doi.org/10.1016/j.postharvbio.2015.05.017>
11. González-Aguilar GA, Buta JG, Wang CY (2003) Methyl jasmonate and modified atmosphere packaging (MAP) reduce decay and maintain postharvest quality of papaya 'Sunrise'. *Postharvest Biology and Technology* 28 (3):361-370. doi:[http://dx.doi.org/10.1016/S0925-5214\(02\)00200-4](http://dx.doi.org/10.1016/S0925-5214(02)00200-4)
12. Llorens A, Lloret E, Picouet PA, Trbojevič R, Fernandez A (2012) Metallic-based micro and nanocomposites in food contact materials and active food packaging. *Trends in Food Science & Technology* 24 (1):19-29. doi:<http://dx.doi.org/10.1016/j.tifs.2011.10.001>

13. Silvestre C, Duraccio D, Cimmino S (2011) Food packaging based on polymer nanomaterials. *Progress in Polymer Science* 36 (12):1766-1782. doi:<http://dx.doi.org/10.1016/j.progpolymsci.2011.02.003>
14. Sothornvit R, Rodsamran P (2008) Effect of a mango film on quality of whole and minimally processed mangoes. *Postharvest Biology and Technology* 47 (3):407-415. doi:<http://dx.doi.org/10.1016/j.postharvbio.2007.08.005>
15. Waghmare RB, Annapure US (2013) Combined effect of chemical treatment and/or modified atmosphere packaging (MAP) on quality of fresh-cut papaya. *Postharvest Biology and Technology* 85:147-153. doi:<http://dx.doi.org/10.1016/j.postharvbio.2013.05.010>
16. Srithammaraj K, Magaraphan R, Manuspiya H (2012) Modified Porous Clay Heterostructures by Organic–Inorganic Hybrids for Nanocomposite Ethylene Scavenging/Sensor Packaging Film. *Packaging Technology and Science* 25 (2):63-72. doi:10.1002/pts.958
17. Srithammaraj K, Magaraphan R, and Manuspiya H. (2008) Surfactant-Templated Synthesis of Modified Porous Clay Heterostructure (PCH). *Advanced Materials Research* 55-57:317-320. doi:10.4028/www.scientific.net/AMR.55-57.317
18. Nakatsuji M, Ishii R, Wang Z-M, Ooi K (2004) Preparation of porous clay minerals with organic–inorganic hybrid pillars using solvent-extraction route. *Journal of Colloid and Interface Science* 272 (1):158-166. doi:<http://dx.doi.org/10.1016/j.jcis.2003.11.039>
19. Polverejan M, Liu Y, Pinnavaia TJ (2002) Aluminated Derivatives of Porous Clay Heterostructures (PCH) Assembled from Synthetic Saponite Clay: Properties as Supermicroporous to Small Mesoporous Acid Catalysts. *Chemistry of Materials* 14 (5):2283-2288. doi:10.1021/cm011559g
20. Polverejan M, Pauly TR, Pinnavaia TJ (2000) Acidic Porous Clay Heterostructures (PCH): Intragallery Assembly of Mesoporous Silica in Synthetic Saponite Clays. *Chemistry of Materials* 12 (9):2698-2704. doi:10.1021/cm0002618
21. Zhou C, Li X, Ge Z, Li Q, Tong D (2004) Synthesis and acid catalysis of nanoporous silica/alumina-clay composites. *Catalysis Today* 93–95:607-613. doi:<http://dx.doi.org/10.1016/j.cattod.2004.06.014>

22. Chmielarz L, Kuśtrowski P, Drozdek M, Dziembaj R, Cool P, Vansant EF (2006) Selective catalytic oxidation of ammonia into nitrogen over PCH modified with copper and iron species. *Catalysis Today* 114 (2–3):319-325. doi:<http://dx.doi.org/10.1016/j.cattod.2006.01.020>
23. Chmielarz L, Kuśtrowski P, Dziembaj R, Cool P, Vansant EF (2007) Selective catalytic reduction of NO with ammonia over porous clay heterostructures modified with copper and iron species. *Catalysis Today* 119 (1–4):181-186. doi:<http://dx.doi.org/10.1016/j.cattod.2006.08.017>
24. Hess C (2013) 7.10 - Ordered Mesoporous and Microporous Materials with Heteroatoms A2 - Reedijk, Jan. In: Poepelmeier K (ed) *Comprehensive Inorganic Chemistry II* (Second Edition). Elsevier, Amsterdam, pp 231-245. doi:<http://dx.doi.org/10.1016/B978-0-08-097774-4.00732-4>
25. Wei L, Tang T, Huang B (2004) Novel acidic porous clay heterostructure with highly ordered organic–inorganic hybrid structure: one-pot synthesis of mesoporous organosilica in the galleries of clay. *Microporous and Mesoporous Materials* 67 (2–3):175-179. doi:<http://dx.doi.org/10.1016/j.micromeso.2003.11.002>
26. Zub YL, Melnyk IV, Stolyarchuk NV, Dobryanska HI, Barczak M, Dabrowski A (2005) Comparative characteristics of texture and properties of hybrid organic–inorganic adsorbents functionalized by amine and thiol groups. *Progress in Solid State Chemistry* 33 (2–4):179-186. doi:<http://dx.doi.org/10.1016/j.progsolidstchem.2005.11.028>
27. de Mello Ferreira Guimarães A, Ciminelli VST, Vasconcelos WL (2009) Smectite organofunctionalized with thiol groups for adsorption of heavy metal ions. *Applied Clay Science* 42 (3–4):410-414. doi:<http://dx.doi.org/10.1016/j.clay.2008.04.006>
28. Delacôte C, Gaslain FOM, Lebeau B, Walcarius A (2009) Factors affecting the reactivity of thiol-functionalized mesoporous silica adsorbents toward mercury(II). *Talanta* 79 (3):877-886. doi:<http://dx.doi.org/10.1016/j.talanta.2009.05.020>
29. Diaz M, Cambier P, Brendlé J, Prost R (2007) Functionalized clay heterostructures for reducing cadmium and lead uptake by plants in contaminated soils. *Applied Clay Science* 37 (1–2):12-22. doi:<http://dx.doi.org/10.1016/j.clay.2006.11.002>
30. Liang X, Xu Y, Sun G, Wang L, Sun Y, Qin X (2009) Preparation, characterization of thiol-functionalized silica and application for sorption of Pb²⁺ and Cd²⁺. *Colloids*

- and Surfaces A: Physicochemical and Engineering Aspects 349 (1–3):61-68.
doi:<http://dx.doi.org/10.1016/j.colsurfa.2009.07.052>
31. Mercier L, Pinnavaia TJ (1998) A functionalized porous clay heterostructure for heavy metal ion (Hg^{2+}) trapping. *Microporous and Mesoporous Materials* 20 (1–3):101-106. doi:[http://dx.doi.org/10.1016/S1387-1811\(97\)00019-X](http://dx.doi.org/10.1016/S1387-1811(97)00019-X)
32. Rostamian R, Najafi M, Rafati AA (2011) Synthesis and characterization of thiol-functionalized silica nano hollow sphere as a novel adsorbent for removal of poisonous heavy metal ions from water: Kinetics, isotherms and error analysis. *Chemical Engineering Journal* 171 (3):1004-1011.
doi:<http://dx.doi.org/10.1016/j.cej.2011.04.051>
33. Nunes CD, Pires J, Carvalho AP, Calhorda MJ, Ferreira P (2008) Synthesis and characterisation of organo-silica hydrophobic clay heterostructures for volatile organic compounds removal. *Microporous and Mesoporous Materials* 111 (1–3):612-619.
doi:<http://dx.doi.org/10.1016/j.micromeso.2007.09.008>
34. Tonlé IK, Ngameni E, Tcheumi HL, Tchiéda V, Carteret C, Walcarius A (2008) Sorption of methylene blue on an organoclay bearing thiol groups and application to electrochemical sensing of the dye. *Talanta* 74 (4):489-497.
doi:<http://dx.doi.org/10.1016/j.talanta.2007.06.006>
35. Mekhloufi M, Zehhaf A, Benyoucef A, Quijada C, Morallon E (2013) Removal of 8-quinolinecarboxylic acid pesticide from aqueous solution by adsorption on activated montmorillonites. *Environmental Monitoring and Assessment* 185 (12):10365-10375.
doi:10.1007/s10661-013-3338-5
36. Zehhaf A, Benyoucef A, Quijada C, Taleb S, Morallón E (2015) Algerian natural montmorillonites for arsenic(III) removal in aqueous solution. *International Journal of Environmental Science and Technology* 12 (2):595-602.
doi:10.1007/s13762-013-0437-3

CHAPTER VI
SILVER-LOADED ON THE SURFACE OF THE POROUS CLAY
HETEROSTRUCTURE (PCH) FOR USING AS ETHYLENE SCAVENGER
IN FOOD PACKAGING

6.1 Abstract

Silver element (Ag) has significant characteristics and advantages such as stable shelf-life, excellent conductor, ethylene scavenger, and antimicrobial. For producing a new ethylene scavenger/sensor film, silver (Ag) was deposited on the surface of the porous clay heterostructure (PCH) which had been prepared by the surfactant-directed assembly of mesostructured silica and synthesized via the polymerization of tetraethoxysilane (TEOS), designated as Ag-PCH. The Ag-PCH was synthesized with various weight percentages of silver (Ag), presented as (N) wt% Ag-PCH. According to the results, the 1 wt%, 3 wt%, and 5 wt% of (N) wt%Ag-PCHs were blended with polypropylene (PP) and fabricated into the nanocomposite films. The characteristics of Ag-PCH and (N)wt%Ag-PCH/PP nanocomposite films were investigated. Additionally, the ethylene adsorption of Ag-PCH was measured by GC. This material is expected to use as freshness indicator packaging.

Keyword: Silver (Ag), Porous clay Heterostructure (PCH), Ethylene scavenger, conductivity, freshness indicator packaging

6.2 Introduction

Ethylene (C₂H₄) acts as a plant hormone which accelerates respiration, leading to maturity and senescence, and ripening of many kinds of fruits. Furthermore, ethylene accumulation can cause yellowing of green vegetables and may be responsible for a number of specific post harvest disorders in fresh fruits and

vegetables. Ethylene can also be removed by using a number of chemical processes. There are many ethylene scavengers such as KMnO_4 , activated carbon, zeolite, and clay. Porous clay heterostructure (PCH) was chosen to study in this work due to the high specific surface areas which show a great amount of gas adsorption. A new PCH was introduced and synthesized by loading silver (Ag) inside the pore structure to perform in ethylene adsorption. Silver (Ag) has significant characteristics and advantages such as stable shelf-life, excellent conductor, ethylene scavenger, and antimicrobial [1-8]. Since the earliest published reports of the antimicrobial properties of silver colloids, silver nanoparticles (AgNP) have been found to be potent agents against numerous species of bacteria, such as *E. coli*, *Enterococcus faecalis*, and *Staphylococcus (aureus and epidermidi)*. AgNPs are also effective against strains of these organisms that are resistant to potent chemical antimicrobials, including MRSA, MRSE, vancomycin-resistant *Enterococcus* (VRE) and extended-spectrum β -lactamase (ESBL) producing *Klebsiella*. In addition, AgNPs are toxic to fungi [9-12]. While AgNPs do likely serve as a source of Ag^+ ions, they may have additional antimicrobial mechanisms. For instance, when normalizing for released Ag^+ concentration, AgNPs have been found to be more toxic to algae than equivalent dosages of AgNO_3 . Contrasting the study cited above, a separate report found that AgNPs had great effectiveness against silver resistant strains of *P. mirabilis* and *E. coli* and highlighted the fact that particles of different sizes, shapes or other characteristics may behave differently, even in the same [13-16].

One of the biggest advantages of inorganic nanoparticles over molecular antimicrobials is the ease with which the former can be incorporated into polymers to form functional antimicrobial materials. This is especially true due to the controlled release properties of AgNPs, which can be engineered to remain potent antimicrobial agents for long periods of time. Thus, AgNP/ polymer nanocomposites are attractive materials for use in both medical devices as well as food packaging materials to preserve shelf life. In addition, since silver particles catalyze the destruction of ethylene gas, fruits stored in the presence of AgNPs have slower ripening times and thus extended shelf lives [17-20]. Despite all of these advances in the use of silver nanostructures for food packaging applications, comprehensive studies in various polymeric systems are still lacking, and much work needs to be done to elucidate key

relationships that influence the antimicrobial strength of various AgNP-based PNC materials [21].

In this work, silver was synthesized in the PCH and evaluated the efficiency in ethylene adsorption to use as ethylene scavenger. The conductivity property of silver was further investigated to present the higher conductivity property and displayed as ethylene scavenger sensor for using in active and smart packagings.

6.3 Materials and Methods

6.3.1 Chemicals and Raw Materials

Pristine sodium bentonite (Na-BTN), with a cation exchange capacity (CEC) of 44.5 meq/100g, was kindly supplied by Thai Nippon Chemical Industry Co., LTD. (Thailand). Cetyltrimethylammonium Chloride (CTAC), performing as the cationic surfactant, and chemical substances such as tetraethoxysilane, silver nitrate (AgNO_3), and ascorbic acid were purchased from Fluka and Acros, respectively. PP (Moplen HP525N, MFI 11) and Surlyn® (PC 350, MFI 5) were provided by HMC Polymers Co., Ltd. (Thailand) and DuPont™.

6.3.2 Synthesis of Porous Clay Heterostructures (PCHs)

Purified bentonite was changed into a quaternary ammonium exchange form by ion exchange with cetyltrimethylammonium chloride (CTAC) and was stirred at 50 °C. After that, the sample was filtered, washed with a mixture of methanol and water, and then air-dried overnight. The obtained organoclay was stirred in dodecylamine at 50 °C for 30 min before adding the tetraethoxysilane (TEOS) at a molar ratio of organoclay:dodecylamine:TEOS of 1:20:150. The resulting suspension was stirred at 37 °C for 4 hours. The suspension was filtered and air-dried overnight to form the as synthesized PCH. Then the surfactant was removed from the as-synthesized PCH by solvent extraction using a mixture of methanol and HCl solution. Typically, 1 g of the as-synthesized PCH was added to 5 ml of HCl and 45 ml of methanol, and was refluxed for 2 hours.

6.3.3 Synthesis of Silver-Loaded Porous Clay Heterostructures

Next, PCH was suspended in the mixture of AgNO_3 and ethanol with various contents of silver in 1 wt%, 5 wt%, 10 wt%, 20 wt%, and 30 wt% to PCHs at 30 °C. After 1 hour, the 0.1 M ascorbic acid was dropped into the suspension to reduce Ag^+ to Ag^0 , designated as Ag-PCH. The Ag-PCH was collected by filtration and air-dried overnight

6.3.4 Preparation of Polypropylene/clay Nanocomposite Film

The 1wt%, 3wt%, and 5wt% of Ag-PCHs, 2wt% of surlyn®, and PP were prepared by using twin-screw extruder (Labtech) with an L/D ratio of 40 and a screw diameter of 20 mm. The operation temperature was performed at 160, 165, 170, 175, 180, 185, 190, 200, 210 and 215°C from hopper to die respectively and the screw speed was 30 rpm.

6.3.5 Fabrication of Nanocomposite Films

The nanocomposite films were prepared by using blown film extrusion machine. The nanocomposite pellets were dried in an oven prior to blowing. The following extrusion conditions were employed at the rotation speed of the screw around 50 rpm and the blowing ratio was 1.52. The barrel and mold temperature were 210 °C. The thickness of the films was controlled to about 40 μm .

6.3.6 Characterization

6.3.6.1 *X-Ray Fluorescence Spectrometry (XRF)*

The elemental analysis of the pristine clay and the modified PCHs was carried out by using X-ray fluorescence technique. The excitation source was an X-ray tube with thin silver as the primary filter, operating at a tube voltage of 35 kV.

6.3.6.2 *X-Ray Diffractometry (XRD)*

An X-ray diffractometer (XRD) was used to obtain the *d*-value of the bentonite and the organoclay to investigate the crystal structure of materials. The ray-X diffraction patterns were measured on a Rigaku Model Dmax 2002 diffractometer with Ni-filtered $\text{CuK}\alpha$ in WAXS mode operation at 45 kV, 200

mA, and on the 2θ range of 2 degree – 10 degree with a scan speed of 0.5 degrees/min and a scan step 0.02 degree. SAXS mode was operated on the 2θ range of 0.1 to 8 degrees with a scan speed of 0.5 degrees/min and a scan step 0.02 degrees.

6.3.6.3 *Surface Area Analysis (SAA)*

The N₂ adsorption desorption–isotherms were obtained at -196°C on a Sorptomatic analyzer. The samples were degassed at 150°C for 15 h in a vacuum furnace before analysis. Specific surface areas were calculated using the BET equation. The pore size distributions were constructed based on The Barrett, Joyner, and Halenda (BJH) method using the adsorption branch of the nitrogen isotherm.

6.3.6.4 *Scanning Electron Microscopy (SEM)*

Scanning electron microscopy was performed with Hitachi S-4800 Model to observe the surface morphology of all modified PCHs at 5 kV. The samples were sputtered with a thin layer of platinum for 180 seconds prior to the observation.

6.3.6.5 *Transmission electron microscopy (TEM)*

JEOL Ltd, Tokyo, Japan was supplied for JEM-1400 electron microscope with an accelerating voltage of 100kV to observe structure of the pores and shape of the silver. The magnification was 60,000 times–80,000 times. The samples were supported on 300 mesh copper grids.

6.3.6.6 *X-ray photoelectron spectroscopy (XPS)*

The structure of modified PCHs were examined by XPS (Kratos axis ultra DLD model) with a monochromatic x-ray source (Al K_α anode). The base pressure during experiments was 3×10^{-9} Torr and analyzed area was $700 \times 300 \mu\text{m}^2$. Pass energy 160 eV was used for wide scan in order to get percentage of atomic concentration of Si2p, C1s, O1s and Ag3d compositions. Moreover, for quantitative analysis, narrow scan with pass energy 80 eV was used for Si2p, C1s, O1s and Ag3d spectra. Then all spectra were referred to the Ag3d peak at 368 eV and 374 eV.

6.3.6.7 *Differential scanning calorimetry (DSC)*

Differential Scanning Calorimeter (METTLER, DSC822) was used to measure the crystallization and melting behavior of the PP/modified PCHs nanocomposites. The samples were heated and cooled from 30-200 °C, using a heating/cooling rate of 10 °C min⁻¹ in a nitrogen.

6.3.6.8 Thermogravimetric Analysis (TGA)

TGA analysis was performed with a TA Instruments TGA 2950 over a temperature range 30-700 °C at a heating rate of 10 °C/min under N₂ atmosphere of 200 ml/min. The decomposition temperature and weight loss were measured.

6.3.6.9 Tensile Properties

Tensile test of PP/modified porous clay nanocomposite films were carried out by a LLOYD Universal Testing Machine model 4206 by ASTM D 638. A gage length of 50 mm was employed with a crosshead speed of 50 mm/min and preload 0.01 N.

6.3.6.10 Ethylene Adsorption

A gas chromatograph (Model 910, BUCK Scientific) with a helium ionization detector was utilized to examine the ethylene adsorption capacity of the porous clays. Ethylene was injected into a chamber to give a specific concentration of 5000 ppm. Ethylene concentration in the chamber was measured periodically, about once per hour. The ethylene adsorption was calculated by taking the difference between the amount of ethylene added and the amount remaining in the headspace.

6.3.6.11 Conductivity Measurement

The electrical conductivity of the mesoporous materials were observed using Impedance test by LCR meter (Agilent E4980A) as the function between Z (ohm) and θ (radian). The clay pellets were covered with platinum and placed between the 2 probes and the tests were run at 20 Volts with varying frequency from 20 Hz to 1 MHz. Finally, the results were calculated by Nyquist's plot to obtain the semi circle and find the resistivity from the intersect of x axis at the high frequency.

6.3.6.12 Keithley Electrometer for Conductivity Measurement

The electrical conductivity of the nanocomposite films were observed using Keithley Electrometer with 6517B Hi-R test. The film was placed between the 2 probes in the vacuum box. The tests were run by varying the voltages in 1, 5, 10, 20 and 100 Volts and then calculated the electrical conductivity from plotting between the current and the applied voltage. The volume resistivity was calculated by Equation (1).

$$\text{Volume resistivity} = \frac{22.9}{\text{thickness,cm}} \times \frac{V}{I} \text{ (ohm} \cdot \text{cm)} \quad (1)$$

6.4 Results and Discussions

6.4.1 Crystallography of Bentonite and modified PCHs

Bentonite (BTN) was stirred with cetyltrimethylammonium chloride (CTAC) to prepare the organoclay. Bentonite and organoclay have a long period structure due to the corresponding XRD diffraction peaks. As seen from Figure 1, the basal spacing of BTN was 1.16 nm (Figure 1(a)). After BTN was treated with CTAC, the new peaks were observed at lower angle (Figure 1 (b)) indicating the increasing of distance between clay layers. The d-spacing of organoclay was 1.90 nm. The results are shown in Table 1.

Table 1 Basal spacing of BTN, organoclay, and porous clay

Sample	2θ (degree)	d-value (nm)
Bentonite	7.62	1.16
Organoclay	4.64	1.90

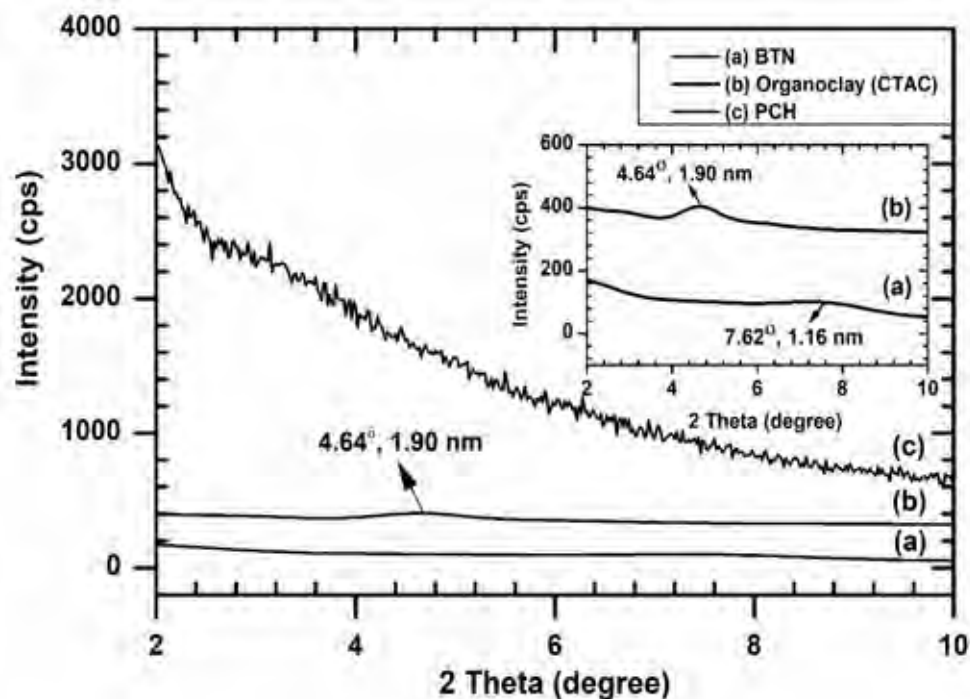


Figure 1 XRD patterns of (a) Bentonite, (b) organoclay (CTAC), and (c) PCH.

After porous modification with silica source, the PCH was examined by SAXS mode (Rigaku Corporation, Japan). In figure 1(c), the results showed that there were no diffraction peaks like BTN and organoclay. Disorder of silica framework which was formed in the galleries of clay and highly shielded the regular inter-stratifications of the clay layers. So the XRD patterns in figure 1 (c) showed only diffuse scattering. It meant that the structure of PCH was pore structure not long period structure. The average pore diameter of PCH was 3.18 nm.

Figure 2 shows XRD patterns of different various ratio of silver content of all Ag-PCHs. Five peaks at 2θ values of 38.0760, 44.2751, 64.3916, and 77.3401 deg corresponding to (111), (200), (220), and (311) planes of Silver are observed and compared with the standard powder diffraction card of DB card number (00-001-1167) [7]. The XRD study indicates that the silver particle successfully embedded in the PCHs.

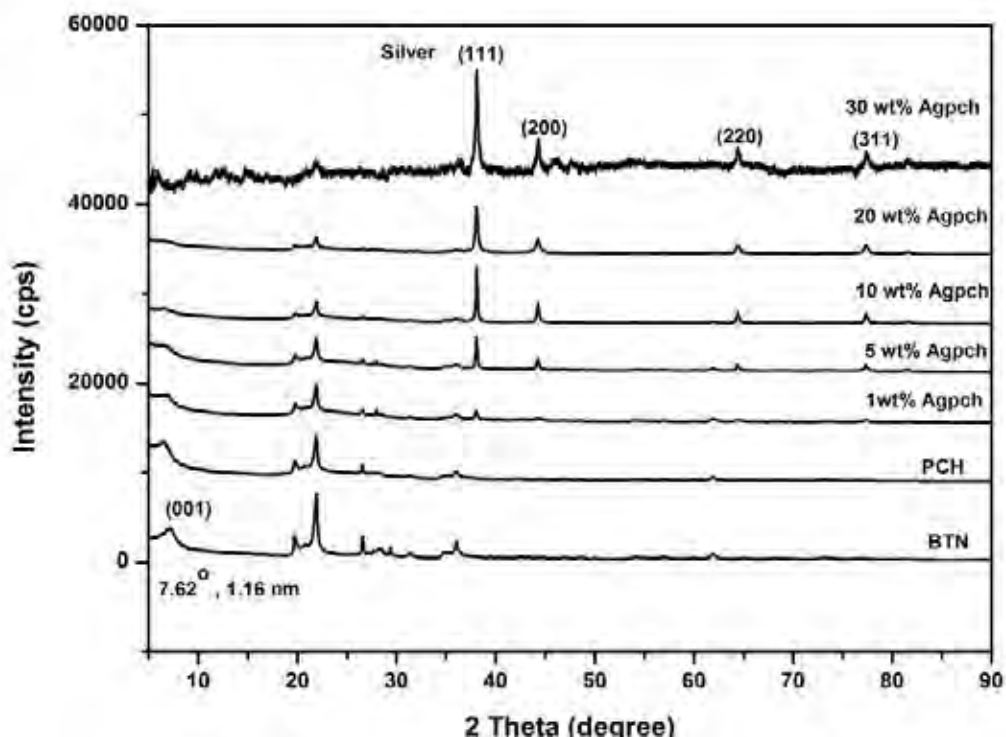
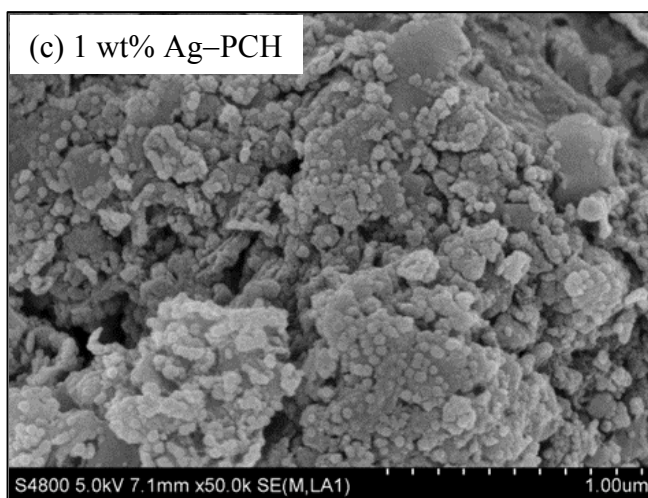
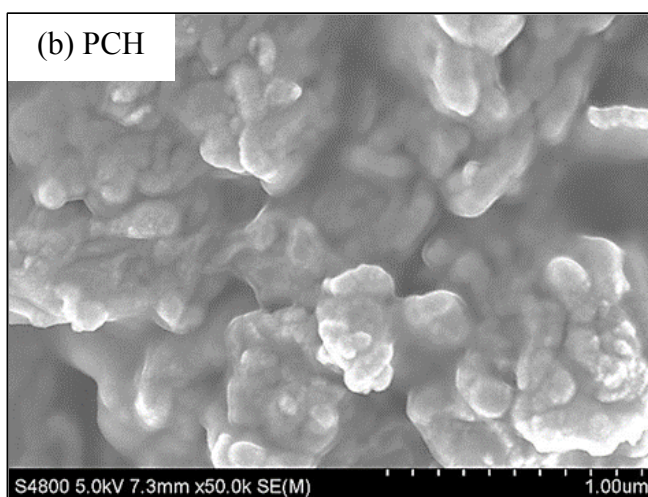
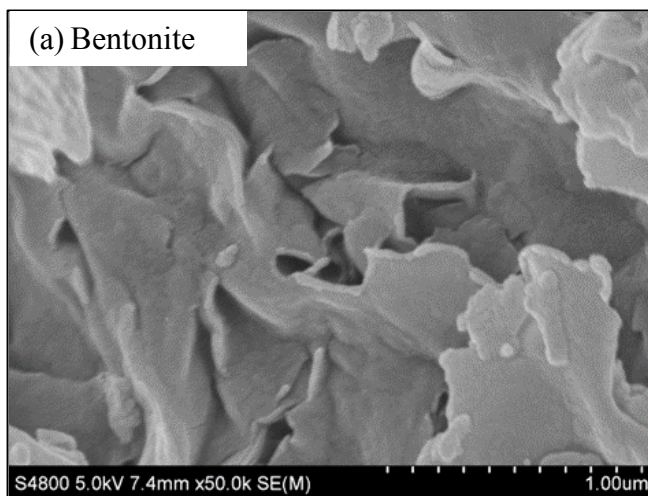
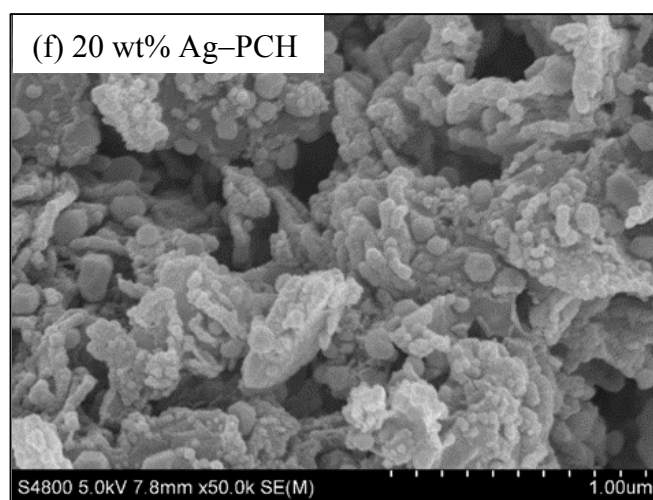
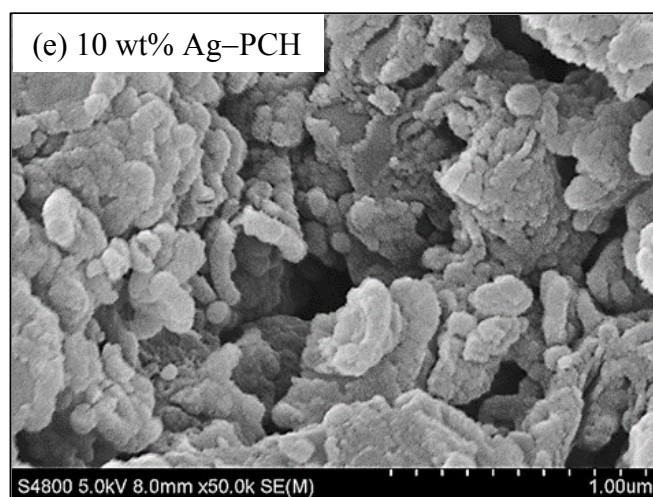
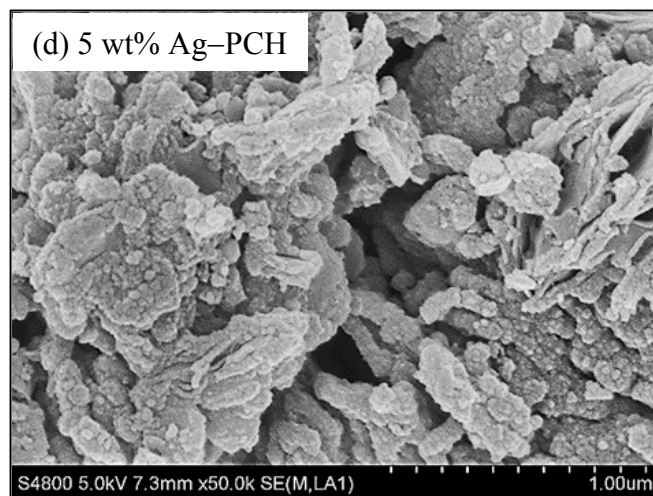


Figure 2 XRD patterns of Bentonite (BTN), porous clay heterostructure (PCH) and all modified PCHs (Ag–PCHs).

6.4.2 Morphology of Bentonite and Modified PCHs

Normally, the Bentonite exhibited a layered or plate-like structure in SEM image (Figure 3(a)). After porous modification, the SEM images of all Ag–PCHs (Figure 3(b) –3(g)) revealed a roughness on the surface of clay layers comparing to pristine clay. Moreover, increasing the weight ratio of silver caused much small grains on the top of the surface of clay.





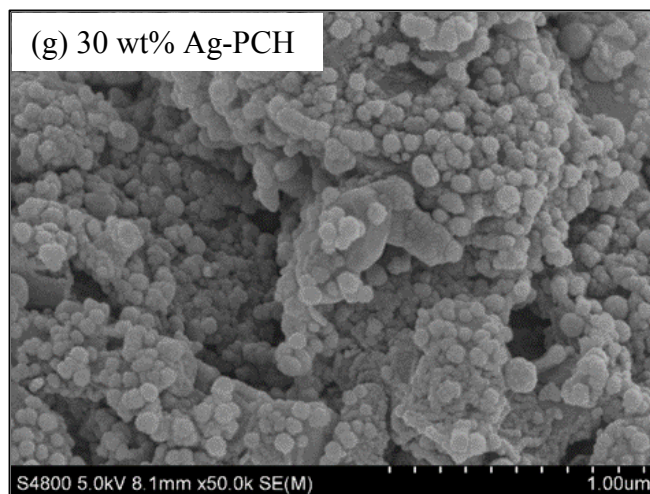
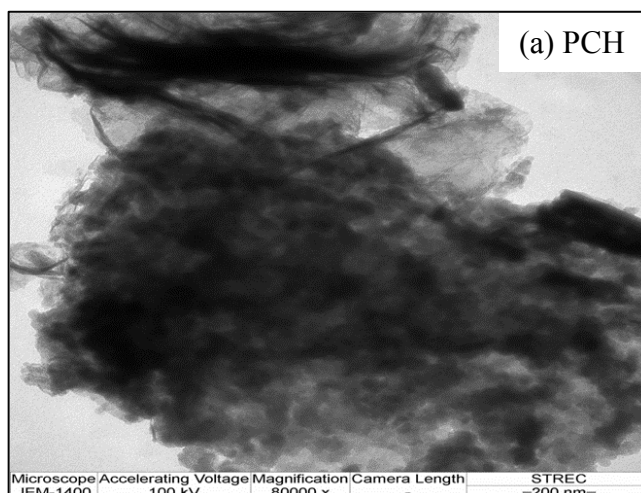


Figure 3 SEM images of (a) BTN, (b) PCH, (c) 1wt% Ag-PCH, (d) 5wt% Ag-PCH, (e) 10wt% Ag-PCH, (f) 20wt% Ag-PCH, and (g) 30wt% Ag-PCH.

The presence of the clay layers was confirmed by the TEM images of representative porous clay heterostructures (Figure 4). From the TEM images, the clay layers were discernible as solid dark lines and revealed aggregated domains of several layers. Although the clay layers were easily observed, the pore structure in the galleries of the clay was more difficult to notice because of their structures. It may claim that the light spot might be the pore structures. TEM image of synthesized Ag-PCH was used to observe the appearance and size of the silver particles. The shape of the silver particles looked like the spherical and the size was around 10 nm – 20 nm (Figure 4 (b) – 4(c)).



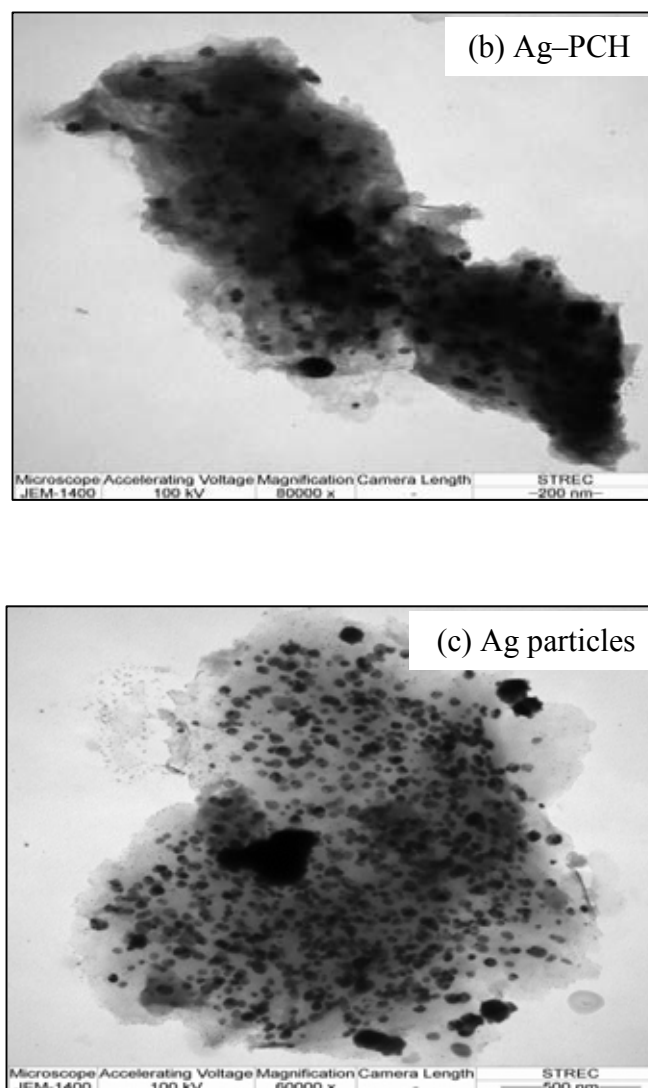


Figure 4 Transmission electron microscopy images of (a) porous clay heterostructure (PCH), (b) silver loaded porous clay heterostructure (Ag-PCH), and (c) silver particles.

6.4.3 Elemental Analysis

After surface modification, the percentage of composition of all modified Ag-PCHs were investigated. From table 2, the result showed that all % element compositions were changed. The % composition of Na in all modified PCHs decreased due to the cationic exchange from CTAC, compared to BTN. Furthermore,

the % Ag composition proportionally increased with increasing the weight percentage of silver loaded in the PCHs.

Table 2 Elemental analysis from XRF result

Sample	% composition of elements									
	O	Si	Na	Mg	Al	K	Ca	Fe	Ag	Total
BTN	39.07	33.56	3.02	3.74	17.86	0.39	1.05	1.31	-	100
PCH	46.83	39.78	0.04	2.07	10.75	0.1	0.03	0.4	-	100
1 wt% Ag-PCH	48.71	39.81	0.70	1.28	7.80	0.18	0.06	0.75	0.71	100
5wt% Ag-PCH	43.82	39.78	0.76	2.28	10.29	0.14	0.02	0.45	4.84	100
10 wt% Ag-PCH	44.95	38.27	0.41	1.14	9.5	0.16	0.02	0.32	7.03	100
20 wt% Ag-PCH	46.93	38.64	0.32	1.62	8.3	0.07	0.02	0.26	5.31	100
30 wt% Ag-PCH	43.33	36.88	0.18	1.61	8.05	0.09	0.01	0.19	13.75	100

6.4.4 Structural Analysis

After modification, the structure of all modified PCHs were examined in order to confirm that silver was successfully incorporated in the PCHs. Figure 5 shows the wide scan of the sample. The binding energies were 531 eV, 284 eV, 102 eV, 368 eV, and 374 eV corresponding to O1s, C1s, Si2p, Ag3d_{3/2}, and Ag3d_{5/2}, respectively. From binding energy, the structure of PCH and Ag-PCH were assigned in the scheme (1).

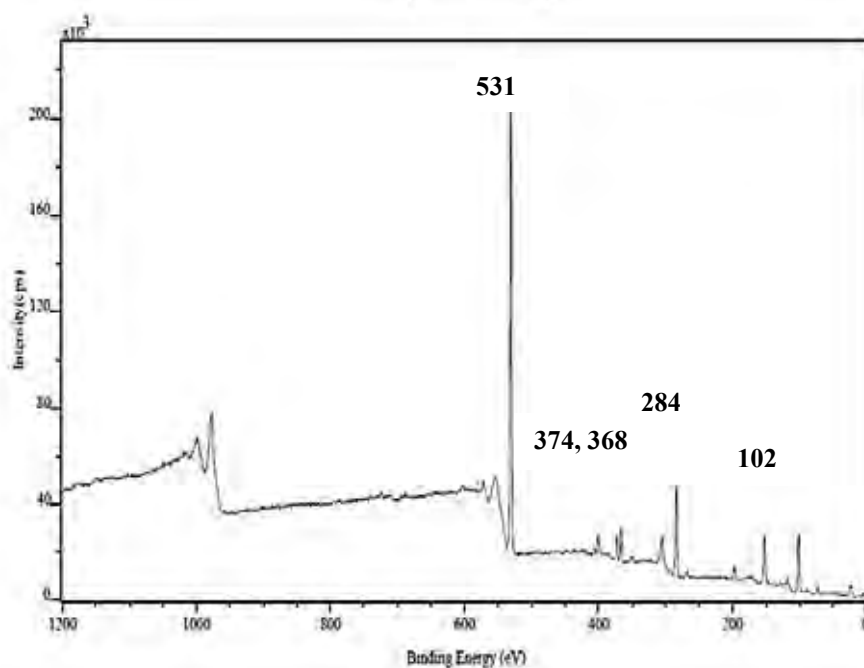
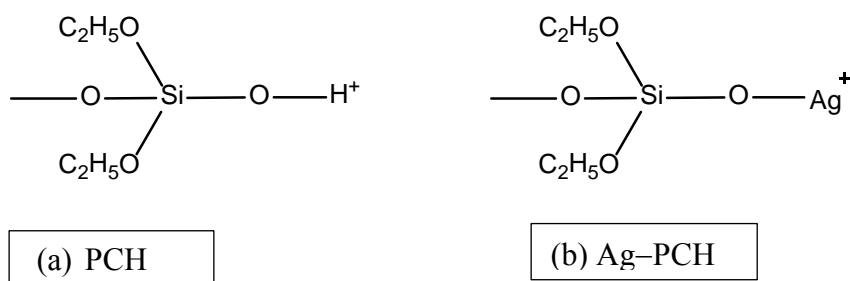


Figure 5 XPS spectra for wide analysis.



Scheme 1 Structure of PCH and Ag-PCH.

6.4.5 Surface Areas Analysis

From N_2 adsorption-desorption, the specific surface area of Bentonite was $31 \text{ m}^2/\text{g}$. After modification, the specific surface areas of PCH and all Ag-PCHs were significantly increased comparing to BTN (Table 3). Average pore diameter and pore volume of PCH and Ag-PCHs were about $3.50 \text{ nm} - 5.50 \text{ nm}$ and $0.20 \text{ cc/g} - 0.60 \text{ cc/g}$, ordered in mesopore range. However, the specific surface areas, average

pore diameter and pore volume of all Ag–PCHs decreased when the amount of silver contents increased. It confirmed that Ag was loaded inside the pore structure.

Table 3 Specific surface areas from the N₂ adsorption-desorption

Sample	Multipoint BET surface area (m ² /g)	Average pore diameter (nm)	BJH pore volume (cc/g)
BTN	31.0	-	-
PCH	437.0	5.45	0.60
1wt%Ag–PCH	401.5	4.10	0.30
5wt%Ag–PCH	342.6	3.75	0.32
10wt%Ag–PCH	318.3	3.49	0.28
20wt%Ag–PCH	309.0	3.76	0.34
30wt%Ag–PCH	109.8	3.94	0.19

6.4.6 Ethylene Adsorption of Ag–PCHs

The adsorption behaviour of ethylene gas, Ag–PCHs was examined by using gas chromatography (GC), Model 910, BUCK Scientific with a helium ionization detector. Ethylene gas was injected into a chamber to give a specific concentration of 5000 ppm. Ethylene concentration in the chamber was measured periodically, about once per hour until saturated condition. The ethylene adsorption was calculated by taking the difference between the amount of ethylene added and the amount remaining in the headspace. Figure 6 showed the adsorption capacity of the Ag–PCHs compared to that of BTN. The concentration of ethylene gas in the chamber proportionally decreased with time consuming and amount of silver contents. It explained that these materials could adsorb the ethylene gas. So Ag–PCHs acted as a good ethylene absorber comparing to all of materials. Among all Ag–PCHs, 10 wt%Ag–PCH represented as the good ethylene scavenger because of high silver loading and high specific surface area.

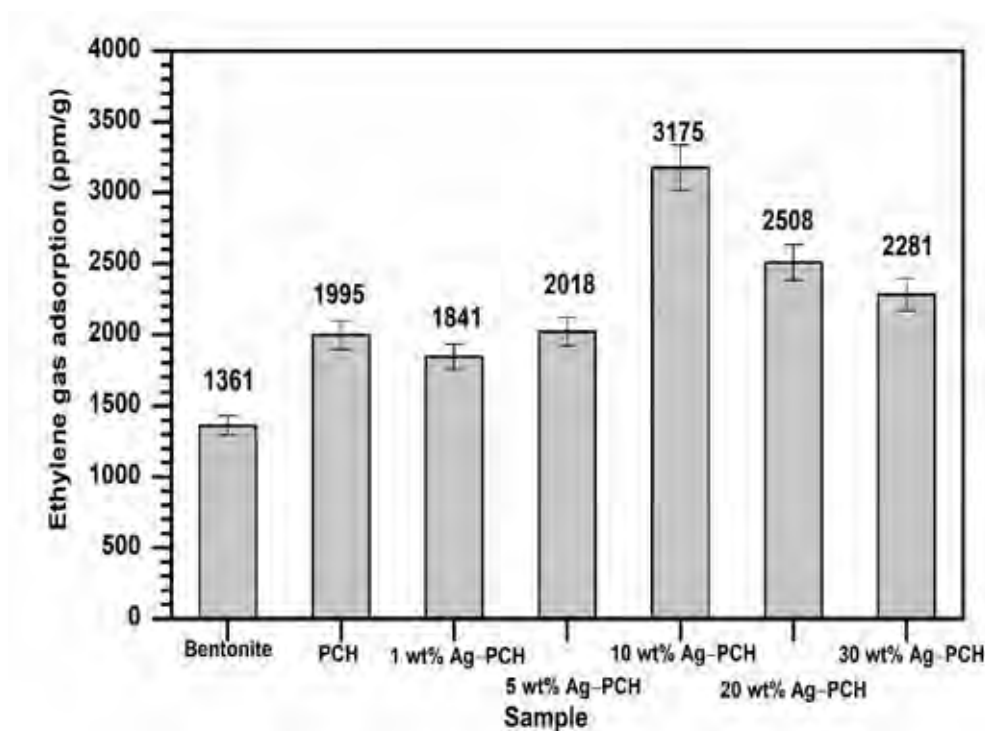


Figure 6 Ethylene adsorption of BTN, PCH, and Ag-PCHs at the equilibrium state.

6.4.7 Conductivity of Bentonite and Ag-PCHs

The electrical conductivity measurement was taken as an approach to the performance of the modified porous clay as the ethylene sensor. From Table 4, the conductivity of bentonite was 1.81×10^{-6} S/cm and the conductivity of all Ag-PCHs were greater than that of BTN. The conductivity of PCH decreased as a result of more organic compound which are non-polar. From the result, the conductivity of all Ag-PCHs increased with the increasing of amount of silver loading. This is explained based on the fact that the silver element shows the largest conductivity values. It concluded that the conductivity of modified PCH increased with content of conducting material (silver) which was loaded in the PCH. From measurement results, it was implied that the silver element plays an important role in conductivity part and it also showed the significant increasing on conductivity value. Although the 30 wt% Ag-PCH showed the highest conductivity value, 10 wt% Ag-PCH was chosen to study further in nanocomposite film via blending with polypropylene. And the

last this 10 wt% Ag–PCH/PP nanocomposite was evaluated about its conductive sensing in the film form.

Table 4. Conductivity of bentonite and Ag-PCHs

Sample	Conductivity (S/cm)
Bentonite	1.81×10^{-6}
PCH	1.3×10^{-7}
1wt%Ag-PCH	1.57×10^{-6}
5wt%Ag-PCH	3.87×10^{-6}
10wt%Ag-PCH	4.38×10^{-6}
20wt%Ag-PCH	4.45×10^{-6}
30wt%Ag-PCH	1.30×10^{-3}

6.4.8 Thermal properties of nanocomposite

According to previous results, 10wt% Ag–PCH was chosen to blend with polypropylene (PP) through twin screw extruder to obtain nanocomposite pellets. The crystallization and melting behavior of PP/MPPCH nanocomposites compared to PP were measured by Differential Scanning Calorimeter (DSC) using Mettler DSC 822 STARe System. The pellets were heated from 30°C to 200°C at a heating rate of 10°C/min in order to eliminate the influence of thermal history and then cooled down from 200°C to 30°C to observe melt crystallization behavior. After that, reheated to 200°C to observe melting behavior.

The crystallinity of samples was calculated by this equation,

$$\% \text{ Crystallinity} = \frac{\Delta H_{\text{sample}}}{\Delta H^{\circ}} \times 100 \quad (2)$$

Where, ΔH_{sample} = enthalpy of fusion of the sample (J/g)

ΔH_{PP} = enthalpy of fusion of completely crystalline (207 J/g)

Melting temperatures of PP and PP/modified Ag-PCHs nanocomposites were observed by DSC heating scan thermograms in Figure 7. The melting temperature of PP is 164.0 °C while the melting temperature of the PP/modified Ag-PCHs nanocomposites is around 163 °C - 164 °C. These results suggested that the additions of a compatibilizer surlyn® ionomer and various types of porous clay have minimal effect on the melting temperatures. For crystallization behaviors of PP and the nanocomposites were presented by DSC cooling scan thermograms in Figure 8 and Table 5. The results showed that the crystallization of PP was significantly affected by both the presence of a compatibilizer surlyn® ionomer and modified porous clays. As shown in Figure. 6, the PP presented the crystallization temperature at 114.5 °C .And the PP/modified Ag-PCHs nanocomposites exhibited quite similar crystallization temperature not different much from PP, whereas the % crystallinity of PP/modified Ag-PCHs nanocomposites displayed the lower percentage of crystallinity than that of pure PP, indicating that the PP-clay interface played an important role in the crystallization behavior. These results referred to the good dispersion of modified PCHs in the PP matrix.

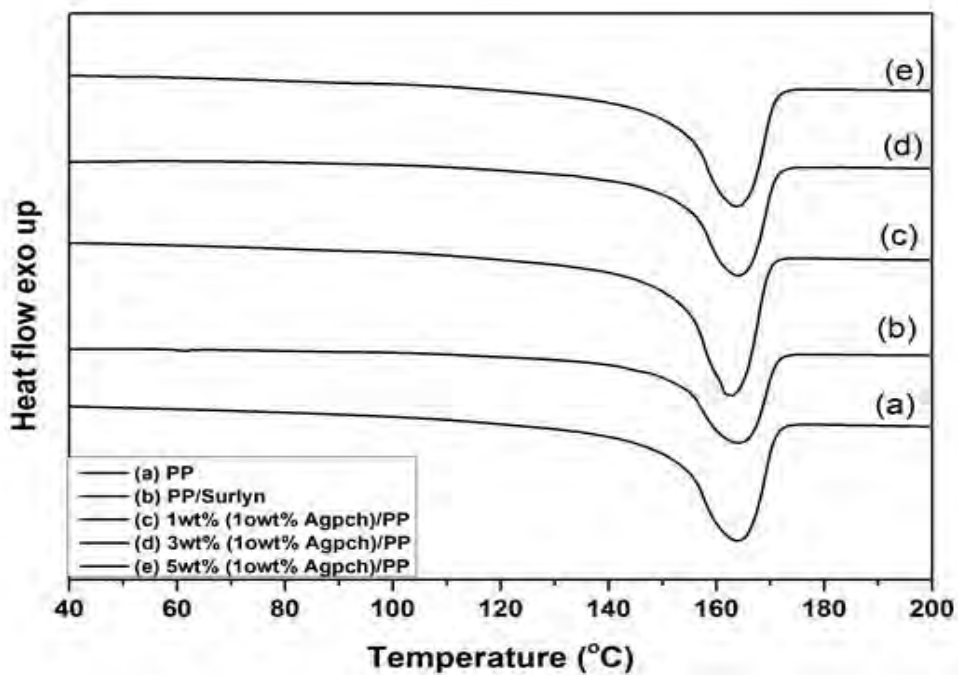


Figure 7 DSC heating scan thermograms of pure PP and PP/modified Ag-PCHs nanocomposites.

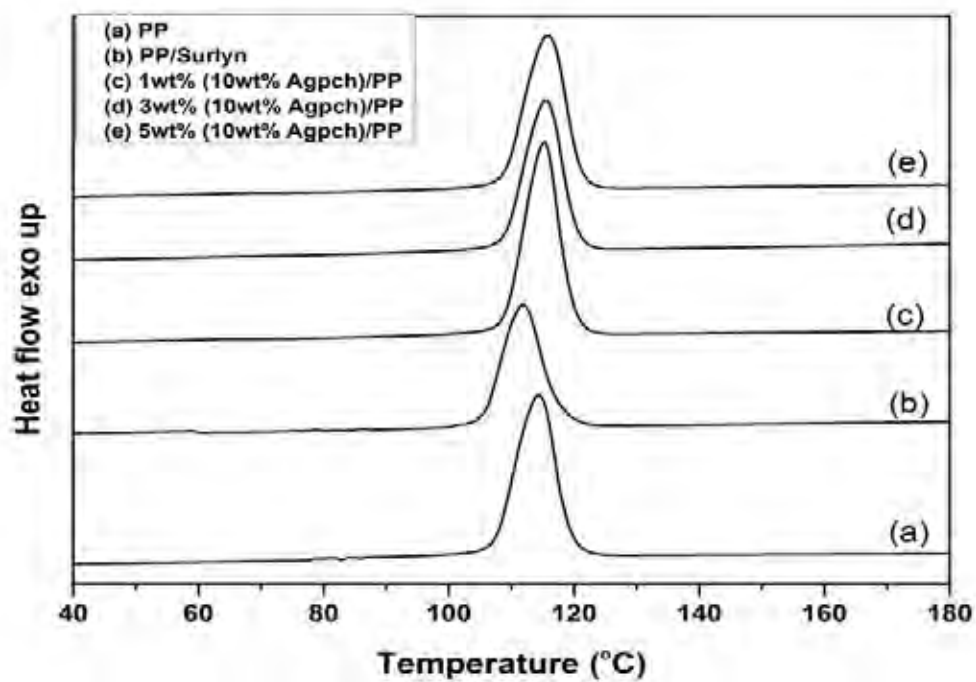


Figure 8 DSC cooling scan thermograms of pure PP and PP/modified Ag-PCHs. Nanocomposites.

Table 5 Crystallization behavior of PP and PP/modified Ag-PCHs nanocomposites

Sample	T _c peak (°C)	T _m peak (°C)	ΔH _m (J/g)	Crystallinity (%)
PP	114.5	164.0	100.55	48.57
2 wt% Surlyn®/PP	111.5	164.1	95.05	45.00
1 wt% (10wt% Ag-PCH)/ 2 wt% Surlyn®/PP	115.9	163.0	99.54	46.64
3 wt% (10wt% Ag-PCH)/ 2 wt% Surlyn®/PP	115.4	164.1	93.36	42.84
5 wt% (10wt% Ag-PCH)/ 2 wt% Surlyn®/PP	115.7	163.8	97.47	43.79

Thermogravimetric analysis (TGA) was used to study the thermal stability of PP/Ag-PCH nanocomposites compared to PP. The degradation temperature of samples was determined by Perkin Elmer Pyris Diamond TG/DTA instrument. The pellets were loaded on platinum pan and heated from 30°C to 700°C at a heating rate of 10°C/min and flow under N₂ 200 ml/min. The increase in thermal stability and melting temperature are due to the intercalation or the separation of the silicate layers as well as better dispersion of the silicate layers. TG-DTA curves of PP and the PP/modified Ag-PCHs nanocomposites were delineated in Figure 9 and all results of thermal properties were listed in Table 6. The thermal degradation of PP and all PP/ modified Ag-PCHs nanocomposites occurred in a single stage, and it indicated that thermal stability of the nanocomposites was marginally increased when compared to that of virgin PP.

In general, the shift considerably toward higher temperature was attributed to the formation of a high-performance carbonaceous-silicate char, building up on the surface. In spite of all these, the results answered that the addition of these modified porous clays just slightly improved the thermal stability of PP which might be responsible for some destruction of clay layers on Ag-PCHs materials or due to

the intercalation or the separation of the silicate layers as well as better dispersion of the silicate layers.

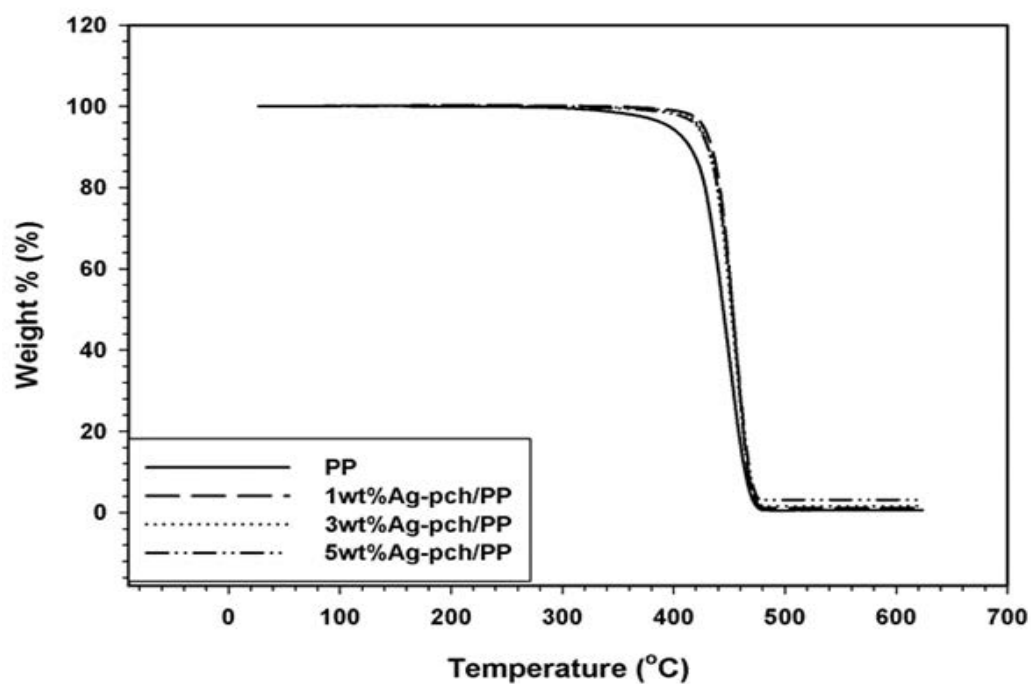


Figure 9 TG-DTA curves of pure PP and modified Ag–PCH nanocomposites.

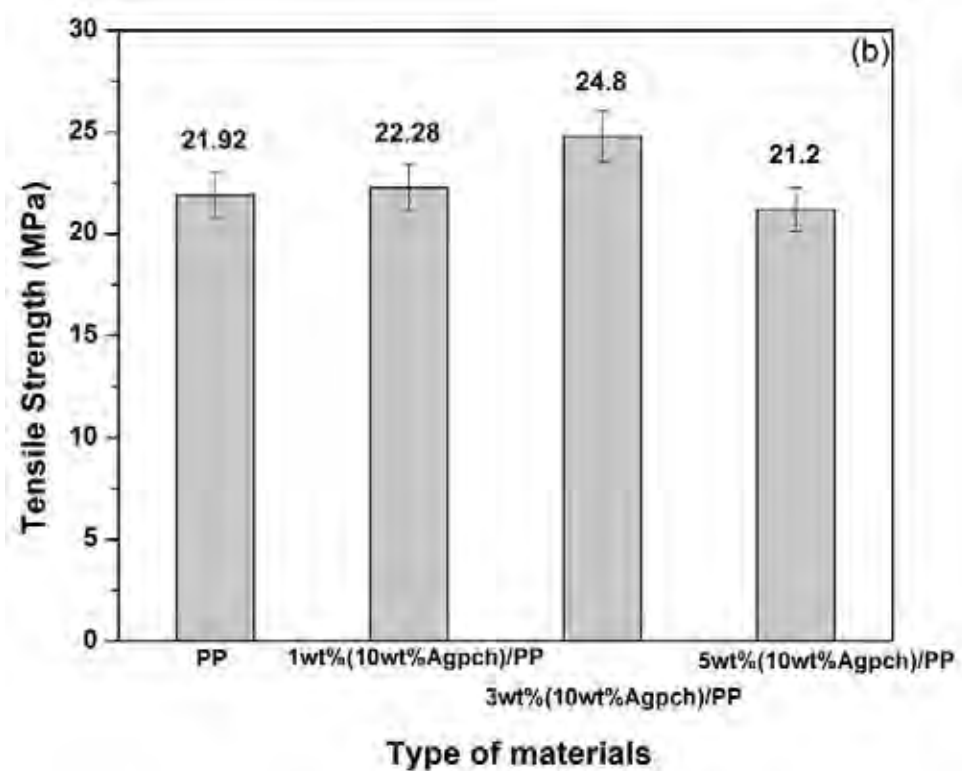
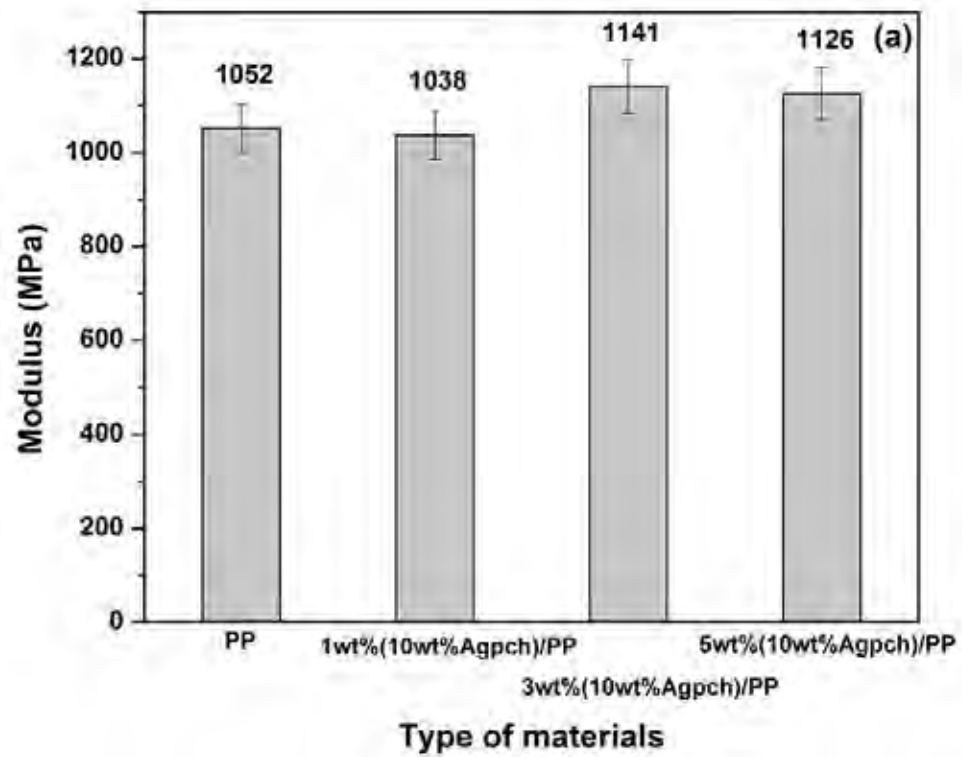
Table 6. Thermal properties of PP and PP/modified PCHs nanocomposites

Sample	T_d peak (°C)	Char residue at 600 °C (%)
PP	452.5	0.07
2 wt% Surllyn®/PP	455.7	0.07
1 wt% (10wt% Ag–PCH)/ 2 wt% Surllyn®/PP	455.7	0.87
3 wt% (10wt% Ag–PCH)/ 2 wt% Surllyn®/PP	456.6	2.67
5 wt% (10wt% Ag–PCH)/ 2 wt% Surllyn®/PP	456.9	4.98

6.4.9 Mechanical Property of Nanocomposite Films

The effect of clay contents on the mechanical properties of all PP/modified PCHs nanocomposites was emphasized on the tensile modulus, tensile strength and % elongation. The results were shown in Figure 10 (a), (b) and (c), respectively. The average values of these mechanical properties were reported in Table 5. Tensile modulus and strength of all Ag–PCH/PP nanocomposites were greater than those of pure PP, on the other hand, the tensile modulus and strength of 5 wt% (10 wt% Ag–PCH)/PP was decreased because the lower content of compatibilizer in PP/clay affected to the poor dispersion of modified porous clay in the composition. The decrease in tensile modulus and tensile strength of PP/clay nanocomposites could also involve with the remaining of some impurities (quartz) in bentonite clay as inhomogeneous aggregates. The aggregations of clays or the impurities act as stress concentrators, allowing crack initiation and propagation, consequently decreasing the mechanical performance of the nanocomposites.

The percentage of elongation was represented in Figure 10 (c). The % elongation of both composites was reduced with increasing the clay contents. The reduction of elongation may be due to the stiffness from Ag–PCHs that acted as the reinforcement, or the greater interaction between filler and polymer matrix, which probably leads to a lower polymeric chain mobility, making the material more rigid. Furthermore, the agglomeration of clay particles also caused the defect in the PP matrix leading to drop the mechanical property.



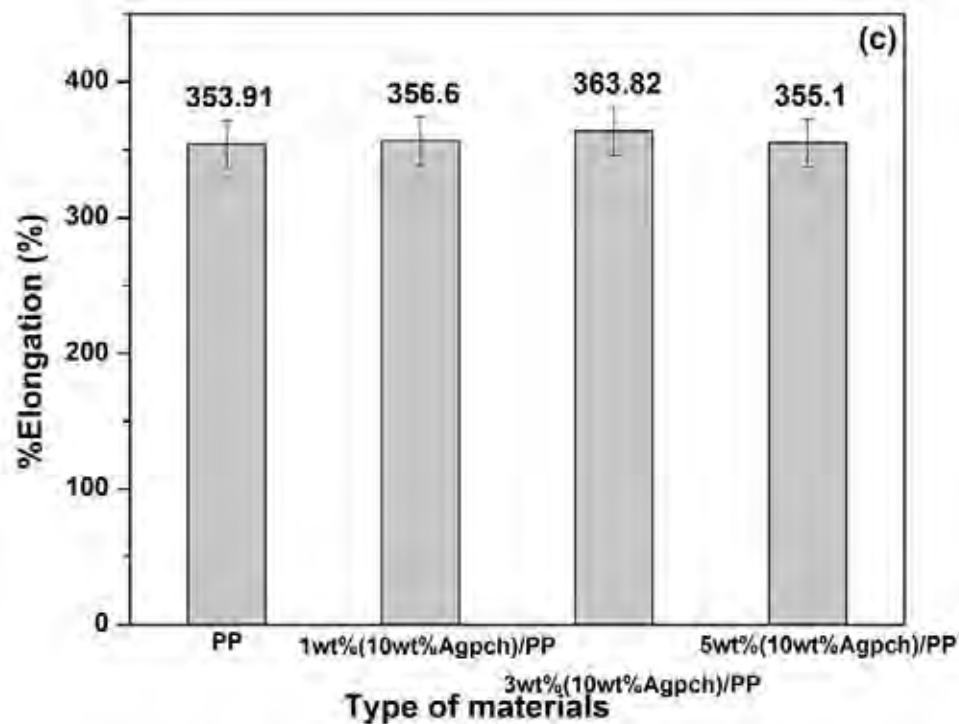


Figure 10 Mechanical properties of PP and 10wt% Ag-PCH/PP composite films with various contents of clay loading: (a) Young's modulus (b) Tensile strength, and (c) %Elongation.

Table 7 Young's modulus, tensile strength, and % elongation of PP and 10wt% Ag-PCH/PP composites with various compositions

Sample	Modulus (MPa)	Tensile strength (MPa)	% Elongation at break
PP	1052 ± 254	21.92 ± 1.68	353.91 ± 8.21
1 wt% (10 wt% Ag-PCH)/ 2 wt% Surlyn®/PP	1038 ± 132	22.28 ± 2.97	356.50 ± 17.12
3 wt% (10 wt% Ag-PCH)/ 2 wt% Surlyn®/PP	1141 ± 230	24.80 ± 4.17	363.82 ± 18.05
5 wt% (10 wt% Ag-PCH)/ 2 wt% Surlyn®/PP	1126 ± 332	21.20 ± 4.60	355.10 ± 23.37

6.4.10 Ethylene Adsorption

Adsorption behaviour of ethylene gas within the PP/modified porous clay composite films was examined using gas chromatography. Figure 11 showed the amount of ethylene adsorption of PP and all the composite films. The amount of ethylene adsorption proportionally increased with the increasing of clay contents. This was explained that the higher amount of clay led to the better ethylene adsorption. It concluded that the silver on the surface of clay adsorbed the ethylene gas and the amount of clay also affected to ethylene adsorption ability. In conclusion, all 10 wt% Ag-PCH/PP composite film performed the better ethylene adsorption than neat PP.

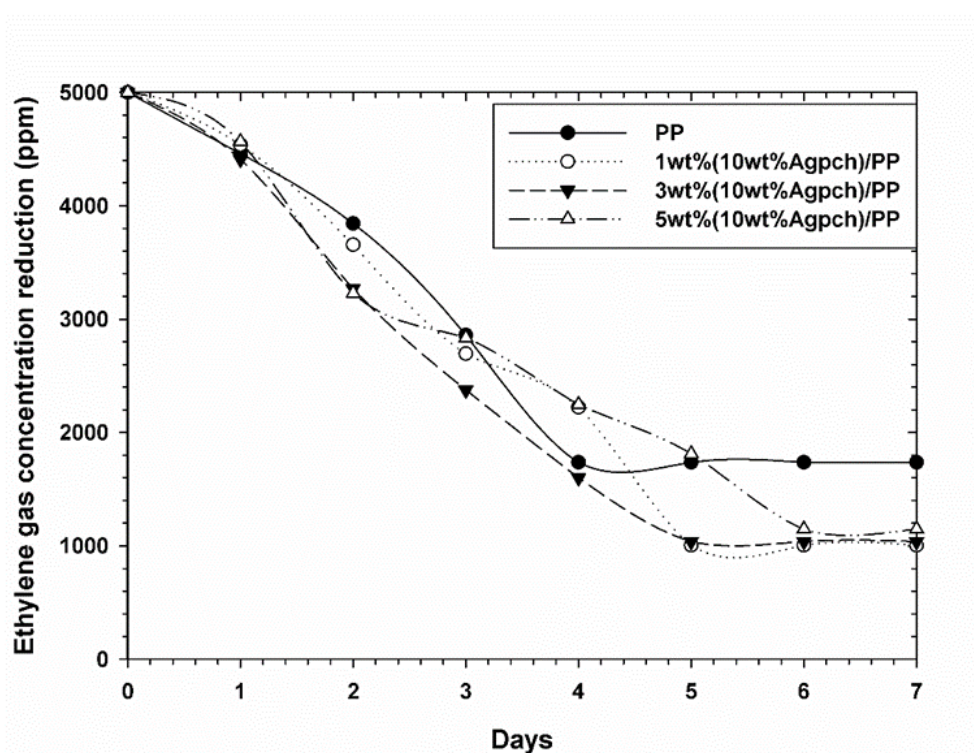


Figure 11 Ethylene reduction capacity of PP, 1wt% (10wt%Ag-PCH)/PP, 3wt% (10wt%Ag-PCH)/PP, and 5wt% (10wt%Ag-PCH)/PP nanocomposite films.

6.4.11 Conductivity of Composite Films

PP/modified Ag-PCHs composite films were the films which consisted of the modified PCHs; loading with silver (Ag) nanoparticles that effected to the conductivity of the films. Whereas, PP is an insulator film, its conductivity did not change when adsorbed the ethylene gas. After investigating the ethylene adsorp-

tion, the PP and PP/modified Ag-PCHs composite films were evaluated the conductivity when adsorbed the ethylene gas. The conductivity of PP/modified porous clay composite films decreased with time. When the films interacted with the ethylene gas, their conductivity decreased. Additionally, the higher content of clay conducted to the higher of the conductivity of the PP/modified Ag-PCHs composite films. Eventually, it can conclude that the PP/modified PCHs composite films performed significantly conductivity changing comparing to PP.

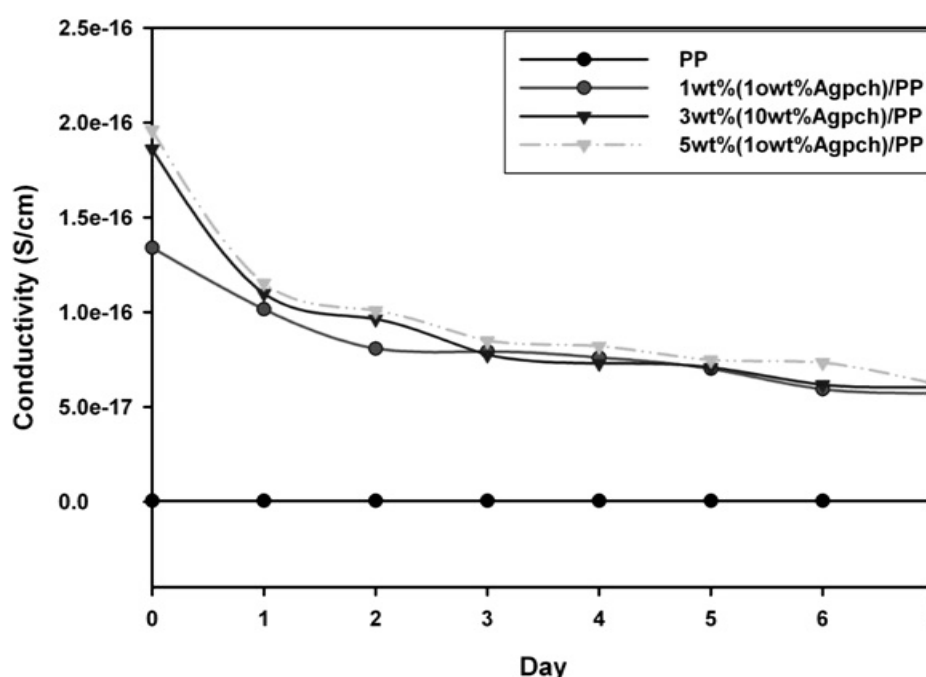


Figure 12 The conductivity of PP and Ag-PCHs/PP composite films as a function of time adsorbing to the ethylene gas.

Sample	Conductivity* (1 st day) (S/cm)	Conductivity** (Equilibrium state) (S/cm)
--------	---	--

PP	5.17×10^{-19}	5.17×10^{-19}
1 wt% (10 wt% Ag-PCH)/ 2 wt% Surlyn®/PP	1.34×10^{-16}	1.01×10^{-16}
3 wt% (10 wt% Ag-PCH)/ 2 wt% Surlyn®/PP	1.86×10^{-16}	1.09×10^{-16}
5 wt% (10 wt% Ag-PCH)/ 2 wt% Surlyn®/PP	1.96×10^{-16}	1.15×10^{-16}

Table 8 Conductivity of polypropylene (PP) and PP/modified PCHs composite films

Note * Conductivity of materials before adsorbing the ethylene gas.

** Conductivity of materials after adsorbing the ethylene gas.

6.5 Conclusion

In this work, the silver (Ag) nanoparticles was successfully embedded into the porous structure of the PCH. According to the results, it concluded that Ag-PCH revealed porous structure due to scattering spectra, and also exhibited the roughly surface and small grains with increasing the contents of silver. Furthermore, the Ag-PCHs performed the higher efficiency in adsorbing ethylene gas, comparing to BTN and PCH. The 10 wt%Ag-PCH was chosen to blend with PP due to it's the best ethylene adsorption and the great conductivity property and then fabricated into PP/clay composite films with various 1 wt%, 3 wt%, 5 wt% Ag-PCH loading. Referred to thermal and mechanical result, all PP/Ag-PCHs composite films presented improving in thermal and mechanical property due to higher Td, higher modulus and tensile strength and also higher elongation at break. Moreover, all PP/Ag-PCHs composite films showed the greater value in ethylene adsorption and conductivity result. In addition, PP/Ag-PCHs composite films also displayed the sensing to the ethylene gas by conductivity dropping. In conclusion, Ag-PCHs and Ag-PCHs/PP composite films eventually claimed that they acted as the ethylene scavenger and ethylene gas sensing films.

6.6 Acknowledgment

This work are financially supported by the Petroleum and Petrochemical College and Centre of Excellent on Petrochemical and Materials Technology, Thailand. Partially fund are supported by the 90th Anniversary of the Chulalongkorn University Fund (Ratchadaphiseksomphot Endowment Fund). The Author would like to thank Assistant Professor Dr. Chiravoot Pechyen from Department of Chemical and Materials Technology, Faculty of Science and Technology, Thailand for providing packaging testing.

6.7 References

1. Zhou, X., Huang, Q., Chen, S., & Yu, Z. (2005). Adsorption of the insecticidal protein of *Bacillus thuringiensis* on montmorillonite, kaolinite, silica, goethite and Red soil. *Applied Clay Science*, 30(2), 87-93.
doi:<http://dx.doi.org/10.1016/j.clay.2005.04.003>
2. Valášková, M., Hundáková, M., Kutláková, K. M., Seidlerová, J., Čapková, P., Pazdziora, E., Rafaja, D. (2010). Preparation and characterization of antibacterial silver/vermiculites and silver/montmorillonites. *Geochimica et Cosmochimica Acta*, 74(22), 6287-6300.
doi:<http://dx.doi.org/10.1016/j.gca.2010.08.025>
3. Turgut Basoglu, F., & Balci, S. (2010). Micro-mesopore analysis of Cu²⁺ and Ag⁺ containing Al-pillared bentonite. *Applied Clay Science*, 50(1), 73-80.
doi:<http://dx.doi.org/10.1016/j.clay.2010.07.004>
4. Rodríguez-Hernández, J. (2017). 3 - Nanostructured antimicrobial materials in the food industry A2 - Grumezescu, Alexandru Mihai Food Preservation (pp. 75-124): Academic Press.
5. Srividya, N., Ghoora, M. D., & Padmanabh, P. R. (2017). 4 - Antimicrobial nanotechnology: research implications and prospects in food safety A2 - Grumezescu, Alexandru Mihai Food Preservation (pp. 125-165): Academic Press.
6. Lv, Y., Liu, H., Wang, Z., Liu, S., Hao, L., Sang, Y., Boughton, R. I. (2009). Silver nanoparticle-decorated porous ceramic composite for water treatment.

- Journal of Membrane Science, 331(1–2), 50–56.
doi:<http://dx.doi.org/10.1016/j.memsci.2009.01.007>
7. Liu, J., Li, X., Zuo, S., & Yu, Y. (2007). Preparation and photocatalytic activity of silver and TiO₂ nanoparticles/montmorillonite composites. *Applied Clay Science*, 37(3–4), 275–280. doi:<http://dx.doi.org/10.1016/j.clay.2007.01.008>
 8. Duncan, T. V. (2011). Applications of nanotechnology in food packaging and food safety: Barrier materials, antimicrobials and sensors. *Journal of Colloid and Interface Science*, 363(1), 1–24. doi:<http://dx.doi.org/10.1016/j.jcis.2011.07.017>
 9. Carja, G., Kameshima, Y., Nakajima, A., Dranca, C., & Okada, K. (2009). Nanosized silver–anionic clay matrix as nanostructured ensembles with antimicrobial activity. *International Journal of Antimicrobial Agents*, 34(6), 534–539. doi:<http://dx.doi.org/10.1016/j.ijantimicag.2009.08.008>
 10. Quang Huy, T., Van Quy, N., & Anh-Tuan, L. (2013). Silver nanoparticles: synthesis, properties, toxicology, applications and perspectives. *Advances in Natural Sciences: Nanoscience and Nanotechnology*, 4(3), 033001.
 11. Praus, P., Turicová, M., Machovič, V., Študentová, S., & Klementová, M. (2010). Characterization of silver nanoparticles deposited on montmorillonite. *Applied Clay Science*, 49(3), 341–345. doi:<http://dx.doi.org/10.1016/j.clay.2010.06.009>
 12. Pehlivan, H., Balköse, D., Ülkü, S., & Tihminliog̃lu, F. (2005). Characterization of pure and silver exchanged natural zeolite filled polypropylene composite films. *Composites Science and Technology*, 65(13), 2049–2058. doi:<http://dx.doi.org/10.1016/j.compscitech.2005.04.011>
 13. Magaña, S. M., Quintana, P., Aguilar, D. H., Toledo, J. A., Ángeles-Chávez, C., Cortés, M. A., Sánchez, R. M. T. (2008). Antibacterial activity of montmorillonites modified with silver. *Journal of Molecular Catalysis A: Chemical*, 281(1–2), 192–199. doi:<http://dx.doi.org/10.1016/j.molcata.2007.10.024>
 14. Li, T., Lin, O., Lu, Z., He, L., & Wang, X. (2014). Preparation and characterization of silver loaded montmorillonite modified with sulfur amino acid. *Applied Surface Science*, 305, 386–395. doi:<http://dx.doi.org/10.1016/j.asusc.2014.03.098>

15. Jia, H., Hou, W., Wei, L., Xu, B., & Liu, X. (2008). The structures and antibacterial properties of nano-SiO₂ supported silver/zinc–silver materials. *Dental Materials*, 24(2), 244-249. doi:<http://dx.doi.org/10.1016/j.dental.2007.04.015>
16. Gupta, R. K., & Dudeja, P. (2017). Chapter 46 - Food packaging Food Supply Safety in India (pp. 547-553). San Diego: Academic Press.
17. Fernandez, A., Picouet, P., & Lloret, E. (2010). Cellulose-silver nanoparticle hybrid materials to control spoilage-related microflora in absorbent pads located in trays of fresh-cut melon. *Int J Food Microbiol*, 142(1-2), 222-228. doi:10.1016/j.ijfoodmicro.2010.07.001
18. Długosz, M., Bulwan, M., Kania, G., Nowakowska, M., & Zapotoczny, S. (2012). Hybrid calcium carbonate/polymer microparticles containing silver nanoparticles as antibacterial agents. *Journal of Nanoparticle Research*, 14(12), 1313. doi:10.1007/s11051-012-1313-7
19. Deng, X., Nikiforov, A. Y., & Leys, C. (2017). 1 - Antimicrobial nanocomposites for food packaging A2 - Grumezescu, Alexandru Mihai *Food Preservation* (pp. 1-34): Academic Pde Paiva, L. B., Morales, A. R., & Valenzuela Díaz, F. R. (2008). *Organoclays: Properties, preparation and applications. Applied Clay Science*, 42(1–2), 8-24. doi:<http://dx.doi.org/10.1016/j.clay.2008.02.006>ress.
20. Cheviron, P., Gouanvé, F., & Espuche, E. (2016). Preparation, characterization and barrier properties of silver/montmorillonite/starch nanocomposite films. *Journal of Membrane Science*, 497, 162-171. doi:<http://dx.doi.org/10.1016/j.memsci.2015.09.039>
21. rabazon, D., & Raffer, A. (2015). Chapter 3 - Advanced characterization techniques for nanostructures *Emerging Nanotechnologies for Manufacturing (Second Edition)* (pp. 53-85). Boston: William Andrew Publishing.

CHAPTER VII

INVESTIGATION OF POLYPROPYLENE/MODIFIED POROUS CLAY HETEROSTRUCTURE NANOCOMPOSITE FILMS: DIELECTRIC PROPERTY AND THERMAL EXPANSION

7.1 Abstract

Polypropylene (PP) was doped with modified PCHs assigned as PP/modified PCHs nanocomposite films. The PP/modified PCHs were HPCH, MPPCH, and Ag-PCH which contained the various type of functional group such as methyl group, thiol group, and metal group (Silver). The effect of dopants were studied base on dielectric property and thermal expansion. According to the dielectric property, the dielectric constant of PP and PP/modified PCHs nanocomposite films decreased by frequency dependent. Moreover, all samples exhibited only one relaxation at 20 KHz, referred to the transition from interfacial polarization to dipolar polarization. Subsequently, adding clay as a filler presented the low thermal expansion coefficient.

Keyword: PP/modified PCHs, nanocomposite film, dielectric property, thermal expansion, multilayer capacitor

7.2 Introduction

Polymer layered silicate nanocomposites have shown great promise in technological sector since they offer significant enhancement in properties. The nanocomposites of polypropylene with organically modified layered silicates and functionalized polypropylene by melt intercalation technique are well known in the field of polymer nanotechnology [1-5]. These nanocomposites are also interesting from research point of view and many attempts have been made to explore the interaction of these clays with polymers using various preparation and characterization techniques [6-10]. As the clays are hydrophobic, major problem in

developing these nanocomposites is of dispersing clay in non-polar polymers such as polypropylene (PP). As a result number of studies on clay modification and use of different compatibilizers have been reported [11-16]. Depending on the state of dispersion of clay platelets in the polymer matrix, the nanocomposites can be classified as intercalated or exfoliated nanocomposites [17]. The intercalated clay-polymer nanocomposites have clay layers dispersed in a polymer matrix with larger inter gallery spacing associated with the insertion of polymer chains into the gallery. In some cases, nanocomposites exhibit exfoliated structure, wherein the silicate layers are completely delaminated and dispersed randomly in the polymer matrix. However in practice, most of the times a combination of intercalated and exfoliated structures is observed and the extent of intercalation or exfoliation depends on the polymer clay interaction and the processing conditions. The reported literature on PP/clay nanocomposites is mostly on three phase system namely PP-compatibilizer-clay. The dispersion of the clay and the properties of these nanocomposites mostly depend on the type, amount of the compatibilizer used and also the modification of clay. The interaction of the compatibilizer is well understood by studying two phase systems consisting of the compatibilizer and the clay. There have been few reports on the compatibilizer/clay systems [18-20]. However, the results are specific to the compatibilizer and the clay used in the study. Our earlier work on dynamics of polymer/clay nanocomposites have shown that the molecular dynamics of the polymer is significantly affected by the clay dispersion [21-25].

In this work, PP and PP/modified PCHs nanocomposite were studied about dielectric property and thermal expansion property in order to understand the effect of various type of dopants and their behaviour. These nanocomposite materials were evaluated for using in capacitor application.

7.3 Materials and Methods

7.3.1 Chemicals and Raw Materials

Pristine sodium bentonite (Na-BTN), with a cation exchange capacity (CEC) of 44.5 meq/100g, was kindly supplied by Thai Nippon Co. Ltd. (Thailand). Cetyltrimethylammonium Chloride (CTAC), performing as the cationic surfactant,

and chemical substances such as tetraethoxysilane, silver nitrate (AgNO_3), and ascorbic acid were purchased from Fluka and Acros, respectively. PP (Moplen HP525N, MFI 11) and Surlyn® (PC 350, MFI 5) were provided by HMC Polymers Co., Ltd. (Thailand) and DuPont™.

7.3.2 Synthesis of Porous Clay Heterostructures (PCHs)

Purified bentonite was changed into a quaternary ammonium exchange form by ion exchange with cetyltrimethylammonium chloride (CTAC) and was stirred at 50 °C. After that, the sample was filtered, washed with a mixture of methanol and water, and then air-dried overnight. The obtained organoclay was stirred in dodecylamine at 50 °C for 30 min before adding the tetraethoxysilane (TEOS) at a molar ratio of organoclay:dodecylamine:TEOS of 1:20:150. The resulting suspension was stirred at 37°C for 4 hours. The suspension was filtered and air-dried overnight to form the as synthesized PCH. Then the surfactant was removed from the as-synthesized PCH by solvent extraction using a mixture of methanol and HCl solution. Typically, 1 g of the as-synthesized PCH was added to 5 ml of HCl and 45 ml of methanol, and was refluxed for 2 hours.

7.3.3 Synthesis of Hybrid Organic–Inorganic Porous Clay Heterostructures with Functional Groups

According to the previous PCH forming step, a mixture of TEOS and MTS in a mole fraction of 0.5:0.5 was added and stirred for a further 12h at 35 °C. For the conductive functional group, the mixture of TEOS and MPTMS, in a mole fraction of 1:2, was added under N_2 atmosphere and stirred for a further 24 h at room temperature. The obtained modified PCHs were collected by filtration and air-dried overnight at room temperature. Then the surfactant was removed from the as-synthesized modified PCH by solvent extraction. The modified PCHs by MTS and MPTMS are named HPCH and MPPCH, respectively.

7.3.4 Synthesis of Silver-Loaded Porous Clay Heterostructures

Next, PCH was suspended in the mixture of AgNO₃ and ethanol at 30 °C. After 1 hour, the 0.1 M ascorbic acid was dropped into the suspension to reduce Ag⁺ to Ag⁰, designated as Ag–PCH. The Ag–PCH was collected by filtration and air-dried overnight.

7.3.5 Preparation of Polypropylene/clay Nanocomposite Film

The 1 wt% of modified PCHs, 2 wt% of surlyn®, and PP were prepared by using twin-screw extruder (Labtech) with L/D = 40 and D = 20 mm. The operation temperature was performed at 160, 165, 170, 175, 180, 185, 190, 200, 210 and 215°C from hopper to die respectively and the screw speed was 30 rpm.

7.3.6 Fabrication of Nanocomposite Films

The nanocomposite films were prepared by using blown film extrusion machine. The nanocomposite pellets were dried in an oven prior to blowing. The following extrusion conditions were employed at the rotation speed of the screw around 50 rpm and the blowing ratio was 1.52. The barrel and mold temperature were 210 °C. The thickness of the films was controlled to about 40 μm.

7.3.7 Characterization

7.3.7.1 *Dielectric Property*

The dielectric properties of the samples were measured at various frequencies and temperatures. The dielectric properties of the samples with a function of temperature (173 K to 373 K) were measured by a LCR meter (HP 4284A) under He atmosphere with the heating and cooling rate of 3 K/min and also collected as a function in diameter. The tests were investigated the capacitance (*C*) of the samples. Then, the dielectric constant (*k*) was calculated from the capacitance by using Equation (1).

$$C = \varepsilon_0 k \frac{A}{d} \quad (1)$$

Where C is capacitance of the composite (F), ϵ_0 is dielectric constant of the free space (8.85×10^{-12} F/m), A is electrode area (m^2), and d is distance between electrodes, i.e. thickness of the samples (m).

7.3.7.2 Thermal Expansion Property

Thermal expansion of the samples was carried out by using a dilatometer. The measurement was performed at the various temperature from 373 K to 173 K under the N₂ atmosphere. The samples were cut into the bar shape (3.00 mm × 7.00 mm × 3.00 mm) before testing. The parameters were calculated by using Equation (2).

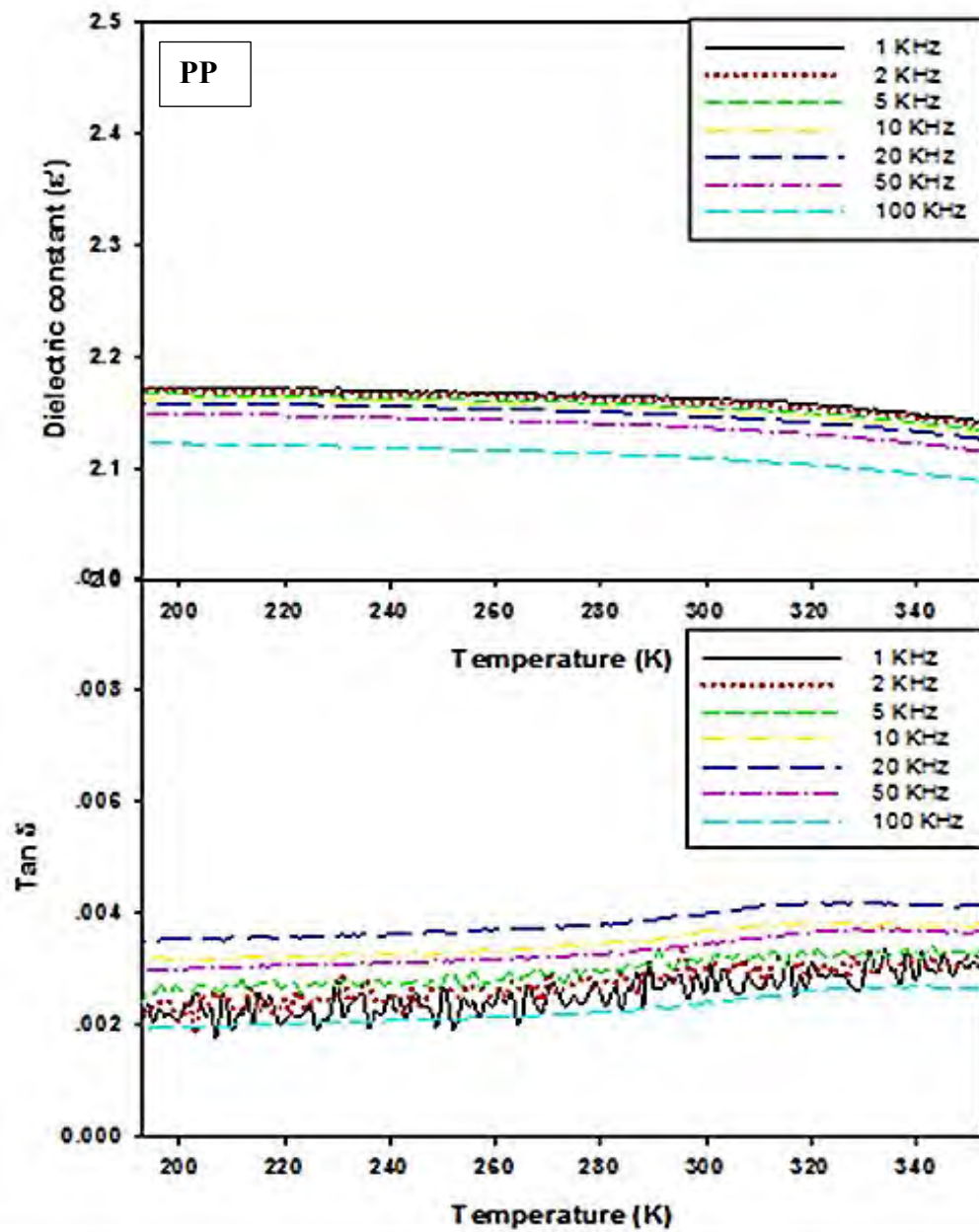
$$\frac{\Delta L}{L_0} = \alpha \Delta T \quad (2)$$

Where ΔL is change in length (m), α is linear expansion coefficient (K^{-1}), ΔT is change in temperature (K).

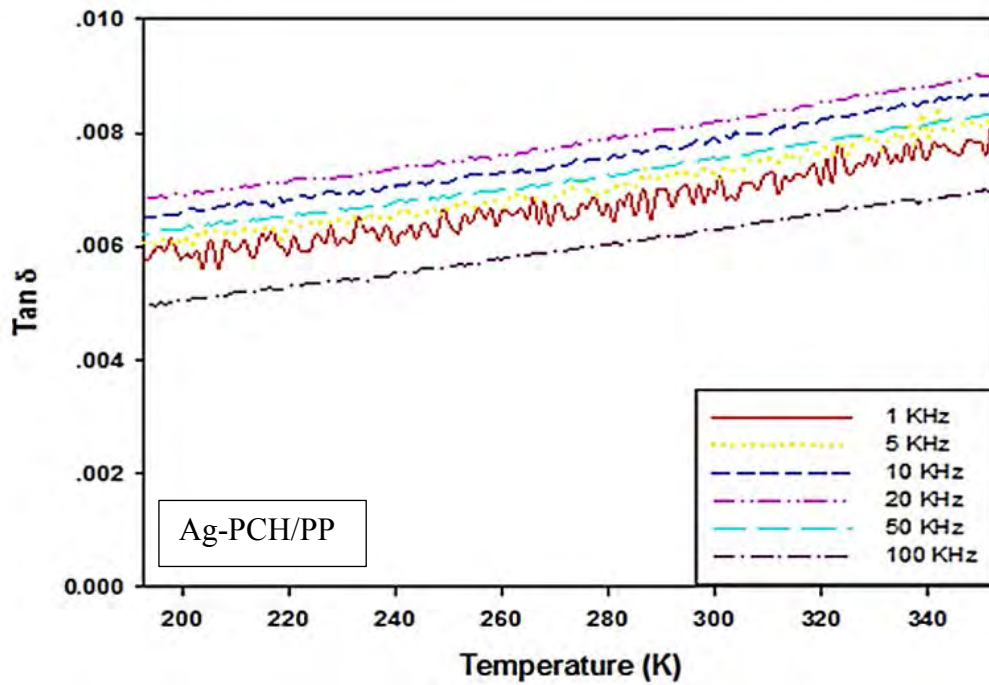
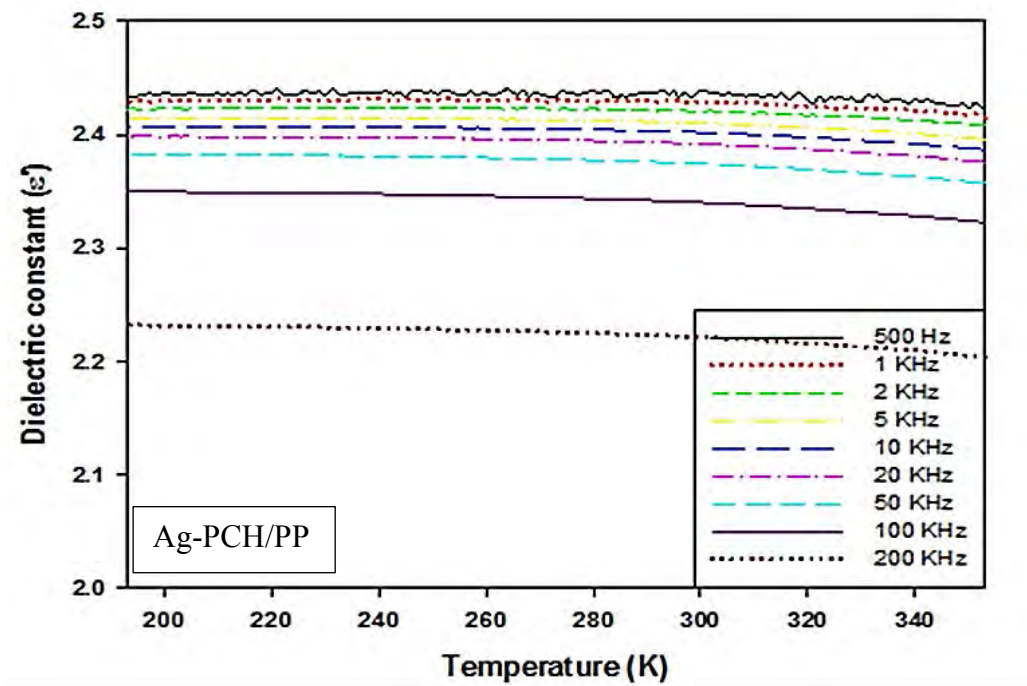
7.4 Results and Discussion

7.4.1 Dielectric property

Normally, the dielectric constant of PP is 2.2-2.3. PP/modified PCHs were examined the electrical property via dielectric property. The experiment was carried out at various frequencies and temperatures. The dielectric properties of the samples with a function of temperature (173 K to 373K) were measured by a LCR meter (HP 4284A) under He atmosphere with the heating and cooling rate of 3 K/min. The results showed that when frequency increased, the dielectric constant decreased. For the function of temperature, the dielectric constant did not change much because it depends on the nature of the materials. Figure 1(b) showed that loss of Ag-PCH exhibited like the straight line which replied that Ag-PCH has the behaviour like the conductive material.



(a)



(b)

Figure 1 Dielectric constant and loss tangent of PP and Ag-PCH at function of temperature.

For the function of frequency (Figure 2), PP presented the lowest dielectric constant while the dielectric constant of nanocomposite revealed higher with different dopants (Table 1). Furthermore, Ag-PCH/PP showed the highest dielectric constant. However, it showed the highest loss too. From the results, the dielectric constant decreased with frequency increasing because of the transition from interfacial polarization to dipole polarization. Interfacial polarization generally takes a longer time to form completely than other polarization. Hence, PP failed to accumulate charges at structure interfaces at high frequency. From the graph, it shows that PP is a good capacitor material at low frequency with a low loss and stable dielectric constant from 100 Hz – 10 kHz.

Concerning about relaxation, the figure showed that there was one relaxation at 20 KHz and it was not shifted. That means clay which added into the PP did not perform any effect. It can explain that the relaxation which occurred is the molecular relaxation due to the vibration of the molecules in the polymer chains. In case of one relaxation frequency, the Arrhenius equation (3) was performed to calculate the relaxation process.

$$\tau = \tau_0 \exp(E_a/k_B T) \quad (3)$$

In Eq. (3), $\tau = 1/f_{\max}$ and f_{\max} is the frequency at the temperature which relaxation peak has the maximum, τ_0 represents the characteristic macroscopic relaxation time and E_a is the so-called activation energy. The plot between $\ln\tau$ vs $1/T$ is plotted in Figure 3 for the relaxation time in the temperature ranges of 173K- 373K. From the plot using Eq. (3), it gives the parameter $\tau_0 = 1.16 \times 10^{-7}$ s, $E_a = 2.72$ eV, and $\tau = 7.96 \times 10^{-6}$ s. From relaxation time (τ), it confirmed that the relaxation occurred through the cooperation motions of polymer segment. To conclude that, relaxation of these nanocomposite materials takes place from α -relaxation of PP related to molecular relaxation in the crystalline phase leading to electrical conduction.

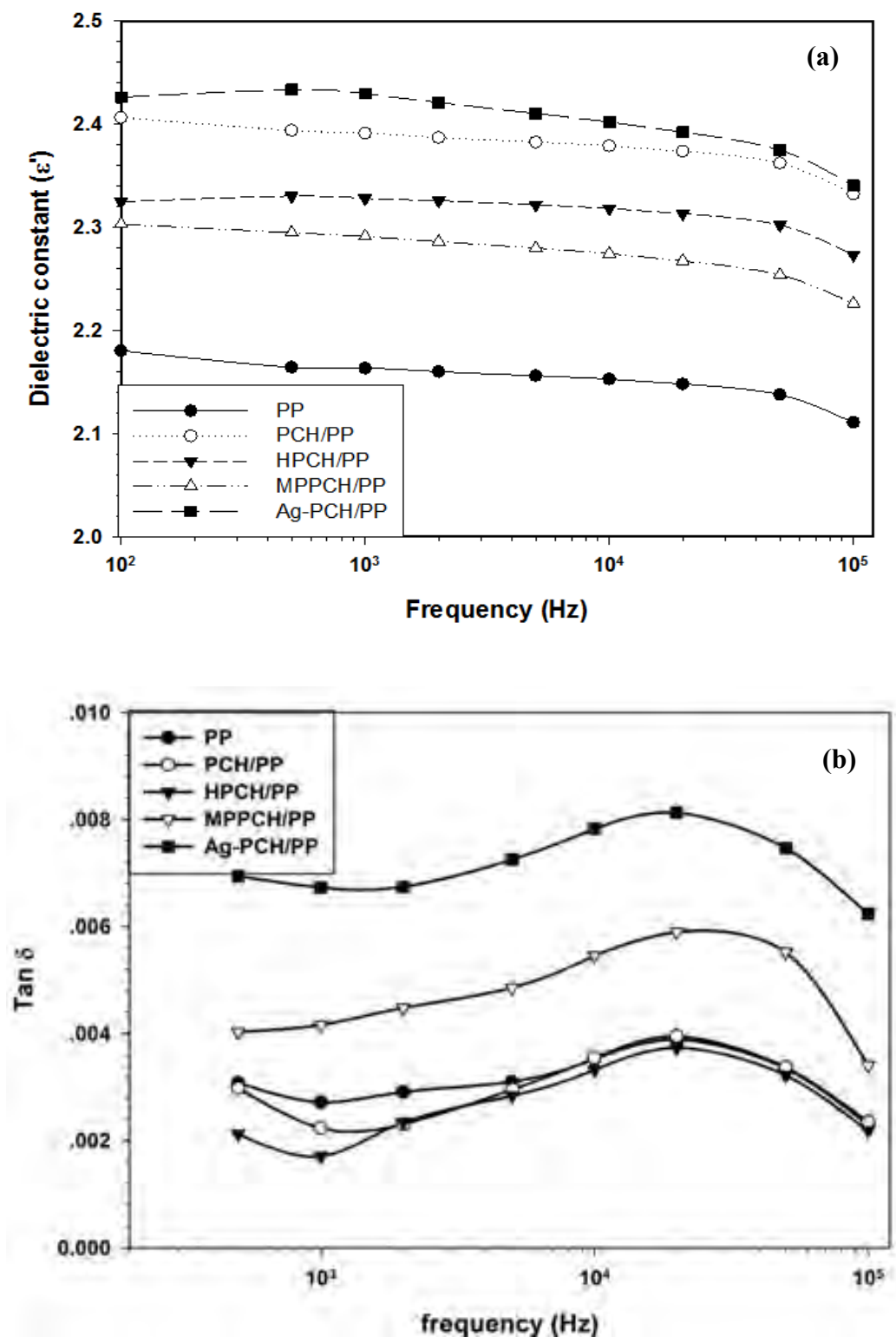
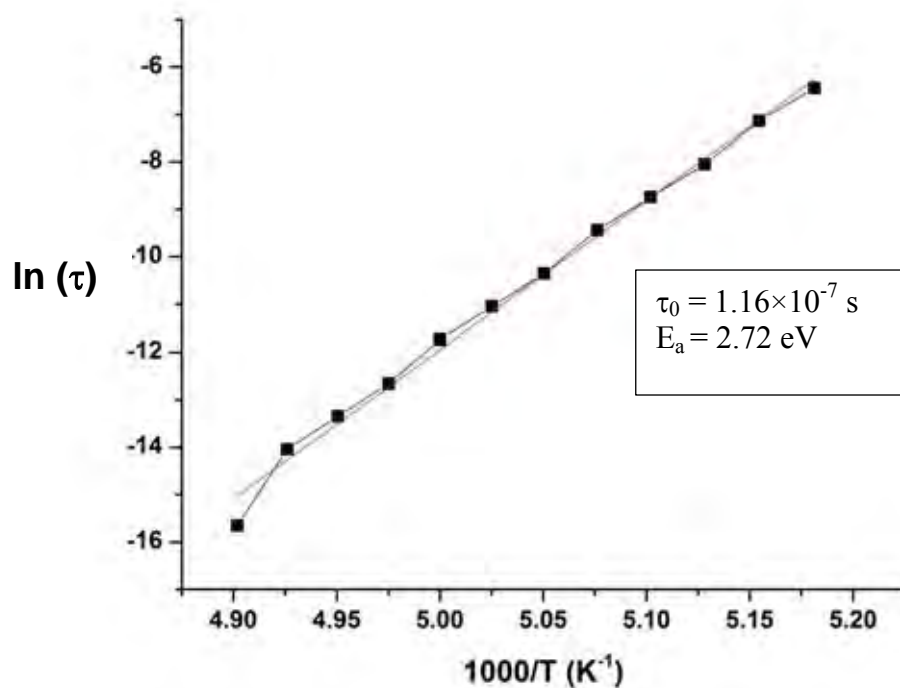


Figure 2 Dielectric constant and loss tangent in function of frequency at 20 °C (293K).

Table 1. Dielectric constant of PP and PP/modified PCHs nanocomposite films

Sample	Dielectric constant (ϵ')
PP	2.15
PCH/PP	2.40
HPCH/PP	2.30
MPPCH/PP	2.26
Ag-PCH/PP	2.43

**Figure 3** Plot of $\ln\tau$ - $1000/T$.

7.4.2 Thermal Expansion

Normally, PP is a negative thermal expansion material which only expand by heating. Figure 4 presented the loop of experimental data. The experiment

was carried out by heating and cooling. And then investigated T_g by intersection of the curve. From Table 2, the results showed that glass transition temperature (T_g) of nanocomposite film was greater than neat PP. As the reinforcement, clay caused the rigid to the molecule so that the molecule cannot move in order to increase the T_g . Moreover, adding clay as fillers resulted in less thermal expansion coefficient.

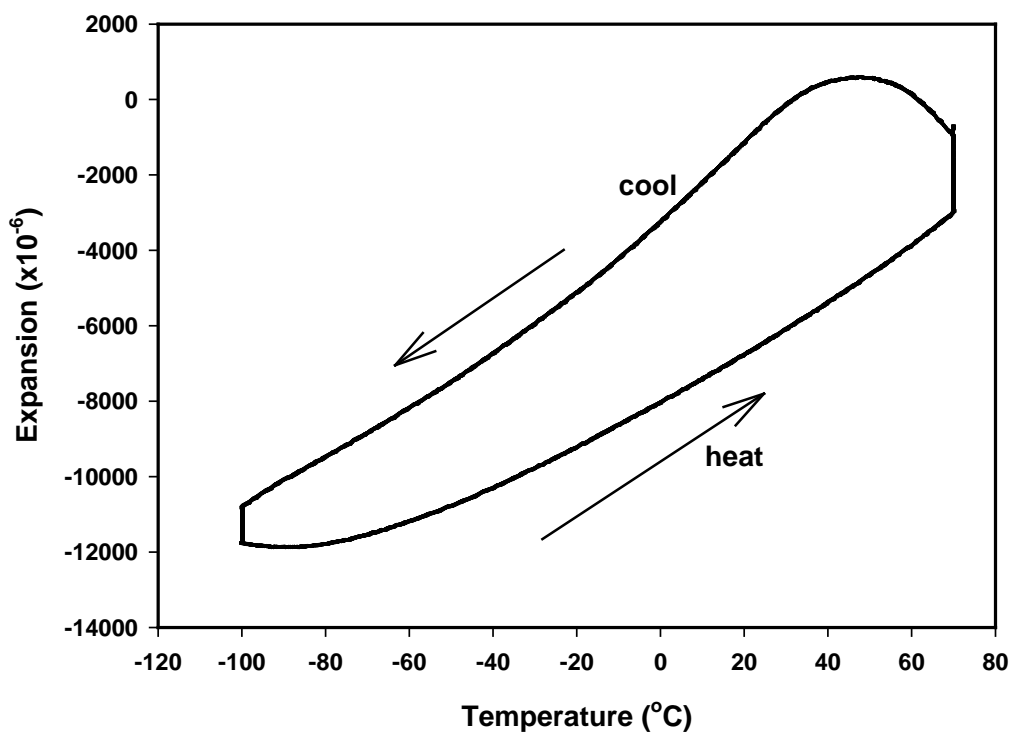


Figure 4 The loop of thermal expansion experiment.

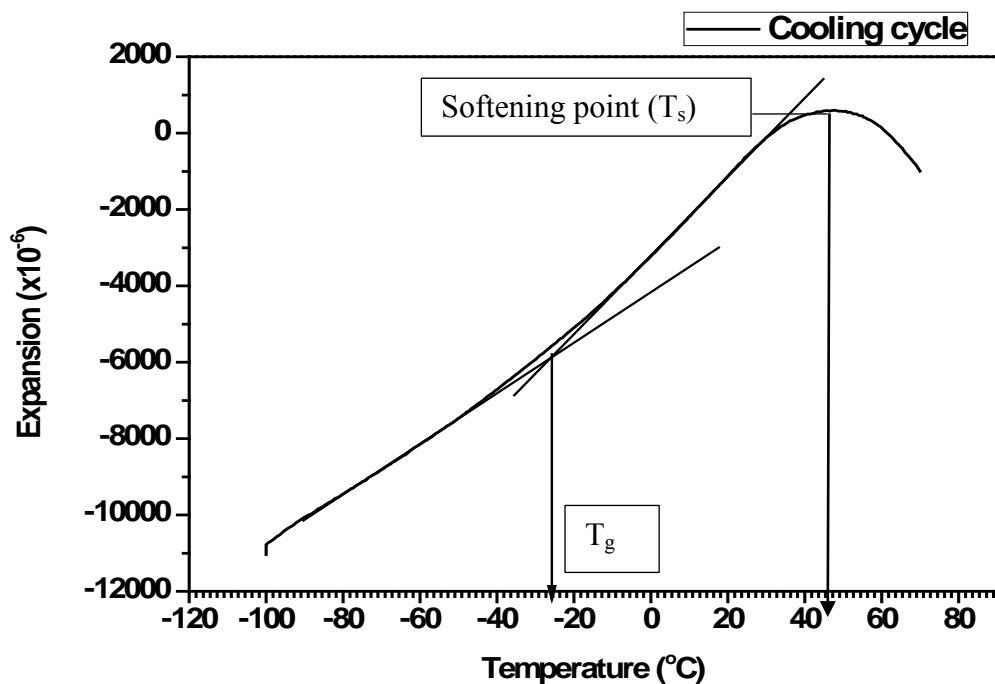


Figure 5 T_g and T_s point of the cooling cycle.

Table 2 The values from thermal expansion analysis

Samples	T _g (°C)	T _s (°C)	$\Delta L/L_0$ (x10 ⁻⁴)	$\alpha_{<Tg-6}$ (x10 ⁻⁶)	α_{RT-6} (x10 ⁻⁶)	$\alpha_{>Tg-6}$ (x10 ⁻⁶)
PP	-25	48	68.21	63.68	101.88	107.87
PCH/PP	-17	54	55.57	67.30	69.90	77.11
HPCH/PP	-15	56	62.93	59.24	61.78	64.53
MPPCH/PP	-14	57	66.66	63.41	83.72	85.06
Ag-PCH/PP	-21	58	61.98	63.85	83.89	87.53

7.5 Conclusion

PP and PP/ modified PCHs nanocomposite films were evaluate and investigate the dielectric constant and thermal expansion. From the result, PP/modified PCHs showed the decreasing of dielectric constant versus frequency increasing. The dielectric constant decreased because of the transition from interfacial polarization to dipolar polarization. In addition, PP and PP/modified PCHs had only one relaxation which is molecular relaxation from PP chain at 20 KHz. Furthermore, adding clay caused T_g of nanocomposite films higher than neat PP and also performed low thermal expansion coefficient. To conclude that, these PP/modified PCHs can perform as a new selective material for using as multilayer film capacitor.

7.6 Acknowledgment

This work is financially supported by the Petroleum and Petrochemical College and Centre of Excellence on Petrochemical and Materials Technology, Thailand. Furthermore, the author would like to acknowledge the research group in the Multifunctional Electronic Materials and Devices Research Laboratory (MeMDRL), Department of Electrical and Computer Engineering, College of Engineering, The University of Texas at San Antonio, Texas, United State for giving the great opportunity in doing the research.

7.7 References

- [1] Varela, C.; Rosales, C.; Perera, R.; Matos, M.; Poirier, T.; Blunda, J.; Rojas, H. Functionalized polypropylenes in the compatibilization and dispersion of clay nanocomposites. *Polym. Composit.*, 2006, 451-458.
- [2] Velasco, J.I.; Ardanuy, M.; Realinho, V.; Antunes, M.; Fernandez, A.I.; Gonzalez-Pena, J.I.; Rodriguez, M.A.; DeSaja, J.A. Polypropylene/Clay nanocomposites: Combined effects of clay treatment and compatibilizer polymers on the structure and properties. *J. Appl. Polym. Sci.*, 2006, 102, 1213-1223.

- [3] Liu, X.; Wu, Q. PP/Clay nanocomposites prepared by grafting– melt intercalation. *Polymer*, 2001, 42, 10013-10019
- [4] Reichert, P.; Nitz, H.; Klinke, S.; Brandsch, R.; Thomann, R.; Mulhaupt, R. Poly (propylene)/organoclay nanocomposite formation: Influence of compatibilizer functionality and organoclay modification. *Macromol. Mater. Eng.*, 2000, 275(2), 8-17.
- [5] Hasegawa, N.; Kawasumi, M.; Kato, M.; Usuki, A.; Okada, A. Preparation and mechanical properties of polypropylene-clay hybrids using a maleic anhydride-modified polypropylene oligomer. *J. Appl. Polym. Sci.*, 1998, 67, 87-92.
- [6] Zhao, Z.; Tang, T.; Qin, Y.; Huang, B. Effects of surfactant loadings on the dispersion of clays in maleated polypropylene. *Langmuir*, 2003, 19, 7157-7159.
- [7] Pozsgay, A.; Frater, T.; Szazdi, L.; Muller, P.; Sajó, I.; Pukanszky, B. Gallery structure and exfoliation of organophilized montmorillonite: Effect on composite properties. *Eur. Polym. J.*, 2004, 40, 27-36.
- [8] Zheng, W.; Lu, X.; Toh, C.; Zheng, T.; He, C. Effect of clay on polymorphism of polypropylene in Polypropylene /Clay nanocomposites. *J. Appl. Polym. Sci: Part B: Polym. Phys.*, 2004, 42, 18101816.
- [9] Modesti, M.; Lorenzetti, A.; Bon, D.; Besco, S. Effect of processing conditions on morphology and mechanical properties of compatibilized polypropylene nanocomposites. *Polymer*, 2005, 46, 10237-10245.
- [10] Wu, J.; Wu, T.; Chen, W.; Tsai, S.; Kuo, W. Preparation and characterization of PP/Clay nanocomposites based on modified polypropylene and clay. *J. Polym. Sci: Part B: Polym. Phys.*, 2005 43, 3242-3254.
- [11] Morlat, S.; Mailhot, B; Gonzalez, D.; Gardette, J. Photo-oxidation of polypropylene/montmorillonite nanocomposites. 1. Influence of nanoclays and compatibilizing agent. *Chem. Mater.*, 2004, 16, 377-383.
- [12] Szazdi, L.; Pukanszky Jr, B.; Foldes, E.; Pukanszky, B. Possible mechanism of intercalation among the components in MAPP modified layered silicate PP nanocomposites. *Polymer*, 2005, 46, 80018010.

- [13] Ding, C.; Jia, D.; He, H.; Guo, B.; Hong, H. How organomontmorillonite truly affects the structure and properties of polypropylene. *Polym. Test.*, 2005, 24, 94-100.
- [14] Ratnayake, U.; Howorth, B. Polypropylene-clay nanocomposites: Influence of low molecular weight polar additives on intercalation and exfoliation behavior. *Polym. Eng. Sci.*, 2006, 1008-1015.
- [15] Zhang, Q.; Fu, Q.; Jiang, L.; Lei, Y. Preparation and properties of polypropylene /montmorillonite layered nanocomposites. *Polym. Int.*, 2000, 49, 1561-1564.
- [16] Korakianiti, A.; Papaefthimiou, V.; Daflou, T.; Kennou, S.; Gregriou, V. Characterization of Polypropylene (PP) Nanocomposites for Industrial Applications. *Macromol. Symp.*, 2004, 205, 71-84. [
- [17] Chiu, F.; Lai, S.; Chen, J.; Chu, P. Combined effects of clay modifications and compatibilizers on the formation and physical properties of melt-mixed polypropylene/clay nanocomposites. *J. Appl. Polym. Sci: Part B: Polym. Phys.*, 2004, 42, 4139-4150.
- [18] Bohning, M.; Goering, H.; Fritz, A.; Brzezinka, K.; Turkey, G.; Schonhals, A.; Schartel, B. Dielectric study of molecular mobility in poly (propylene-graft-maleic anhydride)/clay nanocomposites. *Macromolecules*, 2005, 38, 2764-2774.
- [19] Wang, Y.; Huang, S.; Guo, J. The state of clay dispersion in maleated polypropylene/organoclay nanocomposites via dielectric spectroscopy measurements. *e-Polymer*, 2008, 75, 1-16.
- [20] Wang, Y.; Huang, S. Solution intercalation and relaxation properties of maleated polypropylene/ Organoclay Nanocomposites. *Polym.-Plast. Technol. Eng.*, 2007, 46, 1039-1047.
- [21] Kalgaonkar, R.; Jog, J. Molecular dynamics of copolyester/clay nanocomposites investigated by viscoelastic and dielectric analysis. *J. Polym. Sci: Part B: Polym. Phys.*, 2008, 46, 2539-2555.
- [22] Chanmal, C.; Jog, J. Study of dielectric behavior in PVDF/Clay nanocomposites. *e-Polymers*, 2009, 112, 1-8.

- [23] Akinci, A. Mechanical and structural properties of polypropylene composites filled with graphite flakes. *Mater. Sci. Eng.*, 2009, 35/2, 91-94.
- [24] Galgali, G.; Ramesh, C.; Lele, A. A Rheological study on the kinetics of hybrid formation in polypropylene nanocomposites. *Macromolecule*, 2001, 34, 852-858.
- [25] Hambir, S.; Bulakh, N.; Kodgire, P.; Kalgaonkar, K.; Jog, J. PP/Clay nanocomposites: A study of crystallization and dynamic mechanical behavior. *J. Polym. Sci: Part B: Polym. Phys.*, 2001, 39, 446-450.

CHAPTER VIII

CONCLUSIONS AND RECOMMENDATIONS

8.1 Conclusions

The modified mesoporous clay heterostructure was successfully synthesized through the surfactant-directed assembly of the mesostructured silica of clay. After treatment with TEOS/MTS and TEOS/MPTMS via the co-condensation reaction, the intercalated TEOS/MTS and TEOS/MPTMS were hydrolysed and condensed, leading to the formation of micelles in the interlayer of the clay. The surfactants were removed by solvent extraction and then porous materials were obtained. From the XRD results, after treatment with CTAB, the *d*-spacing of organoclay increases, indicating the successful insertion of the surfactant between the clay layers. According to the N₂ adsorption–desorption, the specific surface areas of the PCHs, HPCHs, and MPPCHs are much higher than those of pure bentonite as the plate–like structure was transformed to a pore structure. From the ethylene adsorption results, the HPCHs have a higher efficiency in adsorbing ethylene gas than the others because the methyl groups that incorporate in the PCH lead to a non polar surface, which causes the best ethylene adsorption. Otherwise, the thiol groups that incorporate in the PCH exhibits the best ethylene sensing by their high sensitivity due to the largest drop of the electrical conductivity when they bind to the ethylene gas by the dipole-dipole interaction. Next, the modified mesoporous clay heterostructure was successfully synthesized through the surfactant-directed assembly of the mesostructured silica of clay and then functionalized with MPTMS/TEOS in ratios of 1:1, 2:1 and 4:1 via the co-condensation reaction. According to the N₂ adsorption–desorption, the specific surface areas of all modified MPPCHs are greater than those of pure bentonite. However, the specific surface areas of all modified MPPCHs decrease with increasing amount of thiol group in the modified MPPCHs. From the ethylene adsorption results, the modified MPPCHs have higher efficiency in adsorbing ethylene gas than that of BTN because the organic group (thiol) that incorporate in the PCH leads to a non-polar surface, comparing to the hydroxyl group of bentonite, which causes the best ethylene

adsorption. And MPPCH (2:1) shows the best result in ethylene adsorbing among the others. For conductivity results, BTN shows high conductivity value due to its inorganic material property. Moreover, all modified MPPCHs containing the organic group (thiol) present higher conductivity than BTN and the conductivity values decrease with the increasing of amount ratio of thiol group in modified MPPCHs. However, MPPCH (2:1) exhibits a great ethylene adsorption and also represents a good conductivity value. Consequently, further experiment is blending the MPPCH (2:1) with polymers (PP) and evaluate these nanocomposite films as ethylene scavenging sensor for tropical fruits in smart packaging applications.

According to the results of chapter VI, it concluded that Ag-PCH revealed porous structure due to scattering spectra, and also exhibited the rough surface and small grains with increasing the contents of silver. Furthermore, the Ag-PCH performed the higher efficiency in adsorbing ethylene gas than BTN and PCH. The 10 wt% Ag-PCH was chosen to blend with PP due to its great ethylene adsorption value and great conductivity result and then PP/clay nanocomposite films with various 1wt%, 3wt%, 5wt% Ag-PCH loading were fabricated. Referred to thermal and mechanical results, all PP/Ag-PCHs nanocomposite films presented improving in thermal and mechanical properties due to higher Td, higher modulus and tensile strength and also higher elongation at break than those of neat PP. Moreover, all PP/Ag-PCHs nanocomposite films showed the greater value in ethylene adsorption and conductivity result than PP. In addition, PP/Ag-PCHs nanocomposite films also displayed the sensing to the ethylene gas by conductivity dropping.

Furthermore, PP and PP/ modified PCHs nanocomposite films were evaluated and investigated the dielectric constant and thermal expansion. From the result, PP/modified PCHs showed the decreasing of dielectric constant versus increasing frequency. The dielectric constant decreased because of the transition from interfacial polarization to dipolar polarization. In addition, PP and PP/modified PCHs had only one relaxation which is molecular relaxation. Furthermore, adding clay caused Tg of the nanocomposite films higher than the neat PP and also performed low thermal expansion.

In conclusion, these PP/modified PCHs can perform as new selective materials for using as ethylene scavenger, ethylene gas sensing films, and multilayer film capacitor. Thus they conduct as multifunctional nanocomposite films.

8.2 Recommendations

With clay contents over 3 wt%, it's difficult to fabricate into blown films. To solve this problem, the compatibilizer, e.g. PP-g-MA and Surlyn®, should be added into the system, and the amount of compatibilizer should be added around 5 wt% - 10 wt%.

REFERENCES

- Aharoni, Y., Copel, A., Gil, M., and Fallik, E. (1996) Polyolefin stretch films maintain the quality of sweet corn during storage and shelf-life. Postharvest Biology and Technology, 7(1-2), 171-176.
- Azeredo, H. M. C. d. (2009) Nanocomposites for food packaging applications. Food Research International, 42(9), 1240-1253.
- Baldwin, E. A., Burns, J.K., Kazokas, W., Brecht, J.K., Hagenmaier, R.D., Bender, R.J., Pesis, D.E. (1999) Effect of two edible coatings with different permeability characteristics on mango (*mangifera indica* l.) ripening during storage. Postharvest Biology and Biotechnology, 17, 215-226.
- Bernardo, C. G. P. M., and Gomes, J. A. N. F. (2002) The adsorption of ethylene on the (110) surfaces of copper, silver and platinum: A dft study. Journal of Molecular Structure: THEOCHEM, 582(1-3), 159-169.
- Bodbodak, S., and Moshfeghifar, M. (2016) 4 - advances in modified atmosphere packaging of fruits and vegetables a2 - siddiqui, mohammed wasim, Eco-friendly technology for postharvest produce quality (pp. 127-183): Academic Press.
- Brabazon, D., and Raffler, A. (2015) Chapter 3 - advanced characterization techniques for nanostructures Emerging nanotechnologies for manufacturing (second edition) (pp. 53-85). Boston: William Andrew Publishing.
- Brody, A., Strupinsky, E.P., Kline, L.R. (2001) Active packaging for food applications. Boca Raton Florida: CRC Press.
- Cao, N., Fu, Y., He, J., (2007) Mechanical properties of gelatin films cross-linked, respectively, by ferulic acid and tannin acid. Food Hydrocolloids, 21, 575-584.
- Carja, G., Kameshima, Y., Nakajima, A., Dranca, C., and Okada, K. (2009) Nanosized silver-anionic clay matrix as nanostructured ensembles with antimicrobial activity. International Journal of Antimicrobial Agents, 34(6), 534-539.
- Chakraverty, A. (2001) Postharvest technology. Enfield, New Hampshire: Scientific Publishers.

- Chevion, P., Gouanvé, F., and Espuche, E. (2016) Preparation, characterization and barrier properties of silver/montmorillonite/starch nanocomposite films. Journal of Membrane Science, 497, 162-171.
- Chmielarz, L., Kuśtrowski, P., Drozdek, M., Dziembaj, R., Cool, P., and Vansant, E. F. (2006) Selective catalytic oxidation of ammonia into nitrogen over pch modified with copper and iron species. Catalysis Today, 114(2–3), 319-325.
- Chmielarz, L., Kuśtrowski, P., Dziembaj, R., Cool, P., and Vansant, E. F. (2007) Selective catalytic reduction of no with ammonia over porous clay heterostructures modified with copper and iron species. Catalysis Today, 119(1–4), 181-186.
- Dainelli, D., Gontard, N., Spyropoulos, D., Zondervan-van den Beuken, E., and Tobback, P. (2008) Active and intelligent food packaging: Legal aspects and safety concerns. Trends in Food Science and Technology, 19(Supplement 1), S103-S112.
- De Chiara, M. L. V., Pal, S., Licciulli, A., Amodio, M. L., and Colelli, G. (2015) Photocatalytic degradation of ethylene on mesoporous TiO₂/SiO₂ nanocomposites: Effects on the ripening of mature green tomatoes. Biosystems Engineering 132(Supplement C), 61-70.
- De Jong, A. R., Boumans, H., Slaghek, T., Van Veen, J., Rijk, R., and Van Zandvoort, M. (2005) Active and intelligent packaging for food: is it the future? Food Addit Contam 22(10), 975-979.
- De Mello Ferreira Guimarães, A., Ciminelli, V. S. T., and Vasconcelos, W. L. (2009) Smectite organofunctionalized with thiol groups for adsorption of heavy metal ions. Applied Clay Science, 42(3–4), 410-414.
- De Paiva, L. B., Morales, A. R., and Valenzuela Díaz, F. R. (2008) Organoclays: Properties, preparation and applications. Applied Clay Science, 42(1–2), 8-24.
- Delacôte, C., Gaslain, F. O. M., Lebeau, B., and Walcarius, A. (2009) Factors affecting the reactivity of thiol-functionalized mesoporous silica adsorbents toward mercury(ii). Talanta, 79(3), 877-886.

- Deng, X., Nikiforov, A. Y., and Leys, C. (2017) 1 - antimicrobial nanocomposites for food packaging a2 - grumezescu, alexandru Mihai, Food preservation (pp. 1-34): Academic Press.
- Diaz, M., Cambier, P., Brendlé, J., and Prost, R. (2007) Functionalized clay heterostructures for reducing cadmium and lead uptake by plants in contaminated soils. Applied Clay Science, 37(1–2), 12-22.
- Długosz, M., Bulwan, M., Kania, G., Nowakowska, M., and Zapotoczny, S. (2012) Hybrid calcium carbonate/polymer microparticles containing silver nanoparticles as antibacterial agents. Journal of Nanoparticle Research, 14(12), 1313.
- Dobrucka, R., and Cierpiszewski, R. (2014) Active and Intelligent Packaging Food – Research and Development – A Review. Polish Journal of Food and Nutrition Science, 64(1), 7-15.
- Duncan, T. V. (2011) Applications of nanotechnology in food packaging and food safety: Barrier materials, antimicrobials and sensors. Journal of Colloid and Interface Science, 363(1), 1-24.
- Erdog̃rul, Ö. and Şener, H. (2005) The contamination of various fruit and vegetable with *Enterobius vermicularis*, *Ascaris* eggs, *Entamoeba histolyca* cysts and *Giardia* cysts. Food Control, 16(6), 557-560.
- Erturk, E. and Picha, D. H. (2008) The effects of packaging film and storage temperature on the internal package atmosphere and fermentation enzyme activity of sweet potato slices. Journal of Food Processing and Preservation, 32(5), 817-838.
- Fagundes, C., Moraes, K., Pérez-Gago, M. B., Palou, L., Maraschin, M., and Monteiro, A. R. (2015) Effect of active modified atmosphere and cold storage on the postharvest quality of cherry tomatoes. Postharvest Biology and Technology, 109, 73-81.
- Fernandez, A., Picouet, P., and Lloret, E. (2010) Cellulose-silver nanoparticle hybrid materials to control spoilage-related microflora in absorbent pads located in trays of fresh-cut melon. Int J Food Microbiol, 142(1-2), 222-228.

- Garcia, M. A., Martino, M.N., Zaritzky, N.E. (1998a) Starch-based coatings: Effect on refrigerated strawberry (*fragaria* × *ananassa*) quality. *Journal of the Science of Food and Agriculture*, 76, 411-420.
- Ghaani, M., Cozzolino, C. A., Castelli, G., and Farris, S. (2016) An overview of the intelligent packaging technologies in the food sector. *Trends in Food Science and Technology*, 51(Supplement C), 1-11.
- Giannakourou, M., Koutsoumanis, K., Nychas, G., and Taoukis, P. (2005) Field evaluation of the application of time temperature integrators for monitoring fish quality in the chill chain. *Int J Food Microbiol*, 102, 323-336.
- González-Aguilar, G. A., Buta, J. G., and Wang, C. Y. (2003) Methyl jasmonate and modified atmosphere packaging (map) reduce decay and maintain postharvest quality of papaya 'sunrise'. *Postharvest Biology and Technology*, 28(3), 361-370.
- Gupta, R. K., and Dudeja, P. (2017) Chapter 46 - food packaging Food supply safety in india (pp. 547-553). San Diego: Academic Press.
- Hassan, F. A. S., and Mahfouz, S. A. (2012) Effect of 1-methylcyclopropene (1-MCP) on the postharvest senescence of coriander leaves during storage and its relation to antioxidant enzyme activity. *Scientia Horticulturae*, 141(Supplement C), 69-75.
- ess, C. (2013). 7.10 - Ordered Mesoporous and Microporous Materials with Heteroatoms A2. In Jan Reedijk and K. R. Poeppelmeier (Eds.), Comprehensive Inorganic Chemistry II (Second Edition) (pp. 231-245). Amsterdam: Elsevier.
- Ishii, R., Imai, Y., Wada, M., Ebina, T., Hanaoka, T., and Mizukami, F. (2006) Adsorption and desorption behaviors of flavor molecules into a microporous pillared clay mineral and the application to flavor capsule composites. *Applied Clay Science*, 33(2), 99-108.
- Jia, H., Hou, W., Wei, L., Xu, B., and Liu, X. (2008) The structures and antibacterial properties of nano-sio₂ supported silver/zinc-silver materials. *Dental Materials*, 24(2), 244-249.

- Khwalidia, K., Perez, C., Banon, S., Desobry, S., and Hardy, J. (2004) Milk Proteins for Edible Films and Coatings. Critical Reviews in Food Science and Nutrition, 44(4), 239-251.
- Kruijf, N. D., Beest, M. V., Rijk, R., Sipiläinen-Malm, T., Losada, P. P., and Meulenaer, B. D. (2002) Active and intelligent packaging: applications and regulatory aspects. Food Additives and Contaminants, 19(sup1), 144-162.
- Li, L., Kaplunov, T., Zutahy, Y., Daus, A., Porat, R., and Lichter, A. (2015) The effects of 1-methylcyclopropane and ethylene on postharvest rachis browning in table grapes. Postharvest Biology and Technology, 107, 16-22.
- Li, T., Lin, O., Lu, Z., He, L., and Wang, X. (2014) Preparation and characterization of silver loaded montmorillonite modified with sulfur amino acid. Applied Surface Science, 305, 386-395.
- Liang, X., Xu, Y., Sun, G., Wang, L., Sun, Y., and Qin, X. (2009) Preparation, characterization of thiol-functionalized silica and application for sorption of Pb²⁺ and Cd²⁺. Colloids and Surfaces A: Physicochemical and Engineering Aspects, 349(1-3), 61-68.
- Liu, J., Li, X., Zuo, S., and Yu, Y. (2007) Preparation and photocatalytic activity of silver and tio₂ nanoparticles/montmorillonite composites. Applied Clay Science, 37(3-4), 275-280.
- Llorens, A., Lloret, E., Picouet, P. A., Trbojevich, R., and Fernandez, A. (2012) Metallic-based micro and nanocomposites in food contact materials and active food packaging. Trends in Food Science and Technology, 24(1), 19-29.
- Lv, Y., Liu, H., Wang, Z., Liu, S., Hao, L., Sang, Y., Liu, D., Wang, J., and Boughton, R. I. (2009) Silver nanoparticle-decorated porous ceramic composite for water treatment. Journal of Membrane Science, 331(1-2), 50-56.
- Magaña, S. M., Quintana, P., Aguilar, D. H., Toledo, J. A., Ángeles-Chávez, C., Cortés, M. A., León, L., Freile-Pelegrín, Y., López, T., and Sánchez, R. M. T. (2008) Antibacterial activity of montmorillonites modified with silver. Journal of Molecular Catalysis A: Chemical, 281(1-2), 192-199.

- Marcinkowsky, A. E. and Berty, J. M. (1973) Ethylene adsorption on oxygenated silver: Evidence for two types of chemisorbed oxygen. Journal of Catalysis, 29(3), 494-499.
- Martínez-Romero, D., Bailen, G., Serrano, M., Guillen, F., Valverde, J.M., Zapata, P., Castillo, S., and Valero, D. (2007) Tools to maintain postharvest fruit and vegetables quality through the inhibition of ethylene action: A review. Critical Reviews in Food Science and Nutrition, 47, 543-560.
- Mehyar, G. F., and Han, J. H. (2004) Physical and Mechanical Properties of High-amylose Rice and Pea Starch Films as Affected by Relative Humidity and Plasticizer. Journal of Food Science, 69(9), E449-E454.
- Mekhloufi, M., Zehhaf, A., Benyoucef, A., Quijada, C., and Morallon, E. (2013) Removal of 8-quinolinecarboxylic acid pesticide from aqueous solution by adsorption on activated montmorillonites. Environmental Monitoring and Assessment, 185(12), 10365-10375.
- Mercier, L. and Pinnavaia, T. J. (1998) A functionalized porous clay heterostructure for heavy metal ion (Hg^{2+}) trapping. Microporous and Mesoporous Materials, 20(1-3), 101-106.
- Meyer, M. D., and Terry, L. A. (2010) Fatty acid and sugar composition of avocado, cv. Hass, in response to treatment with an ethylene scavenger or 1-methylcyclopropene to extend storage life. Food Chemistry, 121(4), 1203-1210.
- Nakatsuji, M., Ishii, R., Wang, Z.-M., and Ooi, K. (2004) Preparation of porous clay minerals with organic-inorganic hybrid pillars using solvent-extraction route. Journal of Colloid and Interface Science, 272(1), 158-166.
- Nunes, C. D., Pires, J., Carvalho, A. P., Calhorda, M. J., and Ferreira, P. (2008) Synthesis and characterisation of organo-silica hydrophobic clay heterostructures for volatile organic compounds removal. Microporous and Mesoporous Materials, 111(1-3), 612-619.
- Ozdemir, M., and Floros, J.D. (2004) Active food packaging technologies. Critical Reviews in Food Science and Nutrition, 44, 185-193.

- Pálková, H., Madejová, J., Zimowska, M., Bielańska, E., Olejniczak, Z., Lityńska-Dobrzyńska, L., and Serwicka, E. M. (2010) Laponite-derived porous clay heterostructures: I. Synthesis and physicochemical characterization. Microporous and Mesoporous Materials, 127(3), 228-236.
- Pehlivan, H., Balköse, D., Ülkü, S., and Tihminliog˘lu, F. (2005) Characterization of pure and silver exchanged natural zeolite filled polypropylene composite films. Composites Science and Technology, 65(13), 2049-2058.
- Polverejan, M., Liu, Y., and Pinnavaia, T. J. (2002) Aluminated derivatives of porous clay heterostructures (pch) assembled from synthetic saponite clay: Properties as supermicroporous to small mesoporous acid catalysts. Chemistry of Materials, 14(5), 2283-2288.
- Polverejan, M., Pauly, T. R., and Pinnavaia, T. J. (2000) Acidic porous clay heterostructures (pch): Intragallery assembly of mesoporous silica in synthetic saponite clays. Chemistry of Materials, 12(9), 2698-2704.
- Praus, P., Turicová, M., Machovič, V., Študentová, S., and Klementová, M. (2010) Characterization of silver nanoparticles deposited on montmorillonite. Applied Clay Science, 49(3), 341-345
- Preeti, S., Ali, A. W., and Sven, S. (2011) Active packaging of food products: Recent trends. Nutrition and Food Science, 41(4), 249-260.
- Quang Huy, T., Van Quy, N., and Anh-Tuan, L. (2013) Silver nanoparticles: Synthesis, properties, toxicology, applications and perspectives. Advances in Natural Sciences: Nanoscience and Nanotechnology, 4(3), 033001.
- Rao, T. V. R., Gol, N. B., and Shah, K. K. (2011) Effect of postharvest treatments and storage temperatures on the quality and shelf life of sweet pepper (*capsicum annum* l.). Scientia Horticulturae, 132, 18-26.
- Rodríguez-Hernández, J. (2017) 3 - Nanostructured antimicrobial materials in the food industry a2 - grumezescu, alexandru Mihai, Food preservation (pp. 75-124): Academic Press.

- Rostamian, R., Najafi, M., and Rafati, A. A. (2011) Synthesis and characterization of thiol-functionalized silica nano hollow sphere as a novel adsorbent for removal of poisonous heavy metal ions from water: Kinetics, isotherms and error analysis. Chemical Engineering Journal, 171(3), 1004-1011.
- Sanjeev, K. and Ramesh, M.N. (2006) Low oxygen and inert gas processing of foods. Critical Reviews in Food Science and Nutrition, 46, 423-450.
- Santos, M. F., Oliveira, C. M., Tachinski, C. T., Fernandes, M. P., Pich, C. T., Angioletto, E., Riella, H. G., and Fiori, M. A. (2011) Bactericidal properties of bentonite treated with Ag⁺ and acid. International Journal of Mineral Processing, 100(1-2), 51-53.
- Scully, A. D., and Horsham, M.A. (2007) Active packaging for fruits and vegetables. USA: Taylor and Francis, Boca Raton Florida.
- Silvestre, C., Duraccio, D., and Cimmino, S. (2011) Food packaging based on polymer nanomaterials. Progress in Polymer Science, 36(12), 1766-1782.
- Sothornvit, R., and Rodsamran, P. (2008) Effect of a mango film on quality of whole and minimally processed mangoes. Postharvest Biology and Technology, 47(3), 407-415.
- Srithamaraj, K., Magaraphan, R., and Manuspiya, H. (2008) Surfactant-templated synthesis of modified porous clay heterostructure (pch). Advanced Materials Research, 55-57, 317-320.
- Srithamaraj, K., Magaraphan, R., and Manuspiya, H. (2012) Modified porous clay heterostructures by organic-inorganic hybrids for nanocomposite ethylene scavenging/sensor packaging film. Packaging Technology and Science, 25(2), 63-72.
- Srividya, N., Ghoora, M. D., and Padmanabh, P. R. (2017) 4 - antimicrobial nanotechnology: Research implications and prospects in food safety a2 - grumezescu, alexandru Mihai, Food preservation (pp. 125-165): Academic Press.

- Terry, L. A., Ilkenhans, T., Poulston, S., Rowsell, L., and Smith, A. W. J. (2007) Development of new palladium-promoted ethylene scavenger. Postharvest Biology and Technology, 45(2), 214-220.
- Tonlé, I. K., Ngameni, E., Tcheumi, H. L., Tchiéda, V., Carteret, C., and Walcarius, A. (2008) Sorption of methylene blue on an organoclay bearing thiol groups and application to electrochemical sensing of the dye. Talanta, 74(4), 489-497.
- Tucker, G., Hanby, E., and Brown, H. (2009) Development and application of a new time-temperature integrator for the measurement of p-values in mild pasteurization processes. Food and Bioprocess Processing, 87, 23-33.
- Tucker, G. S., Brown, H. M., Fryer, P. J., Cox, P. W., Poole, F. L., and Lee, H. S. (2007) A sterilization time-temperature integrator based on amylase from the hyperthermophilic organism *pyrococcus furiosus*. Innovative Food Science and Emerging Technologies, 8, 63-72.
- Turgut Basoglu, F., and Balci, S. (2010) Micro-mesopore analysis of Cu^{2+} and Ag^+ containing al-pillared bentonite. Applied Clay Science, 50(1), 73-80.
- Valášková, M., Hundáková, M., Kutlákova, K. M., Seidlerová, J., Čapková, P., Pazdziora, E., Matějová, K., Heřmánek, M., Klemm, V., and Rafaja, D. (2010) Preparation and characterization of antibacterial silver/vermiculites and silver/montmorillonites. Geochimica et Cosmochimica Acta, 74(22), 6287-6300.
- Waghmare, R. B., and Annapure, U. S. (2013) Combined effect of chemical treatment and/or modified atmosphere packaging (map) on quality of fresh-cut papaya. Postharvest Biology and Technology, 85, 147-153.
- Wei, L., Tang, T., and Huang, B. (2004) Novel acidic porous clay heterostructure with highly ordered organic-inorganic hybrid structure: One-pot synthesis of mesoporous organosilica in the galleries of clay. Microporous and Mesoporous Materials, 67(2-3), 175-179.
- Zehhaf, A., Benyoucef, A., Quijada, C., Taleb, S., and Morallón, E. (2015) Algerian natural montmorillonites for arsenic(iii) removal in aqueous solution. International Journal of Environmental Science and Technology, 12(2), 595-602.

- Zhou, C., Li, X., Ge, Z., Li, Q., and Tong, D. (2004). Synthesis and acid catalysis of nanoporous silica/alumina-clay composites. Catalysis Today, 93–95, 607-613.
- Zhou, X., Huang, Q., Chen, S., and Yu, Z. (2005) Adsorption of the insecticidal protein of bacillus thuringiensis on montmorillonite, kaolinite, silica, goethite and red soil. Applied Clay Science, 30(2), 87-93.
- Zub, Y. L., Melnyk, I. V., Stolyarchuk, N. V., Dobryanska, H. I., Barczak, M., and Dabrowski, A. (2005) Comparative characteristics of texture and properties of hybrid organic–inorganic adsorbents functionalized by amine and thiol groups. Progress in Solid State Chemistry, 33(2–4), 179-186.

APPENDICES

Appendix A Prolonging Shelf-life of Fresh Fruits

After modification, all of modified PCHs were blended with polypropylene (PP) and then fabricated into polypropylene/clay nanocomposite films, called as PCH/PP, HPCH/PP, MPPCH/PP, and Ag-PCH/PP nanocomposite films, respectively. All polypropylene/clay nanocomposite films were evaluated the ability in preserving the freshness of the produce.

Table A1 Ethylene scavenger test for banana shelf-life








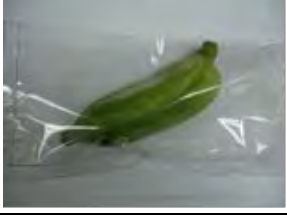







Sample	Day 1	Day 3	Day 10
Control			
PP			
PCH/PP			
HPCH/PP			
MPPCH/PP			

Table A2 Mango prolonging shelf-life test

















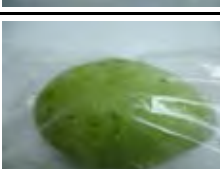
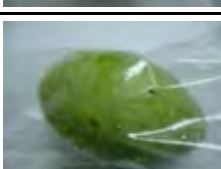
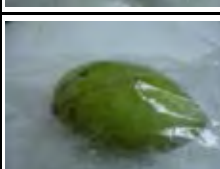
















Sample	Day 1	Day 4	Day 20	Day 27
Control				
PP				
1 wt% MPPCH/PP				
3 wt% MPPCH/PP				
5 wt% MPPCH/PP				

Table A3 Prolonging shelf-life test of Ag-PCH/PP nanocomposite films

Sample	Day 1	Day 14	Day 25
Control			
PP			
1 wt% (10 wt%Ag-PCH)/PP			
3 wt% (10 wt%Ag-PCH)/PP			
5 wt% (10 wt%Ag-PCH)/PP			

Appendix B Percentages of Weight Loss

Furthermore, the nanocomposite films were investigated about an effect on the physiological changes of limes during storage at 25°C. The limes were dipped in distilled water and then packed into the polypropylene/clay nanocomposite films such as Org/PP, PCH/PP, HPCH/PP, MPPCH/PP, and PP as control.

Fruit were weighed on the 1st day after treatment and then measurements were done every 7 days after treatment. Weight loss was calculated as follows:

$$\text{Weight loss (\%)} = \frac{\text{Initial weight (g)} - \text{Final weight (g)}}{\text{Initial weight (g)}} * 100$$

Percentages of weight loss of limes stored at 25 °C for 4 weeks increased during the storage time. The limes dipped in distilled water and packed in HPCH/PP and MPPCH/PP significantly had lower percentages of weight loss than PP since the first week of storage (Figure B1).

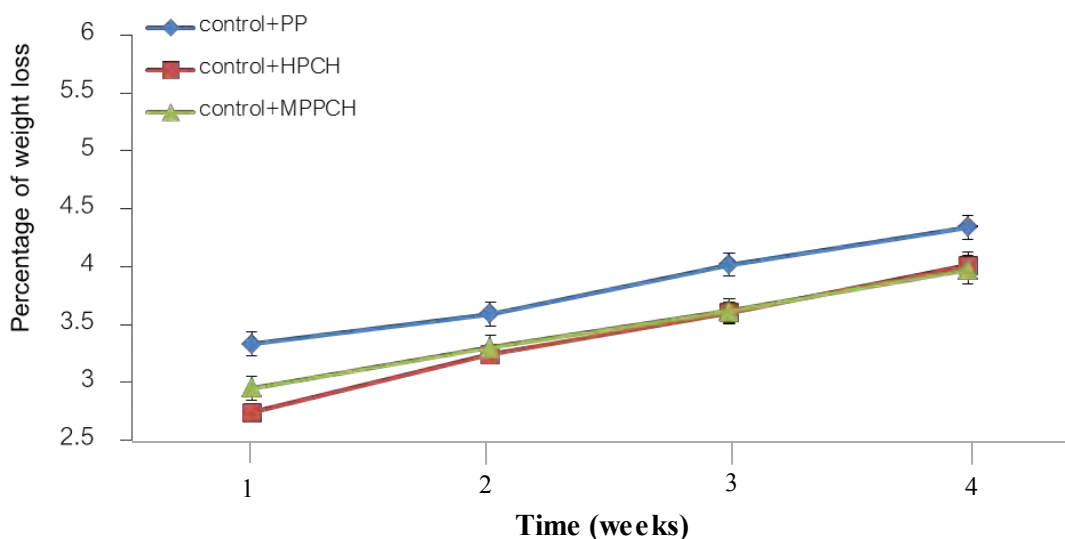


Figure B1 Percentage of weight loss of limes which were packed in polypropylene/clay nanocomposite films and stored at 25 °C for 4 weeks.

Appendix C Disease Incidence

The disease incidence was measured by counting diseased limes in each week and calculated to percentage as follows:

$$\text{Percentage of disease incidence} = \frac{\text{Number of disease fruits}}{\text{Number of total fruits}} * 100$$

The disease incidence of limes was found since the first week and increased throughout the storage times. Limes packed in PP had the highest percentage of the disease incidence while the limes packed in PCH/PP and HPCH/PP did not showed the disease incidence at the last week of storage (Figure C1).

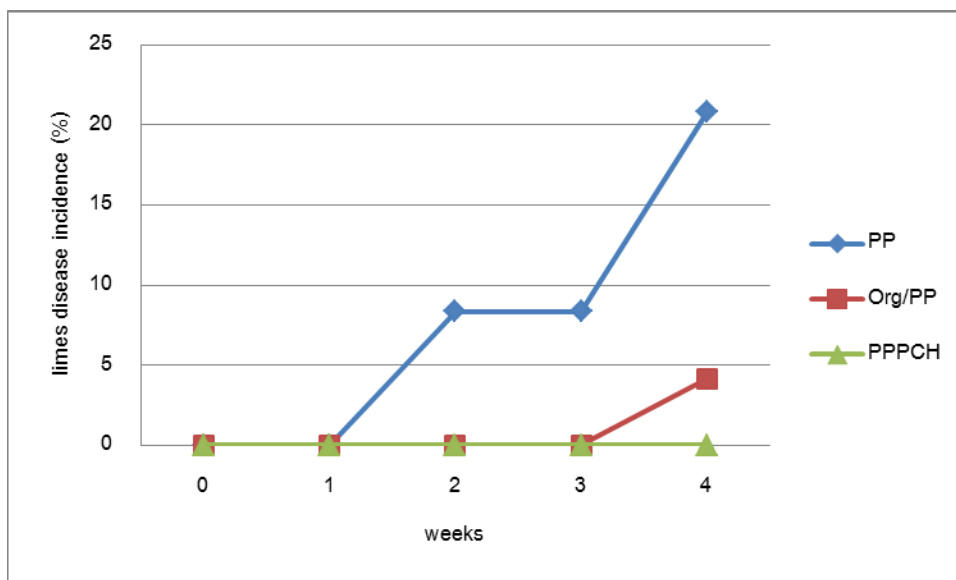


Figure C1 Percentage of lime disease of limes which were packed in polypropylene/clay nanocomposite films during storage at 25°C for 4 weeks.

Appendix D Measurement of Respiration Rate

The respiration rate of lime fruit steadily increased during storage. Limes packed in Org/PP showed the lowest respiration rate in the first and second week (Figure D1). Slightly changes in respiration rate were observed in all treatments of the packages during storage (Figure D2). Limes packed in MPPCH/PP resulted in the lowest respiration rate.

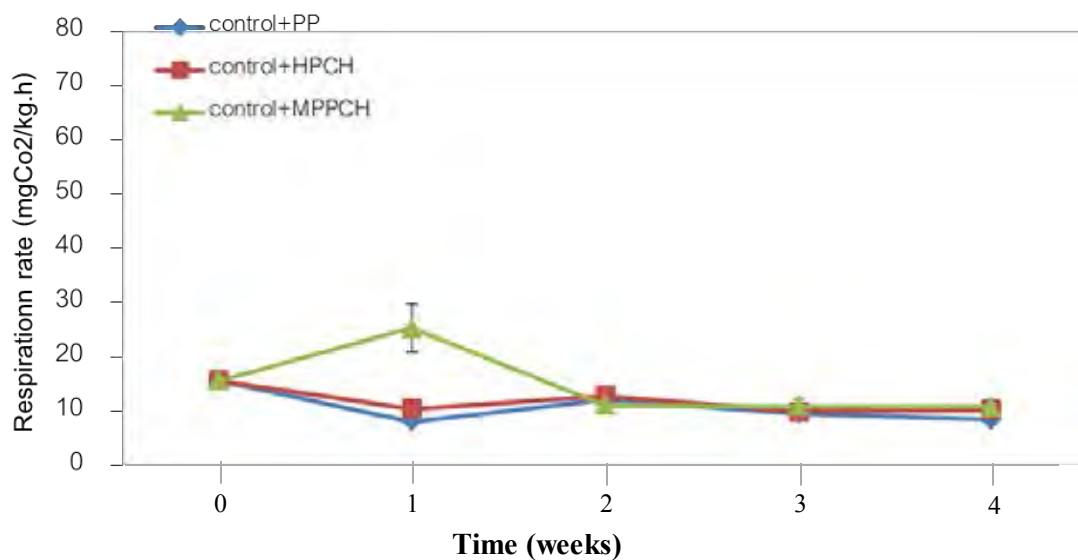


Figure D1 Respiration rate of limes which were packed in polypropylene/clay nanocomposite films during storage at 25°C for 4 weeks.

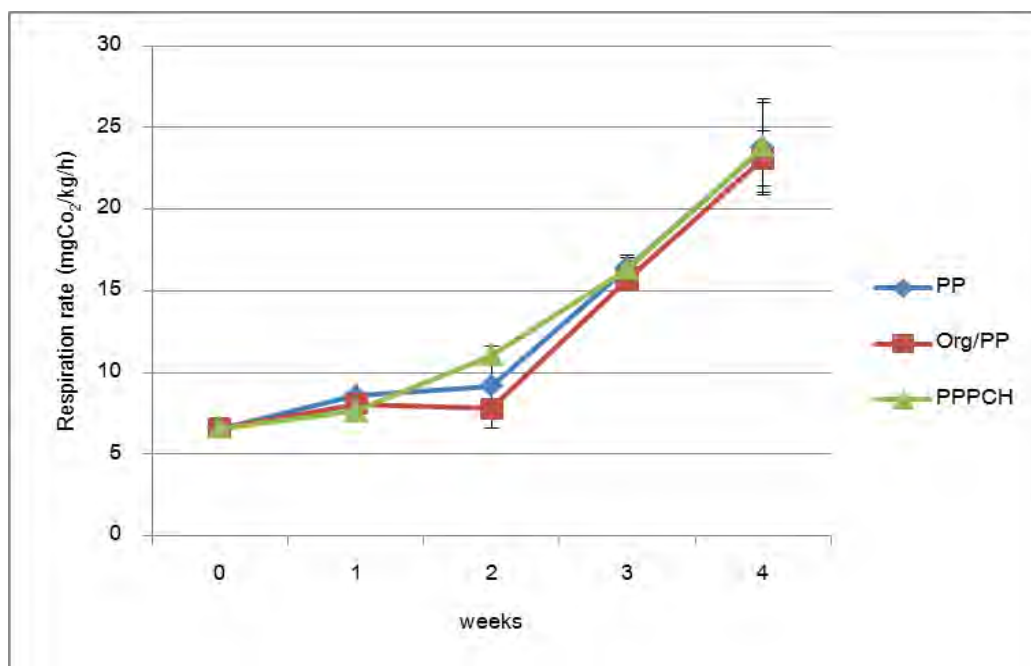


Figure D2 Respiration rate (mgCO₂/kg/h) of limes which were packed in polypropylene/clay nanocomposite films during storage at 25°C for 4 weeks.

Appendix E Antibacterial Test

The antibacterial activity of bentonite, PCH, and all Ag-PCHs was evaluated against bacteria cells by minimum inhibition concentration (MIC) method, based on the National Committee for Clinical Laboratory Standard (Standards, 2006).

For MIC analysis, 100 mL of bacteria in log phase were centrifuged at 400 rpm for 15 min, and the cells were washed twice and suspended in 500 mL of a saline solution or distilled water. Then 10 mL of this prepared bacterial suspension in saline solution or distilled water was added to 9 different concentrations of the samples: 0.1, 0.5, 1.0, 2.0, 5.0, 8.0, 10.0, 12.0, and 14.0 g/L. The antibiotics streptomycin and penicillin were used as positive controls for Gram-negative and Gram-positive bacteria, respectively. Approximately, 100 μ L of the antibiotic solution was added to 10 mL of the bacteria solution as a positive control; for a negative control, 10 mL of the bacteria solution was left without adding anything. By using an incubator shaker, the suspension was shaken for 30 min with an agitation rate of 100 rpm at 37 °C. After half an hour, 10 μ L of the sample solution was dropped on a Muller Hinton Agar (MHA) plate, and the plate was incubated overnight. The MIC value of the samples was recorded as the lowest concentration that killed all bacteria (S.K. Jou and N.A.N.N. Malek, 2016).

Table E1 Minimum Inhibition Concentration (MIC) Result

Bacterial	MIC (mg/ml)						
	% Silver (Ag) and clay						
	1 wt%	5 wt%	10 wt%	20 wt%	30 wt%	PCH	BTN
<i>E.coli</i>	10	2.5	0.156	0.156	0.3125	-	-
<i>E.faecalis</i>	10	0.3125	0.3125	0.3125	0.3125	-	-
<i>S.epidermidis</i>	0.625	0.156	0.156	0.078	0.625	-	-
<i>S.aureus</i>	2.5	0.3125	0.156	0.156	0.625	-	-
<i>S.typhimurium</i>	-	0.625	0.156	0.625	0.3125	-	-
<i>P.aeruginosa</i>	5	0.156	0.078	0.156	0.625	-	-
<i>S.flexneri</i>	-	0.625	0.156	0.625	0.3125	-	-

Note: Accepted value 0.5 mg/l

Appendix F Food Safety Test

All nanocomposite films were submitted to evaluate the quality for using as food packaging. The test was done under the notification of Ministry of Public Health (No. 295) B.E. 2548 (2005): Qualities or standard for container made from plastic. The conditions of testing were followed:

- In-house method LBTY 06370/7 by using ICP-/MS based on TIS- 656-2529 (1986)
- Qualities and standard of dissemination with reference to TIS 656-2529

Table F1 Food Contact results

Sample	PP	PCH/PP	HPCH/PP	MPPCH/PP	Ag-PCH/PP
Lead content	PASS	PASS	PASS	PASS	PASS
Cadmium content	PASS	PASS	PASS	PASS	PASS
Heavy metal (as lead) in 4% concentrated acetic acid extraction	PASS	PASS	PASS	PASS	PASS
Potassium permanganate consumed	PASS	PASS	PASS	PASS	PASS
Residue after evaporation test	PASS	PASS	PASS	PASS	PASS
Migration of color extracted	PASS	PASS	PASS	PASS	PASS

Appendix G Breakdown Strength Measurement

The breakdown strength of the nanocomposite films was observed by using 175Y8S electric puncture tester. The nanocomposite films were placed between the metal plates (sphere shape). All measurements were performed under the air atmosphere. The high value means an insulator material. The less breakdown strength value provides the more conductivity value.

Table G1 Breakdown Strength results

Sample	Breakdown Strength (KV/cm)
PP	281.00 ± 24.69
PCH/PP	83.00 ± 8.93
HPCH/PP	93.48 ± 12.92
1 wt% (MPPCH 2:1)/PP	103.34 ± 4.52
3 wt% (MPPCH 2:1)/PP	97.54 ± 13.13
5 wt% (MPPCH 2:1)/PP	97.28 ± 10.04
1 wt% (10 wt% Ag-PCH)/PP	99.94 ± 9.35
3 wt% (10 wt% Ag-PCH)/PP	96.94 ± 14.77
5 wt% (10 wt% Ag-PCH)/PP	88.38 ± 22.54

CURRICULUM VITAE

Name: Ms. Kornkamol Srithammaraj

Date of Birth: January 23, 1984

Nationality: Thai

University Education:

2002–2005 Bachelor Degree of Chemistry, Faculty of Science, Chiang Mai University, Chiang Mai, Thailand

Publications:

1. Srithammaraj, K., Magaraphan, R., and Manuspiya, H. (2008) Surfactant-Templated Synthesis of Modified Porous Clay Heterostructure (PCH). Advanced Materials Research, 55-57, 317-320.
2. Srithammaraj, K., Magaraphan R, Manuspiya H. (2012) Modified Porous Clay Heterostructures by Organic–Inorganic Hybrids for Nanocomposite Ethylene Scavenging/Sensor Packaging Film. Packaging Technology and Science, 25 (2), 63-72.
3. Srithammaraj, K., Magaraphan R, Manuspiya H. (2017) Influence of Thiol Groups on the Ethylene Adsorption and Conductivity Properties of the Modified Porous Clay Heterostructures (PCHs) Using As Ethylene Scavenger in Smart Packaging. Polymer Bulletin, in press.

Poster Presentations:

1. Srithammaraj, K., Magaraphan, R., and Manuspiya, H. (2008, June 15-19) Mesoporous Heterostructure Derived Conductive Functional Group for Sensor Packaging Application. Paper presented at PPS 24th 2008, Serrano, Italy.
2. Srithammaraj, K., Magaraphan, R. and Manuspiya, H. (2010) Conductive Behaviors of Surface Modified Porous Clay Heterostructure for use as Ethylene Scavenging Sensor. Paper presented at Symposium on Advanced Polymer and Nanomaterials Programme 2010, Patumwan Princess Hotel, Bangkok, Thailand.
3. Srithammaraj, K., Magaraphan R. and Manuspiya, H. (2011, November 13-17) Development of Mesoporous Clay for Entrapping Hormone Gases in Food Packaging. Paper presented at The 12th Pacific Polymer Conference 2011, Jeju Island, Korea.

Oral Presentations:

1. Srithammaraj, K., Magaraphan R. and Manuspiya, H. (2008, April 22-25) Surfactant-Templated Synthesis of Modified Porous Clay Heterostructure. Paper presented at Smart Material 2008, Bangkok, Thailand.
2. Srithammaraj, K., Magaraphan R. and Manuspiya, H. (2009) Surface Modified Porous Clay Heterostructure (PCH) for conductivity Sensor Packaging. Paper presented at Thai-Japan Joint Symposium 2009, Bangkok, Thailand.
3. Srithammaraj, K., Magaraphan R. and Manuspiya H. (2010, October 7-8) Ethylene Scavenger Films Fabricated by Polypropylene/Thiol –Functionalized PCH Nanocomposite. Paper presented at 1st Polymer Conference of Thailand 2010, Bangkok, Thailand.
4. Srithammaraj, K., Magaraphan R. and Manuspiya, H. (2012, January 11-13) Silver-Loaded on the Surface of the Porous Clay Heterostructure (PCH) for sing as Ethylene Scavenger in Food Packaging. Paper presented at PACCON 2012, Chiang Mai, Thailand.